

PERFORMANCE ENHANCEMENT FOR
FILTER BANK MULTICARRIER METHODS
IN MULTI-ANTENNA WIRELESS
COMMUNICATION SYSTEMS

Amr Nagy

In partial fulfillment of the required for the award of Doctor of
Philosophy

Centre for Signal and Image Processing,
Department of Electronic and Electrical Engineering
University of Strathclyde

September 13, 2018

Declaration

This thesis is the result of the author's original research. It has been composed by the author and has not been previously submitted for examination which has led to the award of a degree.

The copyright of this thesis belongs to the author under the terms of the United Kingdom Copyright Acts as qualified by University of Strathclyde Regulation 3.50. Due acknowledgement must always be made of the use of any material contained in, or derived from, this thesis.

Signed: Amr Nagy

Date: September 13, 2018

Acknowledgements

First of all, I would like to thank the Almighty who guides me in all my endeavours. I am heartily thankful to my supervisor, Prof. Stephan Weiss who supported me with a wise guidance, patience and rich knowledge during the progress of my PhD. Also, I would like to express my gratitude for his well-explained illustrations enabled me to develop a solid understanding of the research. I sincerely appreciate his accurate review of this thesis and his valuable comments. Special thanks to my colleagues in room RC3.49 who provided the necessary friendly and quiet environment for the research.

Last, but by no means least, I would like to express my deepest gratitude to my family for their support. Special thanks to my mother, to the memory of my father, my wife, my brothers, and my beloved daughters (Yasmeen and Khadija) for their continuous prayers, wonderful patience, and encouragement all times. It would be outrageous if I missed thanking the Egyptian government for the financial support.

Abstract

This thesis investigates filter bank based multicarrier modulation using offset quadrature amplitude modulation (FBMC/OQAM), which is characterised by a critically sampled FBMC system that achieves full spectral efficiency in the sense of being free of redundancy. As a starting point, a performance comparison between FBMC/OQAM and oversampled (OS) FBMC systems is made in terms of per-subband fractionally spaced equalisation in order to compensate for the transmission distortions caused by dispersive channels. Simulation results show the reduced performance in equalising FBMC/OQAM compared to OS-FBMC, where the advantage for the latter stems from the use of guard bands. Alternatively, the inferior performance of FBMC/OQAM can be assigned to the inability of a per-subband equaliser to address the problem of potential intercarrier interference (ICI) in this system.

The FBMC/OQAM system is analysed by representing the equivalent transmultiplexed channel including the filter banks as a polynomial matrix. The formulated polynomial matrix is demonstrated as a tri-diagonal matrix plus two corner elements which indicates that the induced ICI is limited to the direct adjacent spectrally overlapped subchannels. Based on polynomial matrix algebra, an equaliser is proposed which considers the cross terms between subchannels rather

than performing a per-subband equalisation. The proposed equaliser is obtained through the inversion of the channel polynomial matrix; due to its reduced-rank nature, this inversion requires the extension of pseudo-inversion principles to the domain of polynomial matrices, and the inclusion of a regularisation term for enhanced stability and system performance. Some numerical examples demonstrate the ability of the proposed equaliser to suppress both ISI and ICI.

Furthermore, this thesis combines FBMC/OQAM with multi-antenna architectures. In this scenario, the FBMC/OQAM system will not only suffer from ISI and ICI but also from spatial or inter-antenna interference (IAI). The multiple-input multiple-output (MIMO) channel including the filter bank system is formulated as a polynomial matrix. A polynomial matrix pseudo-inverse of the equivalent channel polynomial matrix is proposed to approximately eliminate ISI, ICI, and IAI. Examples and simulation results are presented to underpin the performance of the proposed architecture.

Contents

Declaration	i
Acknowledgements	ii
Abstract	iii
Table of Contents	viii
List of Figures	xiv
List of Tables	xv
1 Introduction	1
1.1 Motivation and Background	1
1.2 Research Contributions	4

1.3	List of Publications	6
1.4	Outline of the Thesis	7
2	FBMC and MIMO Overview	10
2.1	FBMC/OQAM Modulation	11
2.1.1	OQAM System	13
2.1.2	Synthesis and Analysis Filter Banks	16
2.2	Multi-Antenna Transmission Schemes	20
2.3	FBMC over Dispersive Channels	22
2.4	Conclusions	23
3	FBMC Per-Subband Equalisation Comparison	25
3.1	FBMC Equalisation	26
3.2	FBMC over a Dispersive Channel	28
3.3	Adaptive Equalisation for FBMC	29
3.3.1	Fractionally Spaced Equaliser	30
3.3.2	Concurrent CMA-DD Equaliser	31
3.4	Simulation Results	34

3.5	Concluding Remarks	40
4	Synchronisation and Equalisation of FBMC/OQAM	41
4.1	Background and Motivation	42
4.2	FBMC/OQAM Transmission System	44
4.2.1	Offset QAM	45
4.2.2	Filter Bank Multicarrier System	46
4.3	Equalisation of an FBMC/OQAM System	48
4.3.1	Equivalent Transmission System	48
4.3.2	Equalisation of FBMC System	52
4.4	Polynomial Matrix Inversion via PSVD	54
4.5	Polynomial Matrix Pseudo-Inverse	56
4.6	Concluding Remarks	64
5	Equalisation of Multi-Antenna FBMC/OQAM	65
5.1	Introduction	66
5.2	System Model	68
5.3	Equivalent Polynomial Channel Matrix	70

5.4	MIMO FBMC/OQAM Equalisation	74
5.5	Numerical Example I	76
5.6	Numerical Example II	81
5.7	Conclusions	87
6	Conclusions and Future Work	88
6.1	Conclusions	88
6.2	Future Work	90
	Abbreviations	92
	Mathematical Notation	94
	References	112

List of Figures

2.1	Block diagram of an FBMC/OQAM system in (a) transmitter and (b) receiver.	12
2.2	OQAM pre-processing for two adjacent subchannels, with $\mu = 1 \dots \frac{M}{2}$	14
2.3	OQAM post-processing for two adjacent subchannels, with $\mu = 1 \dots \frac{M}{2}$	15
2.4	Magnitude responses of OFDM and FBMC/OQAM.	18
2.5	MIMO communication system using N_T transmit and N_R receive antennas.	21
3.1	Block diagram of a general FBMC system over a dispersive channel.	28
3.2	Block diagram of a per-subband fractionally spaced equaliser.	30
3.3	Block diagram of the filters inside a concurrent CMA-DD structure.	32

3.4	Flowchart of the per subband concurrent CMA-DD equaliser algorithm for FBMC	35
3.5	Magnitude response of a dispersive channel.	36
3.6	SER performance comparison of FBMC/OQAM to OS-FBMC systems using FS-CMA equaliser per subband.	37
3.7	SER performance comparison of FBMC/OQAM and OS-FBMC systems using concurrent CMA-DD equaliser per subband.	38
3.8	Constellations of the equalised signal of the 12th subband utilising a concurrent CMA-DD equaliser in (a) OS-FBMC and (b) FBMC/OQAM.	39
4.1	Magnitude response of an FBMC/OQAM system with $M = 8$ using PHYDYAS prototype filter.	43
4.2	FBMC-OQAM system model with equaliser $\mathbf{W}[n]$	45
4.3	Inner components of the FBMC/OQAM system with synthesis and analysis filter banks and the channel impulse response $\mathbf{c}[\nu]$	46
4.4	Polyphase components of the OS-FBMC system with synthesis and analysis filter banks and the channel impulse response $\mathbf{c}[\nu]$	48
4.5	Magnitude response of subchannels in an FBMC/OQAM with $M = 4$ using PHYDYAS prototype filter.	50

4.6	Example of a 4×4 polynomial channel matrix $\mathbf{F}(z)$ for an FBMC/OQAM system using PHYDYAS prototype filter.	50
4.7	Magnitude response of subchannels in an OS-FBMC with $M = 4$.	51
4.8	Example of a 4×4 polynomial channel matrix $\mathbf{F}(z)$ for an OS-FBMC system using upsampling factor $K = 5$	51
4.9	Example of 4×4 diagonal matrix $\Sigma(z)$, containing its diagonal terms $\sigma_m[n] \bullet \circ \sigma_m(z)$, with all cross-terms zero or very nearly so.	57
4.10	Example of a 8×8 polynomial channel matrix $\mathbf{F}(z)$ for a FBMC/OQAM system using PHYDYAS prototype filter over a dispersive channel $c[\nu]$ with length of 4.	59
4.11	Example of 8×8 diagonal matrix $\Sigma(z)$, containing its diagonal terms $\sigma_m[n] \bullet \circ \sigma_m(z)$, with all cross-terms zero or very nearly so over a dispersive channel $c[\nu]$ with length of 4.	59
4.12	Example of a 8×8 polynomial equaliser matrix $\mathbf{W}(z)$ of an FBMC/OQAM using PHYDYAS prototype filter.	60
4.13	Example for the joint channel transmission matrix $\mathbf{F}(z)$ and its pseudo-inverse $\mathbf{F}^\dagger(z)$ for an $M = 8$ channel FMBC/OQAM system including a dispersive channel $c[\nu]$ of length 4 when using PHYDYAS prototype filter.	61
4.14	Example for the overall equalised polynomial matrix $\mathbf{G}[\ell]$, for an FMBC/OQAM system with $M = 8$ over a dispersive channel $c[\nu]$ of length 4 when using the PHYDYAS prototype filter.	61

4.15	SER vs regularisation coefficient (ϵ_2) at SNR of 15 dB for the equalised FBMC/OQAM system with $M = 4$ over a dispersive channel of length of 10 coefficients	62
4.16	The PDF of ψ with and without using a regularisation coefficient ϵ_2 during the inversion process of $\mathbf{F}(z)$ for an FBMC/OQAM system with $M = 4$ using PHYDYAS prototype filter over a dispersive channel with length of 10.	63
4.17	SER performances of a per-subband equaliser and the proposed multiband equaliser for FBMC/OQAM with $M = 4$ over a dispersive channel $c[\nu]$ of length 10.	63
5.1	FBMC/OQAM system transmultiplexing signals over a MIMO channel $\mathbf{C}[\nu]$ with N_T transmitters and N_R receivers, and with an equaliser $\mathbf{W}[n]$	69
5.2	Inner component of the MIMO FBMC/OQAM system in polyphase notation.	71
5.3	Example for the equivalent polynomial channel matrix $\mathbf{F}(z) \bullet \text{---} \circ \mathbf{F}[n]$ of a channel with $N_T = 2$ transmitters and $N_R = 2$ receivers, and $M = 4$ subchannels.	73
5.4	Matrix $\Sigma[n] \circ \text{---} \bullet \Sigma(z)$ of approximate singular values of $\mathbf{F}[n]$ as characterised in Fig. 5.3.	76
5.5	Evaluation of non-singular values of $\mathbf{F}(z)$ in Fig. 5.3 on the unit circle.	77

5.6	SER vs regularisation coefficient (ϵ_2) at SNR of 15 dB for the equalised MIMO-FBMC/OQAM system in Fig. 5.8.	78
5.7	Overall response of the equivalent channel $\mathbf{F}(z) \bullet \text{---} \circ \mathbf{F}[n]$, including inner FBMC system of Fig. 5.2, and the equaliser $\mathbf{W}(z) \bullet \text{---} \circ \mathbf{W}[n]$	79
5.8	Response $\mathbf{A}[\ell]$ of the overall MIMO-FBMC/OQAM system as highlighted in Fig. 5.1.	80
5.9	The PDF of ψ with and without using a regularisation constant ϵ_2 during the inversion process of $\mathbf{\Sigma}(z)$	80
5.10	SER Vs SNR for an FBMC/OQAM system over 2×2 MIMO channel when using regularisation coefficient $\epsilon_2 = \{0, 0.05\}$ during the equalisation process.	81
5.11	The equivalent polynomial channel matrix $\mathbf{F}[n]$ of an 2×3 MIMO FBMC/OQAM system with $M = 4$ over a dispersive MIMO channel of length 5.	83
5.12	The diagonal matrix $\mathbf{\Sigma}(z) \bullet \text{---} \circ \mathbf{\Sigma}[n]$ which contains the singular values of $\mathbf{F}(z)$ as depicted in Fig. 5.11	84
5.13	Magnitude response of the non-zero singular values of $\mathbf{F}(z)$ in Fig. 5.11.	85
5.14	The joint channel polynomial matrix $\mathbf{F}(z)$ and its pseudo inverse $\mathbf{F}^\dagger(z)$	86

5.15 Response $\mathbf{A}[\ell]$ of the overall 2×3 MIMO-FBMC/OQAM system as highlighted in Fig. 5.11.	86
--	----

List of Tables

2.1	The SFB output $\mathbf{y}[n]$ when d_3 is an impulse, with transmission over an ideal channel for FBMC/OQAM with $M = 8$	19
2.2	The SFB output $\mathbf{y}[n]$ when d_4 is an impulse, with transmission over an ideal channel for FBMC/OQAM with $M = 8$	20
2.3	The SFB output $\mathbf{y}[n]$ when d_3 is an impulse, with transmission over a dispersive channel for FBMC/OQAM with $M = 8$	23

Chapter 1

Introduction

1.1 Motivation and Background

In the last decade, wireless communication systems have witnessed several developments, such as an increased transmission rate when upgrading from third-generation (3G) wireless communication systems to the fourth generation (4G). Nevertheless, research has continued to push for yet higher data rates for future fifth generation (5G) wireless communication systems [1]. These developments come to meet the increasing requirements of users, who also demand features such as high mobility communications, robustness and low latency transmission.

The increased demands of users, as well as the spread of communication to machine-to-machine links, have made the radio frequency spectrum an increasingly scarce resource [2]. Developing transmission techniques to increase the data throughput becomes essential to overcome this scarcity of the available spectrum. The combination of multicarrier modulation (MCM) schemes and multiple-input

multiple-output (MIMO) architectures represents an attractive strategy to increase the system capacity. Several wireless communication systems have utilised the combination of MIMO and MCM techniques, such as the Worldwide Interoperability for Microwave Access (WiMAX) [3] and the Long Term Evolution (LTE) [4].

MCM is a form of frequency division multiplexing [5], where the data is transmitted across the channel over several frequency bands simultaneously instead of modulating a single carrier [6, 7]. In other words, the wideband communications channel which is generally characterised by frequency selective fading is divided into many subcarriers or subbands that are less frequency selective or perhaps can even be considered as flat fading. Therefore, MCM is robust against broadband dispersions compared to single carrier modulation, and, due to the reduced frequency selectivity, may require less complex synchronisation and equalisation [8].

Orthogonal frequency division multiplexing (OFDM) currently is the most popular and dominant multicarrier modulation technique that is implemented in various broadband communication standards, e.g. wireless local area networks (WLAN), digital audio and video broadcasting (DAB, DVB) [9, 10]. The advantage of OFDM is its robustness against channel dispersion as well as its low complexity, since most computations can be based on the fast Fourier transform (FFT). To mitigate channel dispersion, OFDM however employs a guard interval in the form of a cyclic prefix (CP), which introduces redundancy into the transmission and therefore lowers the spectral efficiency of the approach. Moreover, OFDM utilises rectangular pulse shapes for its subcarrier signals, which leads to poor frequency localisation and potential interference to neighbouring frequency bands, which often has to be addressed by additional channelisation filters in the transmitter and a matched filter in the receiver. If the system is not precisely

synchronised in time and frequency, the orthogonality of the subcarriers is lost, resulting in interference [11, 12]. This may even result in the use of complex equalisers to mitigate intersymbol-interference and cross-talk between subcarriers [13–15], thus negating the simplicity for which OFDM had been adopted originally.

In order to overcome some of the disadvantages of OFDM such as reduced spectral efficiency, tight synchronisation requirements, and high out of band emissions, filter bank based multicarrier (FBMC) modulation has been considered as a potential alternative for OFDM in 5G [16–26]. The main structure of the FBMC system is a filter bank in transmultiplexer configuration. Compared to OFDM, FBMC can contain spectrally well-localised filters, leading to high stop-band attenuation and greatly reduced out-of-band emissions [27]. Because of its higher frequency selectivity, FBMC is considered to be more robust against synchronisation errors than OFDM [29].

Several FBMC methods have been investigated in the literature, such as filtered multitone (FMT) [30], cosine modulated multitone (CMT) [31], or staggered modulated multitone (SMT) which is also termed as filter bank-based multicarrier with offset quadrature amplitude modulation (FBMC/OQAM) [7]. Amongst these FBMC techniques, this thesis investigates FBMC/OQAM [7] based on the pioneering work of Chang who investigated the transmission of amplitude modulation (AM) over parallel band-limited subchannels [32], Saltzberg [33] proposed the transmission of QAM signals using the model presented by Chang, and Hirosaki [34] worked on reducing the system complexity by utilising the digital Fourier transform (DFT). FBMC/OQAM permits overlapping between the adjacent subbands without using guard bands, and thus achieves maximum spectral efficiency [35]. The combination of FBMC and OQAM creates a trans-

parent system between transmitter and receiver that is free of ISI and ICI due to orthogonality conditions when transmitting over an ideal channel [2]. However, when transmitting FBMC/OQAM over dispersive channels, the orthogonality is destroyed leading to ISI and ICI. When transmitting over a multiple-input multiple-output (MIMO) channel, FBMC/OQAM is negatively affected by inter-antenna interference (IAI) in addition to ISI and ICI. Equalisation can be used to restore the orthogonality and mitigate the different interference types. Numerous researchers have investigated the equalisation of FBMC/OQAM over single-input single-output (SISO) channels, e.g. [36–40] and MIMO channels, see e.g. [41–43].

This thesis aims to investigate and analyse FBMC/OQAM in order to develop an effective equalisation approach against ISI, ICI and IAI terms where the channel state information (CSI), i.e. knowledge of the channel impulse response, is only assumed to be known in the receiver. While this excludes better performing joint precoding and equalisation schemes such as in [44–49], it takes into account that often CSI is not available at the transmitter, hence rendering precoder designs impractical. Focussing on the equaliser, a linear algebraic approach is proposed in three phases. First, the transmission channel is formulated as a polynomial matrix based on [50]. Then, algorithms in [52, 53] are used to calculate a polynomial singular value decomposition (PSVD). Finally a pseudo inverse of the equivalent channel matrix is calculated, which represents the proposed equaliser for FBMC/OQAM in SISO [35] and MIMO channels [54].

1.2 Research Contributions

The following are the perceived research contributions made in this thesis:

- **Per-subband equalisation comparison of Filter Bank Based Multicarrier Systems (Chapter 3), [55]**

The use of guard bands in the oversampled filter bank multicarrier (OS-FBMC) system reduces its spectral efficiency. On the other hand, the critically sampled (FBMC/OQAM) system does not use any form of redundancy during the transmission leading to maximum spectral efficiency. Therefore, the symbol error rate (SER) performance of both FBMC systems was compared when transmitting over a dispersive channel and apply an equalisation algorithm working in per subband basis. The simulation results show the degradation in the SER performance of FBMC/OQAM compared to OS-FBMC which calls for developing an equaliser that is capable of combating intersymbol interference (ISI) as well as the intercarrier interference (ICI) induced in FBMC/OQAM due to the spectral overlapping between the subbands.

- **Formulation of the polynomial channel matrix for FBMC/OQAM (Chapter 4), [35]**

The FBMC/OQAM permits an overlapping between the direct adjacent subbands in order to achieve maximum spectral efficiency. However this comes at the cost of spectral leakage between the adjacent subbands when transmitting over a dispersive channel leading to ICI. Therefore, the formulation of a polynomial matrix which represents the transfer functions between subbands in transmitter and receiver including filter bank algorithm and channel was proposed. There are two ways to obtain the equivalent channel polynomial matrix as presented in Chapter 4. The nonzero off-diagonal elements of the channel polynomial matrix show that the induced ICI in FBMC/OQAM comes from the direct adjacent neighbours.

- **Joint equalisation of a FBMC/OQAM using polynomial matrix**

pseudo matrix (Chapter 4), [35]

The cross-talks between the adjacent subbands in FBMC/OQAM degrades the equalisation performance when it works per-subband. Based on the equivalent channel polynomial matrix, equalisation process is proposed to be carried out by inverting this matrix. The rank deficiency of the channel matrix calls for using a polynomial matrix pseudo-inverse. Numerical examples of applying the proposed equaliser are presented. The simulations based results show the capability of the proposed equaliser cooperated with OQAM algorithm to suppress the ISI and ICI affecting the transmitting of FBMC/OQAM via dispersive channels.

- **Equalisation of MIMO FBMC/OQAM System by a Polynomial Matrix Pseudo-Inverse (Chapter 5), [54]**

In order to boost the spectral efficiency, the FBMC/OQAM system is extended to multiantenna techniques. Here, FBMC/OQAM suffers additionally from inter-antenna interference (IAI). Therefore, an equivalent channel polynomial matrix including filter bank and MIMO channel is proposed. The structure of the polynomial matrix reflects the three interference types (ISI, ICI, and IAI). Further, an equaliser that mitigates for all interference types is presented. The proposed equaliser is based on the pseudo-inverse of the MIMO channel matrix which is shown to be a reduced rank matrix.

1.3 List of Publications

- **A. Nagy and S. Weiss:** “Channel Equalisation of a MIMO FBMC/OQAM System Using a Polynomial Matrix Pseudo-Inverse”, IEEE 10th Sensor Array and Multichannel Signal Processing Workshop, Sheffield, UK,

July 2018.

- **A. Nagy and S. Weiss:** “Synchronisation and Equalisation of an FBMC/OQAM System by a Polynomial Matrix Pseudo-Inverse”, IEEE International Symposium on Signal Processing and Information Technology, Bilbao, Spain December 2017.
- **A. Nagy and S. Weiss:** “Comparison of Filter-Bank Based Multicarrier Systems with Fractionally Spaced Equalisation”, 11th International Conference on Mathematics in Signal Processing, Birmingham, UK, December 2016.
- **R. Elliot, A. Nagy, L. Crockett, K. Thompson, S. Weiss, R. Stewart:** “Low-cost frequency-agile filter bank-based multicarrier transceiver implementation”, 2nd IET International Conference on Intelligent Signal Processing, London, UK, December 2015.

1.4 Outline of the Thesis

The thesis is structured as below:

- **Chapter 2** introduces an overview of the concepts and topics that will be used throughout the other chapters of this thesis. First, the fundamentals of FBMC/OQAM modulation scheme are highlighted through presenting its main structure. After that, the main interferences that occur in an FBMC/OQAM system when transmitting over a dispersive channel are explained. Finally, the crucial role of using multiple antennas in a wireless communication system is outlined. In addition, the main factor that hinders

the integration between MIMO and FBMC/OQAM is highlighted which requires a signal processing technique -e.g. an equaliser- which will be discussed in the subsequent chapters.

- **Chapter 3** investigates the application of adaptive per-subband equalisers for oversampled FBMC systems (OS-FBMC) and FBMC/OQAM. The equalisation and timing synchronisation process is achieved by using a fractionally spaced equaliser with updating based on a concurrent constant modulus algorithm (CMA) and decision-direct (DD) approach. The exploited equaliser works on per subband basis for both types of FBMC. Finally, a comparison of equalisation performances -in terms of symbol error rate (SER) versus signal to noise ratio (SNR)- for both cases of FBMC is presented through simulation based results.
- **Chapter 4** delves into the reason behind the performance degradation and inadequately of the per- subband equaliser for FBMC/OQAM. This chapter proposes a polynomial matrix approach that formulates an equivalent channel transfer function, which includes the filter bank components and channel. This polynomial matrix explains the consequences of permitting the overlapping between the adjacent subcarriers in FBMC/OQAM which lead to intercarrier interference (ICI) in addition to intersymbol interference (ISI) when transmitting over a dispersive channel. Further, the proposed equivalent channel polynomial matrix — by using polynomial matrix algebra— is inverted to obtain the solution to an equaliser that can mitigate both ISI and ICI. The inversion process is based on a polynomial matrix pseudo inverse due to the reduced-rank nature of the channel matrix. Some numerical examples are presented to demonstrate the effectiveness of the proposed equaliser in removing ISI and ICI.

- **Chapter 5** investigates the transmission of an FBMC/OQAM system over a MIMO channel. A polynomial matrix representing the equivalent response of the inner MIMO FBMC/OQAM system comprising the filter banks for transmultiplexing as well as the MIMO channel is formulated. The structure of the proposed polynomial matrix reflects the different types of interference: inter-antenna interferences (IAI), ISI, and ICI which degrades the system performance. Accordingly, an equaliser for MIMO-FBMC/OQAM is proposed to combat all types of interference characterised by the proposed polynomial matrix. The rank-deficiency of the equivalent channel matrix has motivated to obtain the polynomial matrix pseudo-inverse. Numerical examples show the ability of the proposed equaliser to mitigate for ISI, ICI, and IAI.
- **Chapter 6** gives final conclusions of the investigated points and the obtained results. Moreover, it outlines the future research work.

Chapter 2

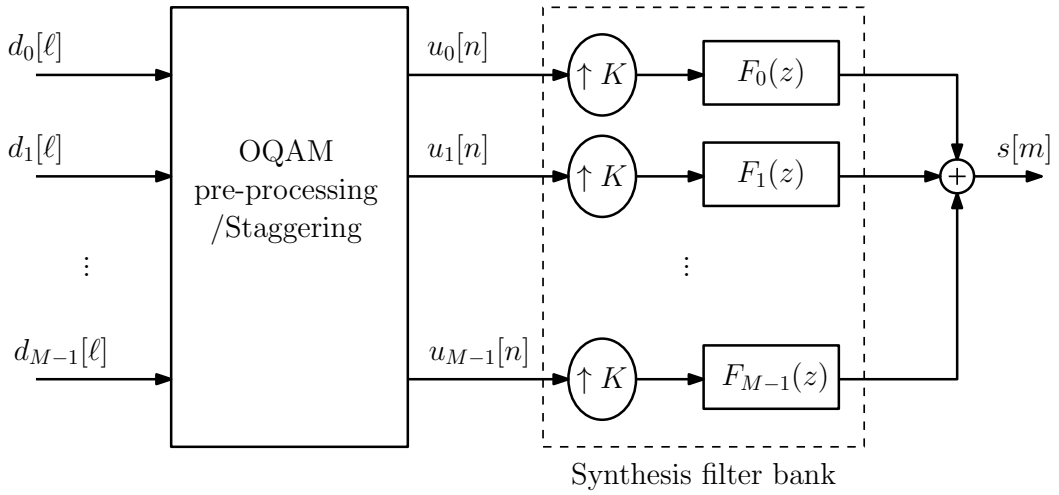
Overview of Filter Bank Based Multicarrier and Multi-Antenna Schemes

In this chapter, the main structure of the FBMC/OQAM system is presented as it is the cornerstone on which this thesis is based. Moreover, a general overview of the multiple antenna architecture and its different advantages and disadvantages are presented to pave the way for combining it with the FBMC/OQAM. The spatial dimension provided by the multi-antenna architecture can be used to contribute to improve the transmission reliability of the FBMC/OQAM system as well as to increase the data throughput.

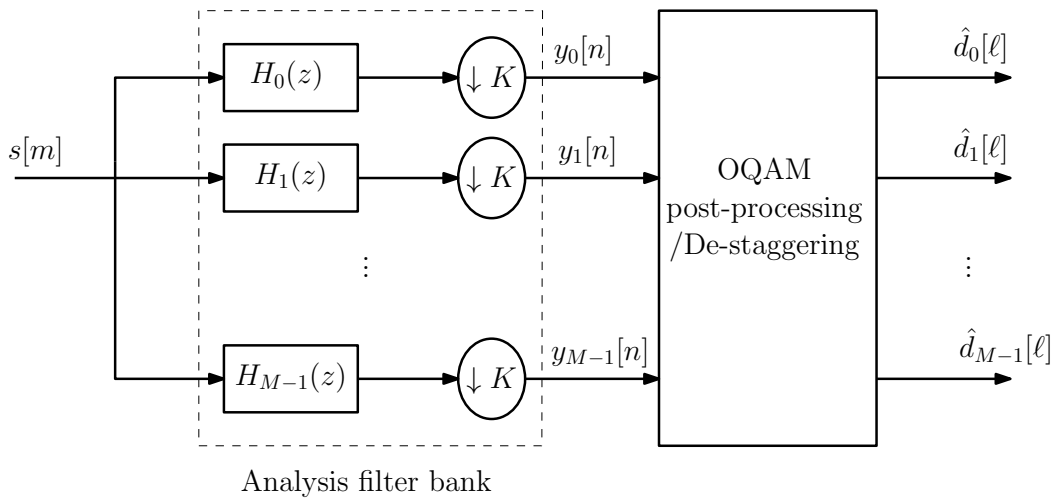
2.1 FBMC/OQAM Modulation

Amongst the different multicarrier modulation techniques, this thesis focuses on FBMC/OQAM, which is also known as OFDM/OQAM or staggered multitone (SMT) [27]. FBMC/OQAM is an attractive multicarrier modulation (MCM) approach, which has been developed over the course of several research projects sponsored by the European Commission such as PHYDYAS I and II, see e.g. [22, 56, 57, 60]. The choice of the FBMC/OQAM system to be investigated in this thesis is based on several advantages which make it a more appealing MCM technique for future wireless communications when compared to conventional OFDM with CP and other FBMC approaches, such as FMT. Mainly, FBMC/OQAM achieves maximum spectral efficiency since it avoids any form of redundancy through e.g. guard bands or guard periods compared to CP-OFDM or FMT. Moreover, FBMC/OQAM uses highly frequency-selective filters, and consequently exhibits less out of band emission compared to OFDM which uses a prototype filter with a periodic sinc characteristic on the frequency domain.

The FBMC/OQAM system is classified as a critically sampled multicarrier modulation system which is working in the transmultiplexer configuration as the input of the analysis filter bank (AFB) at the receiver side, which is fed by the output of the synthesis filter bank (SFB) at the transmitter side [58]. The general block diagram of the FBMC/OQAM system is shown in Fig. 2.1. It can be shown that FBMC/OQAM works through two main subsystems: a filter bank system and an OQAM pre- and post-processing. Each subsystem (filter bank and OQAM) is represented by a block at the transmitter side (OQAM pre-processing and SFB), as shown in Fig. 2.1(a), and another matching block in the receiver side (OQAM post-processing and AFB), as shown in Fig. 2.1(b). The low rate QAM signal $d_i[\ell] \in \mathbb{C}, i = 0 \cdots M - 1$, with symbol time index ℓ is mapped



(a)



(b)

Figure 2.1: Block diagram of an FBMC/OQAM system in (a) transmitter and (b) receiver.

onto $u_i[n] \in \mathbb{C}$ by the OQAM pre-processing block, where M is the number of subchannels. Then, the OQAM signal $u_i[n]$ is multiplexed by SFB to generate a high rate signal $s[m] \in \mathbb{C}$, with time index m running $2K$ times faster than the index ℓ , where $K = \frac{M}{2}$ is the upsampling and downsampling factor used in SFB and AFB respectively. The value of K reflects that FBMC/OQAM is a critically sampled system. On the other hand, in the absence of the OQAM system and using $K > M$, the FBMC system becomes an oversampled system with guard bands leading to a loss in spectral efficiency. When considering an ideal channel, the detected low rate signal $\hat{d}_i[\ell]$ is obtained by demultiplexing the received signal using the AFB then processed by the OQAM post-processing.

2.1.1 OQAM System

The OQAM system represents the initial and terminal processes of the FBMC/OQAM system as shown in Fig. 2.1, and plays a crucial role in the FBMC/OQAM system, where it establishes the orthogonality in the real field between the adjacent overlapping subchannels. On the transmitter side, the OQAM pre-processing block staggers between the in-phase (real) and quadrature (imaginary) components of each complex-valued QAM symbol in $d_i[\ell]$ to generate two new symbols. Therefore, the output of the OQAM pre-processing $u_i[n]$ is running at a rate that is twice as fast as that of the input QAM signals $d_i[\ell]$ i.e. ($n = 2\ell$). As shown in Fig. 2.2, the sequence of the output OQAM symbols relies on the subchannel index. For odd subchannels with index $2\mu - 1, \mu = 1 \dots \frac{M}{2}$, the output signal can be formulated as

$$u_{2\mu-1}[2\ell] = \Re\{d_{2\mu-1}[\ell]\}, \quad (2.1)$$

$$u_{2\mu-1}[2\ell + 1] = j\Im\{d_{2\mu-1}[\ell]\}, \quad (2.2)$$

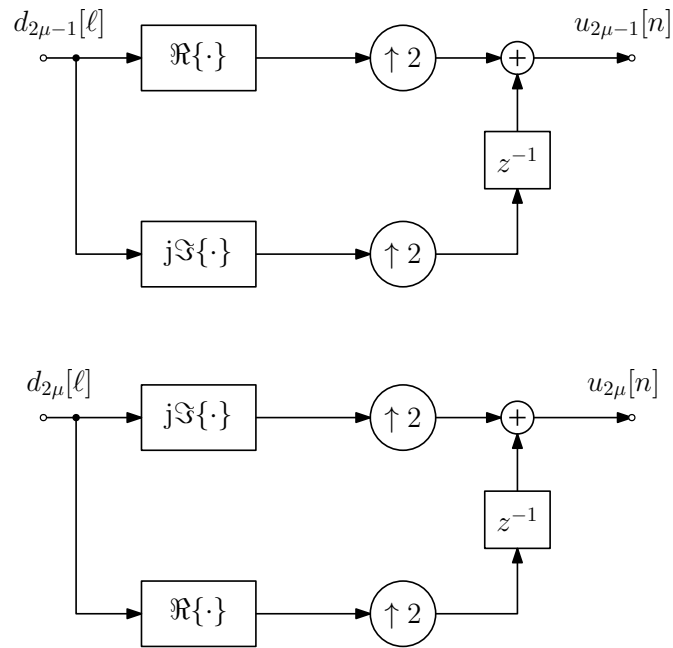


Figure 2.2: OQAM pre-processing for two adjacent subchannels, with $\mu = 1 \dots \frac{M}{2}$.

where $\Re\{\cdot\}$ and $\Im\{\cdot\}$ denote the real and imaginary parts of a complex-valued symbol respectively.

In contrast, in the even subchannels with index 2μ , $\mu = 1 \dots \frac{M}{2}$, the OQAM output is given by

$$u_{2\mu}[2\ell] = j\Im\{d_{2\mu}[\ell]\}, \quad (2.3)$$

$$u_{2\mu}[2\ell + 1] = \Re\{d_{2\mu}[\ell]\}. \quad (2.4)$$

The OQAM post-processing is shown in Fig. 2.3, where the real and imaginary components of the AFB output $y_i[n]$ are alternately combined to form the estimated output signal $\hat{d}_i[\ell]$. Similar to the OQAM pre-processing, the de-

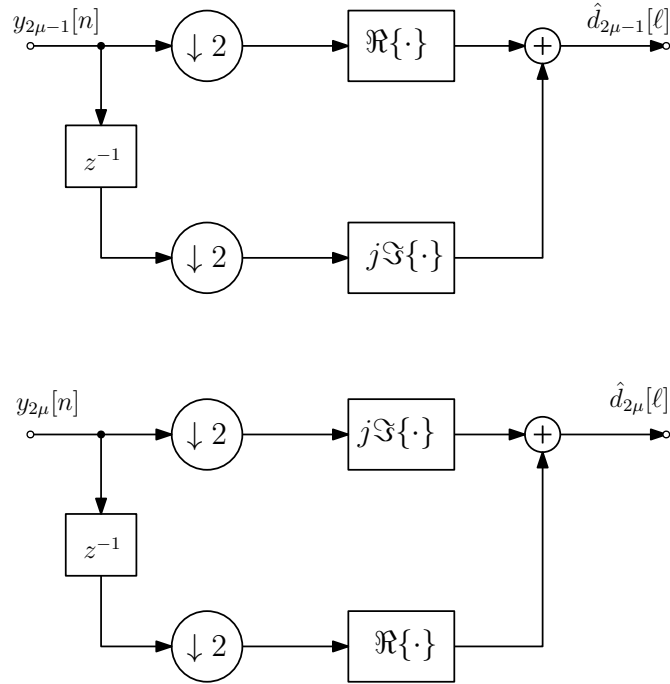


Figure 2.3: OQAM post-processing for two adjacent subchannels, with $\mu = 1 \dots \frac{M}{2}$.

staggering operation is carried out based on the subchannel index as

$$\hat{d}_{2\mu-1}[\ell] = \Re\{y_{2\mu-1}[2\ell]\} + j\Im\{y_{2\mu-1}[2\ell + 1]\}, \quad (2.5)$$

$$\hat{d}_{2\mu}[\ell] = \Re\{y_{2\mu}[2\ell + 1]\} + j\Im\{y_{2\mu}[2\ell]\}. \quad (2.6)$$

The purpose of this staggering and de-staggering is to enable perfect reconstruction — in the absence of a dispersive channel and any synchronisation errors — of the inner filter bank system, which is otherwise fundamentally limited by the Balian-Low theorem [59]. This theorem states that perfect symbol density, timing- and frequency localisation (i.e. critical sampling) as well as orthogonality cannot be satisfied simultaneously. With the above symbol assignment, the orthogonality condition for complex-valued symbols is replaced by the less stringent orthogonality condition for the real parts only.

2.1.2 Synthesis and Analysis Filter Banks

As shown in Fig. 2.1, the synthesis filter bank is constructed of M parallel branches to multiplex the OQAM signals in $u_i[n]$ over the corresponding i th subchannel. Each branch in the SFB is equipped with an upsampler and a filter $F_i(z)$. The transmitted signal $s[m]$ is composed by adding the SFB output signals. On the receiver side, the analysis filter bank consists of M parallel branches to perform the dual operations to the SFB. The received signal $s[m]$ is first demultiplexed to the corresponding subbands and then downsampled by a factor of K to generate the output signals $y_i[n]$. Both the upsampling and downsampling factors are set to have the same value of $K = \frac{M}{2}$ across all branches.

The filter bank system divides the available channel bandwidth equally amongst the signals over all branches of the SFB and AFB, and as such implements a uniform FBMC system. Consequently, the filters in the SFB, $F_i(z)$, $i = 0 \dots (M - 1)$, can be generated by modulating complex exponential with a well designed prototype filter.

This thesis considers the design of the prototype filter presented in [28, 60], which has been developed as part of the physical layer for dynamic spectrum access and cognitive radio (PHYDYAS) project [60]. In this thesis, it is denoted as PHYDYAS prototype filter, which refers to a low pass finite impulse response (FIR) filter $p[m]$ of order $L_p = KM - 1$ [58]

$$p[m] = \frac{1}{VM} \left(a[0] + 2 \sum_{i=1}^{V-1} (-1)^i a[i] \cos\left(\frac{2\pi i}{VM}(m+1)\right) \right), \quad (2.7)$$

where V is the overlapping factor with the value set to be 4, $m = 1 \dots L_p$, and the $a(i), i = 0 \dots V - 1$ are the frequency coefficients obtained based on the frequency

sampling technique used in the filter design [60]. These coefficients are optimised to obtain a highly frequency-selective filter and minimise the interference induced between the adjacent overlapped subchannels. The values of these coefficients are set as [28]

$$\begin{aligned}
 a(0) &= 1 \\
 a(1) &= 0.9719598, \\
 a(2) &= \frac{\sqrt{2}}{2}, \\
 a(3) &= \sqrt{1 - (a(1))^2} = 0.235147.
 \end{aligned} \tag{2.8}$$

Fig. 2.4 illustrates a comparison between the magnitude response of the PHYDYAS prototype filter used in FBMC/OQAM and that used in OFDM. It can be noted that FBMC/OQAM benefits from higher frequency selectivity filters compared to the OFDM.

Therefore, the modulated i th filter in the SFB can be expressed by

$$f_i[m] = p[m] e^{j\frac{2\pi i}{M}(m-D)}, i = 1 \dots M, \tag{2.9}$$

where D is the delay applied to the SFB to be causal [60], $D = \frac{L_p-1}{2}$.

In the receiver, the i th filter in the AFB is the time-reversed complex-conjugated version of the corresponding filter in the SFB, such that

$$\begin{aligned}
 h_i[m] &= f_i^*[L_p - 1 - m] \\
 &= p[L_p - 1 - m] e^{-j\frac{2\pi i}{M}(D-m)} \\
 &= p[m] e^{j\frac{2\pi i}{M}(m-D)}.
 \end{aligned} \tag{2.10}$$

As mentioned earlier, the FBMC/OQAM system is a critically sampled MCM

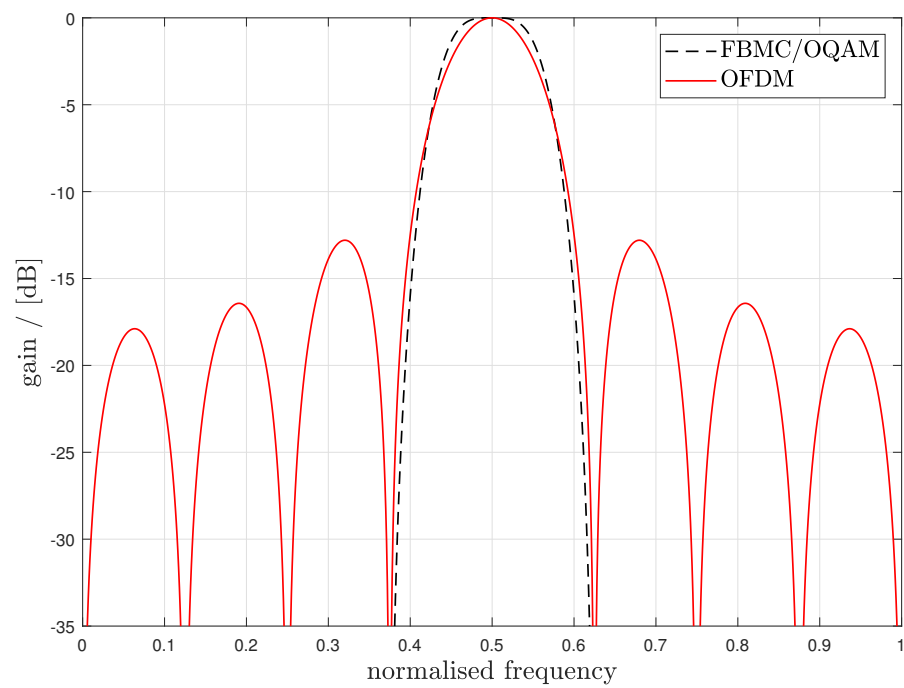


Figure 2.4: Magnitude responses of OFDM and FBMC/OQAM.

Table 2.1: The SFB output $\mathbf{y}[n]$ when d_3 is an impulse, with transmission over an ideal channel for FBMC/OQAM with $M = 8$.

	$n = -3$	$n = -2$	$n = -1$	$n = 0$	$n = 1$	$n = 2$	$n = 3$
$y_1[n]$	0	0	0	0	0	0	0
$\Re\{y_2[n]\}$	0	-0.125	0	0.239	0	-0.125	0
$\Im\{y_2[n]\}$	0.043	0	-0.206	0	0.206	0	-0.043
$\Re\{y_3[n]\}$	0.069	0	-0.564	1	-0.564	0	0.069
$\Im\{y_3[n]\}$	0	0	0	0	0	0	0
$\Re\{y_4[n]\}$	0	-0.125	0	0.239	0	-0.125	0
$\Im\{y_4[n]\}$	-0.043	0	0.206	0	-0.206	0	0.043
$y_5[n]$	0	0	0	0	0	0	0

system that permits the spectral overlapping between the subcarriers. However, the design of the PHYDYAS prototype filter limits the spectral leakage to only affect directly adjacent subbands.

As an example for the real-valued orthogonality of the combined FBMC and OQAM system, Table 2.1 indicates the AFB output signals $y_i[n]$, $i = 1 \dots 5$ over the first five successive subchannels, in a FBMC/OQAM system with $M = 8$, when the corresponding middle subchannel input $d_3[\ell]$ at the transmitter is excited by an impulse, all other inputs set to zero, and under the assumption of an ideal channel. It can be noted that the received signal $y_3[n]$ is affected by the spectral leakage from $y_2[n]$ and $y_4[n]$ while next-adjacent subchannels ($i = 1$ and $i > 4$) have negligible effects on $y_3[n]$.

In case a single, even subchannel is excited, such as $d_4[\ell]$, Table 2.2 denotes the SFB output signals $y_i[n]$, $i = 2 \dots 6$. It worth to emphasise the crucial role of the OQAM system in eliminating the induced interference by alternately discarding the real and imaginary interfered symbols, which are represented by the shaded cells in the Tables 2.1 and 2.2.

Table 2.2: The SFB output $\mathbf{y}[n]$ when d_4 is an impulse, with transmission over an ideal channel for FBMC/OQAM with $M = 8$.

	$n = -3$	$n = -2$	$n = -1$	$n = 0$	$n = 1$	$n = 2$	$n = 3$
$y_2[n]$	0	0	0	0	0	0	0
$\Re\{y_3[n]\}$	0.005	0	-0.125	0	0.239	0	-0.125
$\Im\{y_3[n]\}$	0	-0.043	0	0.206	0	-0.206	0
$\Re\{y_4[n]\}$	0	-0.069	0	0.564	1	0.564	0
$\Im\{y_4[n]\}$	0	0	0	0	0	0	0
$\Re\{y_5[n]\}$	0.005	0	-0.125	0	0.239	0	-0.125
$\Im\{y_5[n]\}$	0	0.043	0	-0.206	0	0.206	0
$y_6[n]$	0	0	0	0	0	0	0

2.2 Multi-Antenna Transmission Schemes

The MCM schemes discussed so far aim to transmultiplex signals over a transmission channel, which can be dispersive and corrupted by additive white Gaussian noise (AWGN). The dispersive component of this channel has been characterised by a channel impulse response $c[m]$, which typically is spanned by a pair of transmit and receive antennas. However, most modern communication systems rely on multiple antennas, i.e. to transmit over a multiple-input multiple-output (MIMO) system instead of a single-input single-output (SISO) system. MIMO transmission offers a range of advantages; for example, Foschini and Gans [61], Foschini [62] and Telatar [63] established an increase in the system capacity when antenna arrays are used at both link terminals. This capacity increase can be exploited in various ways; for example Alamouti [64] and Tarokh [65] elaborated on the improved reliability that a MIMO communications system offers over a SISO one. Generally, this capacity increase can be exploited in the form of a multiplexing gain, an antenna gain, or a diversity gain [66].

In the time domain, a MIMO channel spanned by N_T transmit and N_R receive antennas can be denoted by a matrix $\mathbf{C}[m] \in \mathbb{C}^{N_R \times N_T}$ of impulse responses,

$$\mathbf{C}[m] = \begin{bmatrix} c_{1,1}[m] & \cdots & c_{1,N_T}[m] \\ \vdots & \ddots & \vdots \\ c_{N_R,1}[m] & \cdots & c_{N_R,N_T}[m] \end{bmatrix}, \quad (2.11)$$

where m stands for the time index m and $c_{ij}[m]$ represents the impulse response between the j th transmitter and the i th receiver. When transmitting a signal vector $\mathbf{s}[m] \in \mathbb{C}^{N_T}$ over this MIMO channel $\mathbf{C}[m]$, corrupted by AWGN $\mathbf{n}[m] \in \mathbb{C}^{N_R}$, then the received signals $\mathbf{r}[m] \in \mathbb{C}^{N_R}$ can be expressed as

$$\mathbf{r}[m] = \mathbf{C}[m] * \mathbf{s}[m] + \mathbf{n}[m], \quad (2.12)$$

where $(*)$ denotes the convolution operation.

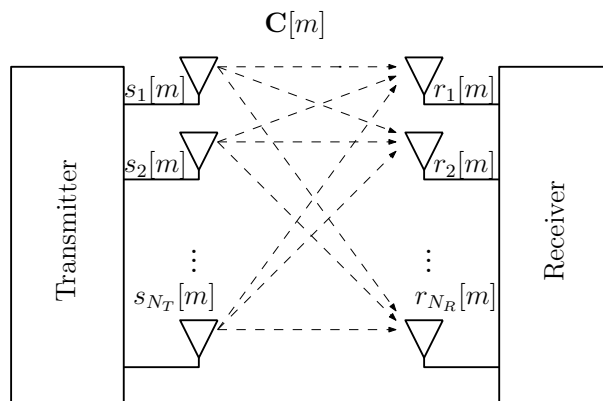


Figure 2.5: MIMO communication system using N_T transmit and N_R receive antennas.

2.3 FBMC over Dispersive Channels

The main objective of the OQAM pre- and post- processing is to obtain the orthogonality in the real field between the adjacent subcarriers. The cross terms induced by the spectral overlapping between the adjacent subchannels is eliminated in the OQAM system as long as the transmission channel is ideal. However, this orthogonality is destroyed when transmitting over dispersive channels. When transmitting FBMC/OQAM over a realistic SISO channel, the received signal $s[m]$ is distorted by the dispersion, i.e. the multipath fading of the channel $c[m] \in \mathbb{C}$ as well as contaminated by additive white Gaussian noise (AWGN) $n[m]$ as

$$r[m] = c[m] * s[m] + n[m] . \quad (2.13)$$

Example. The earlier example of transmitting a pulse in the $i = 3$ rd subcarrier as shown in Table 2.1 is now repeated over a dispersive channel of order four, and in the absence of AWGN. Previously, in the ideal channel case, interference was limited to the shaded components, which are discarded in the OQAM post-processing block. However, Tab. 2.3 shows the received signals $y_i[n], i = 1 \dots 5$ in this dispersive case, and thus illustrates how interference now spreads to discarded and non-discarded components alike. The non-shaded components retaining interference, are now passed to the output of the OQAM post-processing block and represent the remaining interference in the received FBMC/OQAM signal, in terms of ISI within the $i = 3$ rd band, but also as ICI to the adjacent signals for $i = 2$ and $i = 4$.

When transmitting over a MIMO channel $\mathbf{C}[m] \in \mathbb{C}^{N_R \times N_T}$ with channel impulse responses $c_{ij}[m]$ between the j th transmitter and the i th receiver, then the

Table 2.3: The SFB output $\mathbf{y}[n]$ when d_3 is an impulse, with transmission over a dispersive channel for FBMC/OQAM with $M = 8$.

	$n = -3$	$n = -2$	$n = -1$	$n = 0$	$n = 1$	$n = 2$	$n = 3$
$y_1[n]$	0	0	0	0	0	0	0
$\Re\{y_2[n]\}$	0.011	-0.116	-0.058	0.239	0.058	-0.137	-0.011
$\Im\{y_2[n]\}$	0.039	0.035	-0.199	-0.068	0.213	0.034	-0.054
$\Re\{y_3[n]\}$	0.053	0.003	-0.447	0.814	-0.510	0.049	0.050
$\Im\{y_3[n]\}$	-0.016	0.030	0.135	-0.410	0.377	-0.094	-0.033
$\Re\{y_4[n]\}$	-0.007	-0.076	0.065	0.121	-0.092	-0.047	0.034
$\Im\{y_4[n]\}$	-0.030	0.031	0.114	-0.090	-0.093	0.068	0.009
$y_5[n]$	0	0	0	0	0	0	0

received signal at the i th antenna is given by

$$r_i[m] = \sum_{j=1}^{N_T} c_{ij}[m] * s_j[m] + n_i[m]. \quad (2.14)$$

Therefore, the orthogonality between the subchannels is not only destroyed due to ISI and ICI as in SISO but also by the spatial cross-talk between the transmitted streams which is referred as inter-antenna interference (IAI). Therefore, in order to restore the orthogonality between the subchannels in both the SISO and MIMO cases, the OQAM system requires mitigation against the negative effects of the dispersive channels.

2.4 Conclusions

This chapter has reviewed FBMC/OQAM as a multicarrier modulation (MCM) schemes, consisting of an inner filter bank, and an outer OQAM system that staggers symbols, and by doing so enables full spectral efficiency by limiting or-

thogonality to the real part only. It has been demonstrated that a SISO dispersive channel destroys this orthogonality, and introduces intersymbol interference (ISI) within a subcarrier, as well as inter-carrier interference (ICI) between adjacent subcarriers. Even if the channel is not dispersive but imposes a delay, the orthogonality may be compromised, and the system requires synchronisation in order to be transparent.

This thesis will therefore explore approaches to equalisation and synchronisation of such MCM schemes. Specifically, Chapter 3 will explore a per-subcarrier approach, which targets ISI. Chapter 4 will propose a more comprehensive equaliser that is capable of mitigating both ISI and ICI terms.

This chapter has also briefly touched on MIMO transmission. The MIMO channel, as will be demonstrated later, additionally introduces inter-antenna interference or cross-talk. Therefore, Chapter 5 will extend the work of Chapter 4 to the MIMO case, where a proposed equaliser, in addition to ISI and ICI, can also mitigate IAI.

Chapter 3

Per-Subband Equalisation Comparison Between Different FBMC Systems

The previous chapter has provided an overview of an interesting multicarrier modulation scheme particularly FBMC/OQAM system. FBMC systems considered for the inclusion in several emerging communication applications e.g. future wireless communications (5G) [24], underwater acoustic communication [67], and optical communications [68], due to their aforementioned advantages of high spectral efficiency and robustness to synchronisation errors. Generally, FBMC is a transparent modulation system, i.e. it can retrieve the transmitted signals at the receiver perfectly when transmitting over an ideal channel. However, when transmitting over a dispersive channel, the received signals generally suffer from inter-symbol interference (ISI) and inter-carrier interference (ICI), which usually leads to degradation in the system performance. Therefore, it is mandatory to

utilise some countermeasures such as equalisation and timing synchronisation to channel dispersion. Therefore, this chapter investigates the application of simple per-subband equalisation for two types of FBMC: an oversampled FBMC system (OS-FBMC) and a critically sampled FBMC/OQAM system. To assess the performance, we compare the symbol error rate (SER) of the two FBMC systems when utilising different types of per-subband equalisers.

3.1 FBMC Equalisation

A switch from orthogonal frequency division multiplexing to more general filter bank based multicarrier (FBMC) methods is considered for 5G due to better resilience to synchronisation errors [29]. This advantage of FBMC systems may rely on redundancies in terms of guard bands. Sub-channels, however, are not free of inter-symbol interference, therefore requiring equalisation when transmitting over dispersive channels [69].

Amongst FBMC methods, the critically sampled FBMC/ offset quadrature amplitude modulation (OQAM) system by [7] has gained attention because of its high spectral efficiency, for which e.g. [70], [71] have applied precoding and equalisation at the subband level. In contrast oversampled (OS) FBMC systems in e.g. [69] offer a lower spectral efficiency compared to FBMC/OQAM, but enable better synchronisation and a lower achievable minimum mean square error of a subsequent equaliser [72]. The purpose of this chapter is to compare the OS-FBMC case in [72] to the critically sampled case of an FBMC/OQAM system, whereby in both cases the aim is to employ in the receiver a simple adaptive filter in each subchannel to perform equalisation and synchronisation.

Equalisers generally require high orders to invert channel impulse responses of even moderate length [73] with as a rule of thumb recommending 10 equaliser coefficients for every sample of the channel impulse response. Also since the channel coefficients do not necessarily coincide with the sampling grid at the symbol rate, the equaliser is likely required to implement a fractional delay which may also require significant length [74]. These considerations apply to symbol spaced equalisers, where the adaptive filter operates at the receiver's symbol rate. In contrast, operating fractionally spaced equalisers (FSE) on sub-channels can in theory lead to perfect channel equalisation even with a finite length equaliser, which typically can have a much shorter response than its symbol spaced counterpart [75].

Several researchers have investigated the application of the per sub-band equaliser in a FBMC system such as minimum mean square error (MMSE) [87,89] or decision feedback equalisation [51,91]. The fractionally spaced equalisers can be updated by different adaptive algorithms e.g. least mean square (LMS), recursive least squares (RLS), affine projection for trained adaptation, decision directed schemes, as well as blind algorithms including the constant modulus algorithm (CMA). Here, I use the latter, which relies on a blind CM criterion and does not require any information on the transmit signals in the subbands other than that they consist of a CM alphabet such as quaternary phase shift keying (QPSK).

Therefore, the following sections will compare FMBC/OQAM and OS-FBMC systems using a fractionally spaced equaliser for synchronisation and equalisation. Since CM algorithms are robust but tend to converge much slower than training-based adaptive equalisers, a concurrent CM-decision directed (DD) scheme [76–79] will be employed, which incorporates a DD scheme that works as well as a training based approach if decisions are correct.

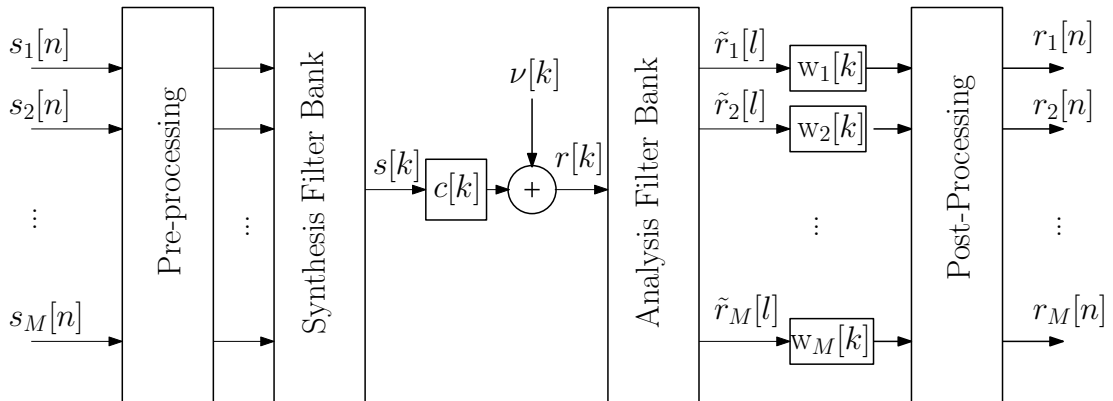


Figure 3.1: Block diagram of a general FBMC system over a dispersive channel.

3.2 FBMC over a Dispersive Channel

The general block diagram of an FBMC system is depicted in Fig. 3.1. A total of M transmit signals $s_m[n]$, $m = 1 \dots M$ are multiplexed by a synthesis filter bank, involving up-sampling by $K \geq M$. The multiplexed signal $s[k]$ propagates through a dispersive channel with impulse response $c[k]$, and is corrupted by additive white Gaussian noise $v[k]$. In the receiver, the signal $r[k]$ is again demultiplexed by an analysis filter bank into M sub-channels $r_m[n]$, $m = 1 \dots M$, involving decimation by K .

The oversampling ratio $K/M \geq 1$ controls the redundancy and therefore bandwidth efficiency of the FBMC system. The pre- and post-processing blocks that are shown in Fig. 3.1 will take on specific roles for FBMC/OQAM and OS-FBMC, and their per subband equalisation.

FBMC/OQAM is a critically sampled system with maximum spectral efficiency as the transmitted signal $s[k]$ runs at a rate M times the symbol rate [7]. FBMC/OQAM permits an overlap between directly adjacent sub-carriers in or-

der to achieve maximum spectral efficiency. This spectral overlap of adjacent sub-channels is compensated by transmitting OQAM symbols, where the real and imaginary parts are transmitted with a half-symbol period delay. The pre-processing in Fig. 3.1 thus consists of staggering $\text{Re}\{s_m[n]\}$ and $\text{Im}\{s_m[n]\}$, $m = 1 \cdots M$, such that the synthesis filter bank inputs run at twice the symbol rate. A matched de-staggering operation is contained in a post-processing block in the receiver, with inputs $\hat{r}_m[l]$ again running at twice the symbol rate.

Spectral guard bands in FBMC systems with oversampling, $K > M$, permit the use of a modulated filter bank without further pre-processing. Both FBMC systems — OS-FBMC and FBMC/OQAM — suffer from interference when transmitting over a dispersive channel. Therefore, a fractionally spaced equaliser per subband for both FBMC systems will be investigated to mitigate these interferences. In order to operate such a fractionally spaced equaliser, I wish to obtain a twice oversampled output $\hat{r}_m[l]$, with the post-processing containing a further decimation by two. Efficient implementations of such systems as in [80] can be extended with some modifications to the case where it is required to obtain outputs at twice the symbol rate, see e.g. [81].

3.3 Adaptive Equalisation for FBMC

The length of the channel impulse response $c[k]$ as experienced by the m^{th} sub-channel will generally appear shortened by the oversampling factor K compare to a transmission over the same channel at symbol rate; however, the channel is likely to include fractional delays w.r.t. the symbol time n , which can counteract this shortening [74]. The residual channel impulse response seen by the m^{th} sub-channel will lead to intersymbol interference (ISI), but will also cause

a loss of timing synchronisation in the FBMC system, resulting in intercarrier interference (ICI). In order to equalise the channel on a per subband basis and enable robustness towards timing synchronisation errors, the following subsections will use a per subband equaliser with a fractionally spaced architecture as described by [82] and advocated for FBMC by e.g. [69], [72] operating on the signals $\hat{r}_m[l]$, $m = 1 \dots M$ in Fig. 3.1. The deployment of such a fractionally spaced equaliser is specifically motivated by its enhanced resolution w.r.t. fractionally spaced delays, resulting in either fewer required equaliser coefficients or enhanced performance [75] w.r.t., for example, the minimum mean squared error of the equaliser.

3.3.1 Fractionally Spaced Equaliser

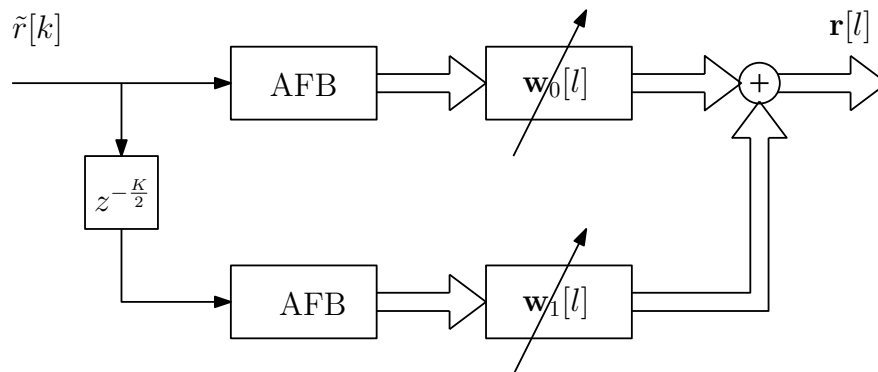


Figure 3.2: Block diagram of a per-subband fractionally spaced equaliser.

For both OS-FBMC and FBMC/OQAM, a total of M fractionally spaced equalisers are applied, one to each of the signals $\hat{r}_m[l]$, $m = 1 \dots M$ as depicted in Fig. 3.2 [72]. In case of OS-FBMC, high selectivity of the filter banks and a guard band due to $K > M$ means that the equaliser will not be exposed to any ICI as illustrated in Chapter 4 in Figs. 4.7 and 4.8. For FBMC/OQAM, the permitted spectral overlap between the adjacent subchannels will lead to induce

ICI when transmitting over a dispersive channel as shown in Figs. 4.5 and 4.6.

As shown in Fig. 3.2, the equalisation operation is carried out by two blocks $\mathbf{w}_0[l]$ and $\mathbf{w}_1[l]$ in two parallel branches. Several algorithms can be used to adapt the fractional delay equaliser coefficients. Here, $\mathbf{w}_0[l]$ and $\mathbf{w}_1[l]$ denote the polyphase components of the fractionally spaced equaliser and operate independently in every subband. In the first branch, the received signal $r[k]$ is first de-multiplexed by the AFB, then is filtered by the first polyphase component of the equaliser $\mathbf{w}_0[l]$. A delayed version of the received signal $r[k]$ is de-multiplexed and fed to the second polyphase component of the equaliser in the second branch. The outputs of the two equalisers are added to produce sub-channel signals in case of OS-FBMC. For FBMC/OQAM, the equalised signals are de-staggered by the OQAM post-processing.

3.3.2 Concurrent CMA-DD Equaliser

The constant modulus algorithm (CMA) is a stochastic gradient based technique which considered as the most widespread blind channel equalisation principle [83]. Since the input signals of the FBMC $s[n]$ have quadrature amplitude modulation (QAM) constellations, the produced symbols have a constant modulus γ which enables the use of the CMA equaliser for the FBMC. The cost function of the constant modulus algorithm ξ_{CM} can be formulated as

$$\xi_{CM} = E \left\{ \sum_{m=1}^M (\gamma^2 - |r_m[l]|^2)^2 \right\}, \quad (3.1)$$

where $E\{\cdot\}$ denotes the expectation operation. The optimum coefficients of the CM equaliser $w_{CM,opt}$ can be calculated by forcing the equaliser output $r_m[l]$ into

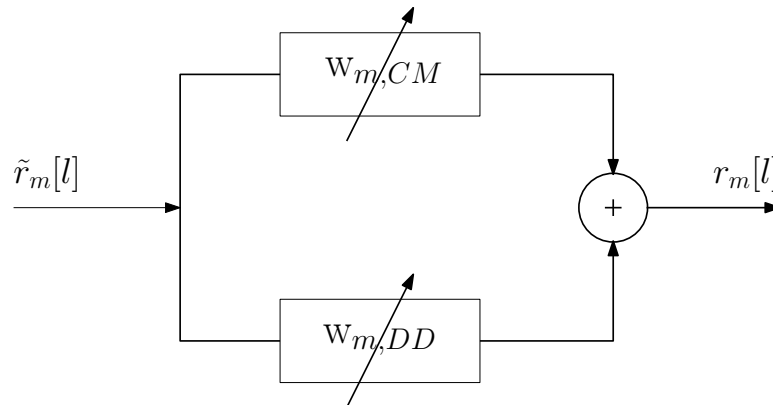


Figure 3.3: Block diagram of the filters inside a concurrent CMA-DD structure.

a constant modulus γ as

$$\mathbf{w}_{CM,opt} = \arg \min_{\mathbf{w}_{CM}} \xi_{CM}. \quad (3.2)$$

It can be noted that the CMA cost function is a biquadratic equation; therefore it is not guaranteed to be convex, and is likely to exhibit local minima. Nevertheless, for longer channels, the CMA equaliser may converge slowly. Therefore a CMA equaliser \mathbf{w}_{CM} concurrently operating with a decision-directed (DD) equaliser \mathbf{w}_{DD} is utilised such that $\mathbf{w} = \mathbf{w}_{CM} + \mathbf{w}_{DD}$ as depicted in Fig. 3.3 [76, 77].

The cost function of the DD algorithm ξ_{DD} can be formulated as

$$\xi_{DD} = E \left\{ \sum_{m=1}^M |q(r_m[l]) - r_m[l]|^2 \right\}, \quad (3.3)$$

where $q(\cdot)$ is a decision function that maps its output to the nearest QAM constellations alphabet. Therefore, \mathbf{w}_{DD} can be optimised as

$$\mathbf{w}_{DD,opt} = \arg \min_{\mathbf{w}_{DD}} \xi_{DD}. \quad (3.4)$$

The concurrent CMA-DD equalisation process runs in an iterative manner to update $\mathbf{w}[n]$ which is started by initialising the filters' coefficient vectors \mathbf{w}_{CM} and \mathbf{w}_{DD} by an appropriate length L_f for both components such that $L_f \geq L_c$, where L_c denotes the length of the channel $c[k]$. Moreover, the step sizes μ_{CM} and μ_{DD} are assigned appropriately according to the filter length L_f . Then, the output signal of the AFB $\tilde{r}_m[l]$ is filtered as

$$r_m[l] = \tilde{r}_m[l](\mathbf{w}_{m,CM}^H[l] + \mathbf{w}_{m,DD}^H[l]), \quad (3.5)$$

where $r_m[l]$ is the output of the equalisation process of the m^{th} subband. The CMA update can be written as

$$\mathbf{w}_{m,CM}[l+1] = \mathbf{w}_{m,CM}[l] + \mu_{CM} \sum_{m=1}^M \tilde{r}_m[l] e_{m,CM}^*[l], \quad (3.6)$$

where $e_{m,CM}[l]$ indicates the error signal during the CM equalisation of the m^{th} subband which is formulated as

$$e_{m,CM}[l] = r_m[l](\gamma^2 - |r_m[l]|^2). \quad (3.7)$$

After the CM update, an intermediate signal $\hat{r}_m[l]$ is calculated as

$$\hat{r}_m[l] = \tilde{r}_m[l](\mathbf{w}_{m,CM}^H[l+1] + \mathbf{w}_{m,DD}^H[l]). \quad (3.8)$$

The concurrent CMA-DD equaliser uses CMA update at every step; if the update does not alter the symbol decision, this decision is deemed correct, and an additional DD update is invoked as illustrated in Fig. 3.4. Using a DD-based normalised LMS algorithm (NLMS), its convergence is as fast as an NLMS provided

no decision errors are incurred as

$$w_{m,DD}[l+1] = w_{m,DD}[l] + \mu_{DD} \sum_{m=1}^M F(q(\hat{r}_m[l]) - q(r_m[l])) \tilde{r}_m[l] e_{m,DD}^*[n], \quad (3.9)$$

where $e_{m,DD}[l] = q(r_m[l]) - r_m[l]$ and $F(\Phi) = 1$ when $\Phi = 0$, otherwise $F(\Phi) = 0$. In other words, $F(\Phi)$ controls the contributions of the DD algorithm to the whole equalisation system. The concurrent CMA-DD equaliser can be updated based on the update of its two components as

$$w_{m,}[l+1] = w_{m,CM}[l+1] + w_{m,DD}[l+1]. \quad (3.10)$$

3.4 Simulation Results

The FBMC/OQAM and OS-FBMC systems are compared for $M \in \{32, 64\}$ transmit signals consisting of uncorrelated quaternary phase shift keying sequences. The OS-FBMC system uses upsampling factors of $K \in \{36; 70\}$, i.e. a redundancy of 12.5% and 9.375%, respectively. The channel $c[k]$ is of length $L_c = 6$ with decaying power delay profile based on the channel model specification of COST 207 (Typical Urban) [84]. The channel $c[k]$ was randomised, where 1000 channel realisations were used in order to be averaged over the simulation. Each channel realisation is assumed to be stationary during the processing of a random input QAM streams with length of 50000 symbols. Fig. 3.5 illustrates the magnitude response of one of the channel realisations used in the simulations.

Fractionally spaced CMA and concurrent CMA-DD equalisers are simulated over different instantiations of a channel and transmit signals, with an equaliser

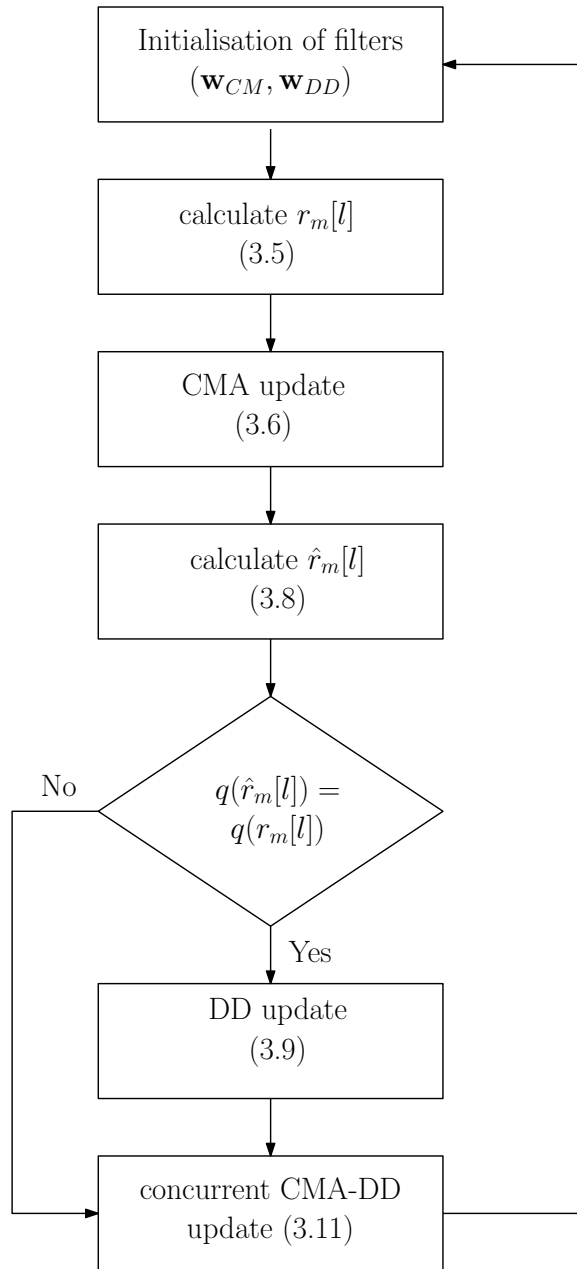


Figure 3.4: Flowchart of the per subband concurrent CMA-DD equaliser algorithm for FBMC .

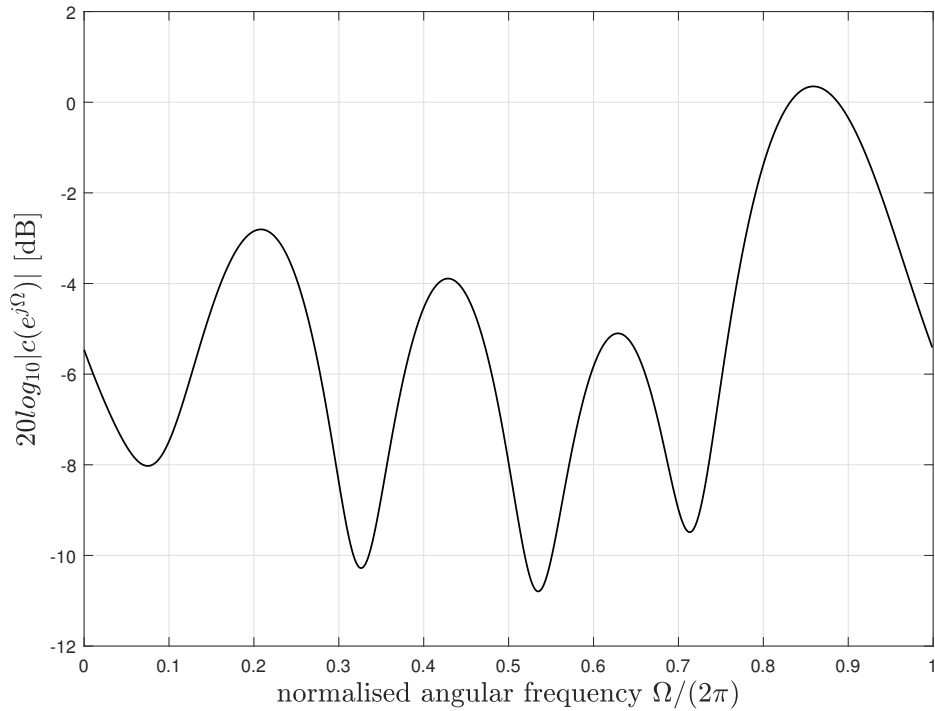


Figure 3.5: Magnitude response of a dispersive channel.

length of $L_f = 10$ coefficients and the centre tap initialised to unity, see e.g. [73]. The step size for the CMA algorithm was selected empirically at approx. 10% of its maximally possible value. For the concurrent CMA-DD algorithm, the CMA step size μ_{CM} is chosen to be 0.0001 which is much smaller than the DD step size μ_{DD} which is chosen to be 0.01 [77].

The CMA algorithm is very likely to result in a rotated constellation causing a phase ambiguity [77]. While the DD scheme could cause considerable error propagation due to the incorrect hard decision. Therefore, in the concurrent CMA-DD equaliser, the update of the DD is only held when the equaliser hard decisions before and after the CMA update are the same as shown in the flow chart in Fig. 3.4.

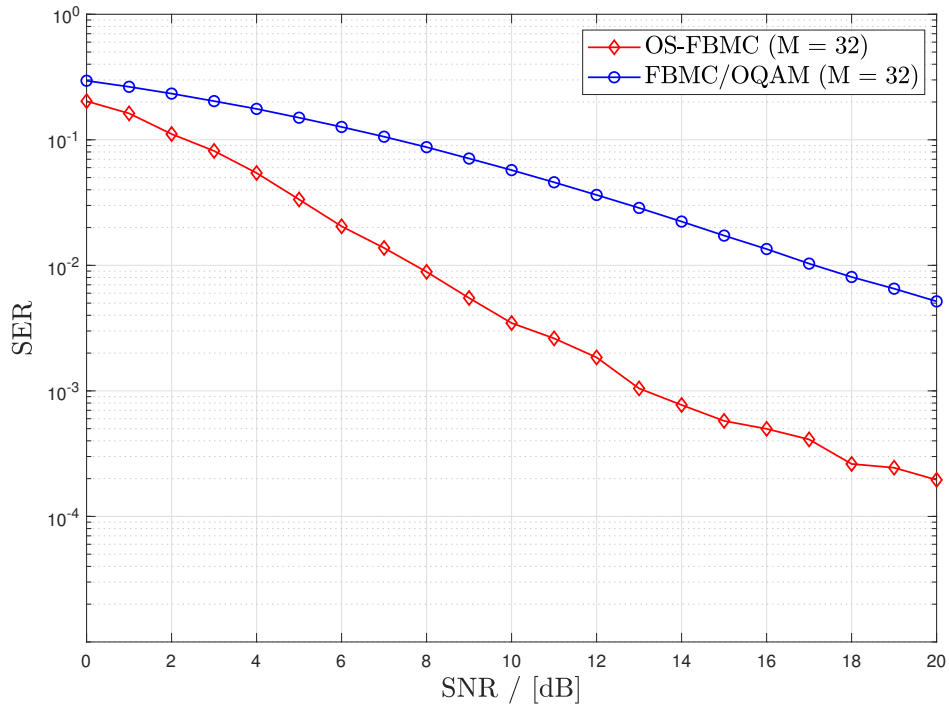


Figure 3.6: SER performance comparison of FBMC/OQAM to OS-FBMC systems using FS-CMA equaliser per subband.

Symbol error ratio (SER) results are summarised in Figs. 3.6 and 3.7 when using the fractionally spaced CMA and concurrent CMA-DD equalisers respectively. Both figures were averaged over the all subchannels and over the various simulations once an approximate steady-state performance has been reached. For the FBMC/OQAM system with $M = 32$, updating the fractionally spaced equaliser with the CMA only led to a poor adaptation compared to the case of the OS-FBMC system, and hence the SER performance of the OS-FBMC outperform the SER performance of the FBMC/OQAM as shown in Fig. 3.6. The concurrent CMA-DD scheme yielded better adaptation, and the FMBC/OQAM and OS-FBMC systems both converged. Higher multiplexing with $M = 64$ provides slightly enhanced performance for both systems, as in this case, the effective channel length is shorter than for $M = 32$, thus easing the burden on the equaliser.

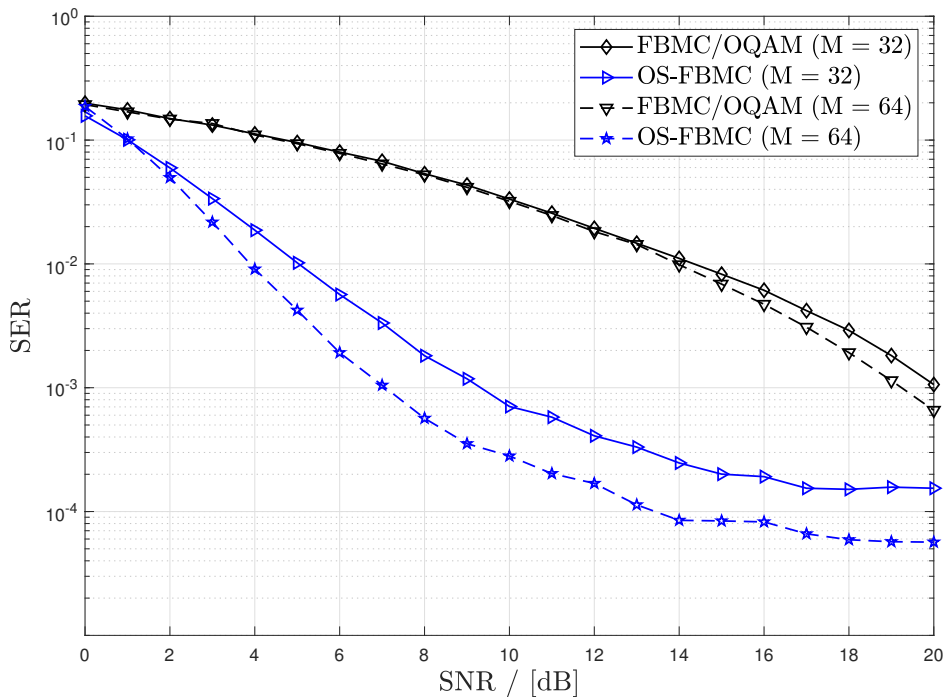
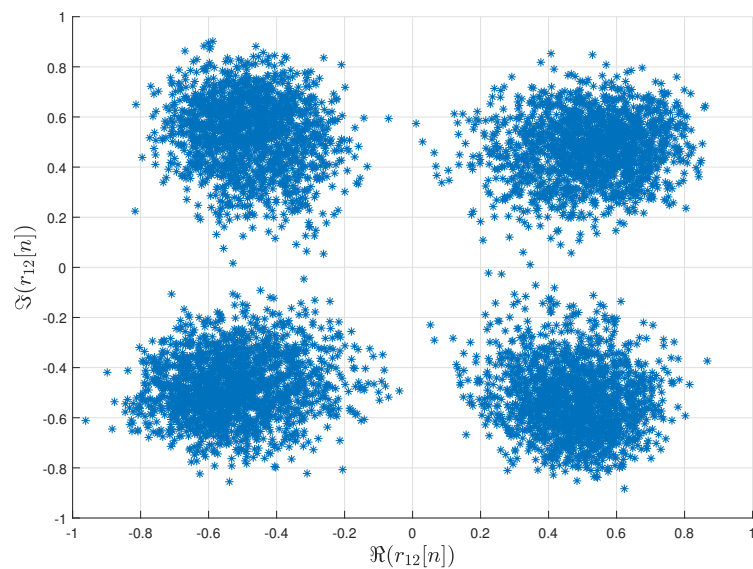
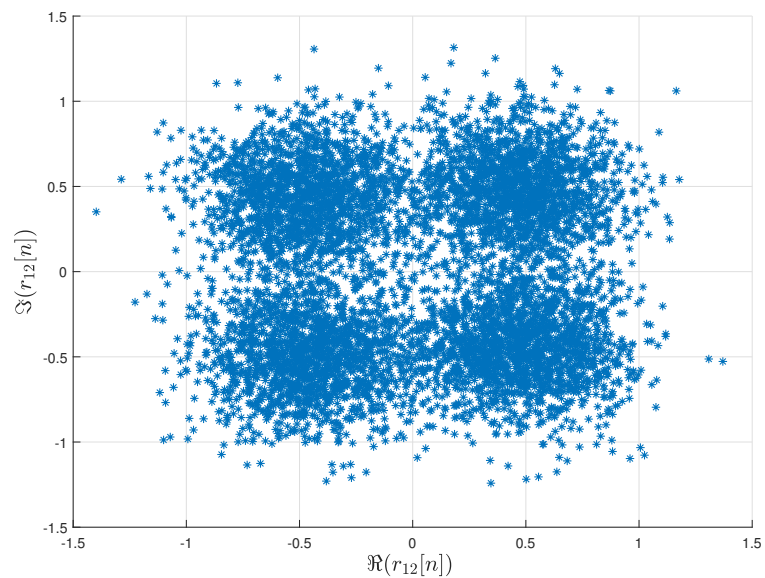


Figure 3.7: SER performance comparison of FBMC/OQAM and OS-FBMC systems using concurrent CMA-DD equaliser per subband.

Importantly, according to Fig. 3.7, OS-FBMC gives a systematically better SER performance than FBMC/OQAM, which only starts to catch up for higher SNR values. Fig. 3.8 depicts the signal constellations of the 12th sub-channel which is affected by the lowest magnitude response of the dispersive channel $c[k]$ at SNR = 20dB. It can be noted that the concurrent CMA-DD equaliser applied to OS-FBMC performs more robustly than in case of the FBMC/OQAM system. Since FBMC/OQAM compared to OS-FBMC suffers not only from ISI but also ICI, and the selected equalisation algorithms belong to the family for stochastic gradients methods, the FBMC/OQAM equaliser experiences a greater level of gradient noise.



(a)



(b)

Figure 3.8: Constellations of the equalised signal of the 12th subband utilising a concurrent CMA-DD equaliser in (a) OS-FBMC and (b) FBMC/OQAM.

3.5 Concluding Remarks

In this chapter, the critically sampled FBMC/OQAM system has been compared with an oversampled FBMC system when applying per-channel equalisation using a fractionally spaced CMA and concurrent CMA-DD equalisers. Based on a concurrent CMA and DD updating, this equaliser has been adapted to provide ISI suppression and symbol synchronisation. While the OS-FBMC system is free of ICI, in the FBMC/OQAM approach ICI is present and creates an additional interference term; further, this leads to a higher excess error at low SNR.

Therefore, even though FBMC/OQAM strives for a higher spectral efficiency, it appears to sacrifice some of the robustness that is expected of FBMC systems for 5th generation wireless communications [17,20,23,24]. Therefore, these results motivated me to investigate an equalisation scheme that considers the cross-talk terms induced between the subbands in the FBMC/OQAM system causing ICI. To that end, the FBMC/OQAM system over SISO and MIMO channels is analysed by proposing an equivalent channel transfer function, which includes the filter bank components and channel in the form of a polynomial matrix as in (4.4) and (5.5) and can be used to easily characterise all interference types as illustrated in Figs, 4.10 and 5.3 for SISO and MIMO respectively. Further, the proposed equaliser is obtained by inverting the channel polynomial matrix as in (4.11) and (5.13).

Chapter 4

Synchronisation and Equalisation of FBMC/OQAM

The previous chapter has demonstrated the increased robustness of a per-subband equaliser applied to an OS-FBMC system compared to an FBMC/OQAM system if the transmission channel is dispersive, or simply if the overall system is not synchronised. The guard bands in the OS-FBMC system reduce inter-carrier interference (ICI) to a negligible level while on the contrary, FBMC/OQAM, as a critical sampled multicarrier system, suffers from ICI in addition to inter-symbol interference (ISI). Therefore, in order to better exploit FBMC/OQAM with its higher spectral efficiency, this chapter proposes an equalisation approach for FBMC/OQAM that aims to mitigate both ISI and ICI. The proposed approach describes the equivalent transmultiplexed channel including the filter banks as a polyphase matrix of transfer functions. Then, polynomial matrix algebra is used to equalise this system. Moreover, I demonstrate that the reduced-rank nature of the channel polynomial matrix in the proposed approach requires a polynomial

matrix pseudo-inverse. I demonstrate how the overall FBMC/OQAM system is orthogonalised, thus removing ISI and ICI by means of examples and computer simulations.

4.1 Background and Motivation

Multicarrier modulation techniques have been central to the development of wide-band wireless communications standards for more than a decade. Within fifth generation communications systems, particularly filter bank-based multicarrier (FBMC) techniques are emerging as candidates for radio front-ends [16–26]. Such FBMC systems are popular because they offer increased robustness against synchronisation errors compared to e.g. orthogonal frequency division multiplexing (OFDM) systems [29]. The approach in [7] that combines FBMC with offset quadrature amplitude modulation (OQAM), referred to as an FBMC/OQAM system, has attracted attention as it is a critically sampled transceiver without any guard intervals, and hence theoretically is able to maximise spectral efficiency [26].

As explained in Chap. 2, FBMC/OQAM consists of two main blocks: a synthesis filter bank (SFB) in the transmitter and an analysis filter bank (AFB) in the receiver. The prototype filters are much more frequency-selective than e.g. in OFDM, which can significantly reduce the out-of-band emission and allow a flexible spectrum usage [2]. Since a critically sampled Discrete Fourier transform(DFT)-modulated filter banks themselves cannot be perfectly reconstructing, incorporating OQAM can lead to perfect reconstruction even under critical sampling and in the absence of guard bands. The latter enables maximum spectrum efficiency [6], but as a consequence, FBMC/OQAM must permit

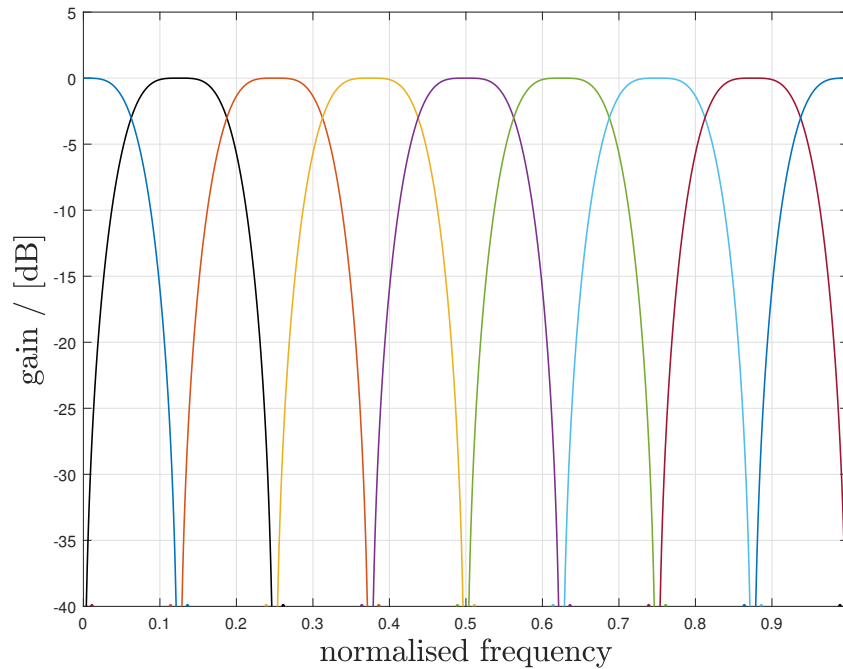


Figure 4.1: Magnitude response of an FBMC/OQAM system with $M = 8$ using PHYDYAS prototype filter.

an overlap of spectra between at least adjacent subcarriers as shown in Fig. 4.1.

Because of this spectral overlap, in a dispersive environment or an unsynchronised FBMC/OQAM transmission, each subcarrier in the receiver is affected by interference from at least adjacent subcarriers, resulting not just in inter-symbol interference (ISI) but also inter-carrier interference (ICI). The mitigation of this interference has received considerable attention in the research community, see e.g. [85–97].

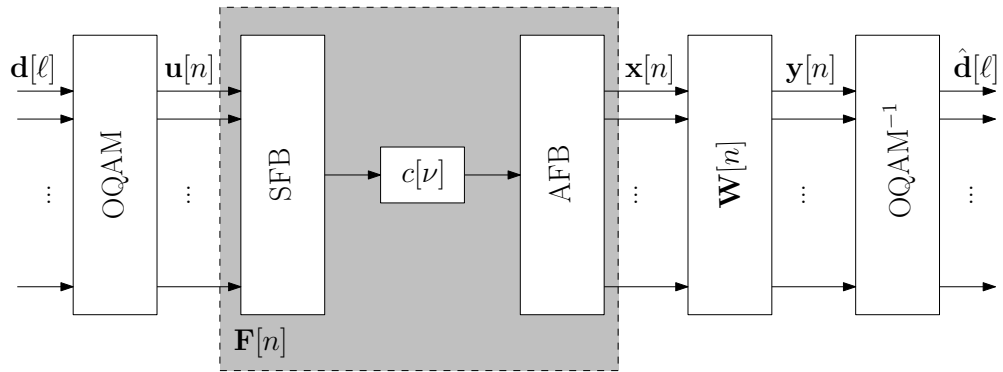
This chapter proposed an equalisation approach to suppress the interference contaminating the transmission of an FBMC/OQAM system over a dispersive channel. The joint equalisation of an FBMC/OQAM system is similar to the concept of subband adaptive filtering in a critically sampled system [98], where

leakage between adjacent channels necessitates the use of cross-terms rather than pure per-band processing. Similar to [70], [71], a linear algebraic approach is used to equalise this broadband system, but here relies on the system description by polynomial matrices, which leads to the novel definition of a polynomial matrix pseudo-inverse to address the FBMC/OQAM interference mitigation.

This chapter is organised as follows: a general structure of the FBMC/OQAM system is introduced in Sec. 4.2. Then, the proposed equalisation approach is presented via the formulation of the channel polynomial matrix and obtaining its inverse in Secs 4.3 and 4.4. Due to the rank deficiency of the equivalent channel polynomial matrix, the polynomial pseudo-inverse is proposed in Sec. 4.5. The concluding remarks are presented in Sec 4.6.

4.2 FBMC/OQAM Transmission System

FBMC/OQAM consists mainly of two components: an inner filter bank, and an outer OQAM system, as shown in Fig. 4.2. In the inner system, a filter bank transmultiplexes a vector $\mathbf{u}[n] \in \mathbb{C}^M$ over a channel with impulse response $c[\nu]$ to generate a demultiplexed output $\mathbf{x}[n] \in \mathbb{C}^M$, with the time index n running $M/2$ times slower than the index ν . The outer system consists of OQAM staggering and de-staggering blocks, which maps a transmit vector $\mathbf{d}[\ell] \in \mathbb{C}^M$ onto $\mathbf{u}[n]$, with index ℓ now running M times slower than ν , and at half the speed of the index n . The de-staggering then generates an output $\hat{\mathbf{d}}[\ell] \in \mathbb{C}^M$ from $\mathbf{x}[n]$.

Figure 4.2: FBMC-OQAM system model with equaliser $\mathbf{W}[n]$.

4.2.1 Offset QAM

The functions of the OQAM component of the FBMC/OQAM system are carried out by two blocks: OQAM pre-processing in the transmitter and OQAM post-processing in the receiver. The input to the OQAM pre-processing are M parallel QAM signals in $\mathbf{d}[\ell]$, where M is the number of subchannels. The complex-valued QAM symbols in $\mathbf{d}[\ell]$ are demultiplexed into their real and imaginary components alternatingly. The sequence of the components is dependent on the sub-channel index, and alternates between adjacent channels.

The reverse process is executed by the OQAM post-processing, where the signals in $\mathbf{y}[n]$ are demultiplexed and the imaginary and real components are alternatingly discarded. The discarding operation again depends on the sub-channel index i.e. alternately changes in odd and even indexed subcarriers, as explained in the numerical example in Chapter 2.

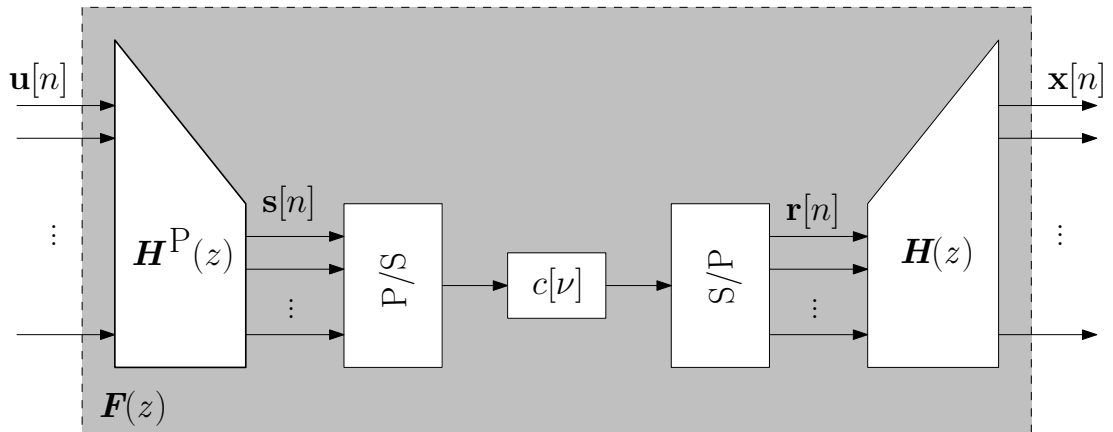


Figure 4.3: Inner components of the FBMC/OQAM system with synthesis and analysis filter banks and the channel impulse response $c[\nu]$.

4.2.2 Filter Bank Multicarrier System

The inner component of the FBMC/OQAM transceiver is an M -channel DFT filter bank operated as a transmultiplexer, with the analysis filter bank (ASB) on the receiver side and the synthesis filter bank (SFB) in the transmitter as shown in Fig. 4.2. The input $\mathbf{u}[n] \in \mathbb{C}^M$ and output $\mathbf{x}[n] \in \mathbb{C}^M$ are operated at a $K = \frac{M}{2}$ times slower rate than the multiplexed data is transmitted over the channel $c[\nu]$.

In contrast to FBMC/OQAM, the OS-FBMC system consists only of the inner filter bank without any outer pre- or postprocessing. Guard bands are inserted between the adjacent subbands with an up-sampling factor $K > M$. The input $\mathbf{d}[\ell] \in \mathbb{C}^M$ and output $\hat{\mathbf{d}}[\ell] \in \mathbb{C}^M$ are operated at a $K > M$ times rate than the multiplexed data is transmitted over the channel $c[\nu]$. Since the filter banks contain decimators, which are not linear time-invariant (LTI) system block but linear periodically time varying (LPTV) [99], the direct analysis using classical tools such as the z transform is not applicable. However, a polyphase representation and the exploitation of noble identities [99] can bypass these restrictions. Therefore, a polyphase analysis of the FBMC system is performed below.

In the receiver, the analysis filter bank (ASB) is formed by a DFT filter bank. In polyphase notation, the input is first demultiplexed by a serial to parallel converter (s/p) before feeding into a polyphase analysis matrix $\mathbf{H}(z) : \mathbb{C} \rightarrow \mathbb{C}^{M \times K}$, as seen in Figs. 4.3 and 4.4 . This matrix consists of transfer functions describing a multiple-input multiple-output system, which can be factored into a network of polyphase components of the filter banks prototype filter, followed by the modulating transform, i.e. a DFT matrix [100, 101].

In the transmitter, a matching DFT synthesis filter bank can also be expressed in polyphase notation. Here, the up-sampling by K is swapped with the filtering operation, such that a polyphase synthesis matrix first operates on the M inputs of $\mathbf{u}[n]$ for FBMC/OQAM as shown in Fig. 4.3 and directly on the M inputs of $\mathbf{d}[\ell]$ for OS-FBMC as shown in Fig. 4.4, before K outputs are multiplexed by a parallel to serial p/s converter, to generate the signal to be transmitted over the channel $c[\nu]$. The polyphase synthesis matrix generally should be the inverse of polyphase analysis matrix. Here, the polyphase analysis matrix $\mathbf{H}(z)$ is selected to be paraunitary, such that $\mathbf{H}(z)\mathbf{H}^P(z) = \mathbf{I}$, where $\{\cdot\}^P$ denotes the parahermitian operations, such that $\mathbf{H}^P(z) = \mathbf{H}^H(1/z^*)$, i.e. consisting of a Hermitian transposition and time reversal. Then for the polyphase synthesis matrix we select $\mathbf{H}^P(z) : \mathbb{C} \rightarrow \mathbb{C}^{K \times M}$, such that the overall system becomes transparent i.e. the system inputs are equal to the system outputs.

The design of the prototype filter plays a crucial role in generating the sub-channels filters in both SFB and AFB [60]. As shown in Fig. 4.1, the prototype filter used in this chapter is based on the designs presented in [28, 58, 102] which will be denoted as the ‘physical layer for dynamic access and cognitive radio’ (PHYDYAS) prototype filter. These prototype filters have been used due to their high frequency selectivity; in particular the PHYDYAS prototype ensures

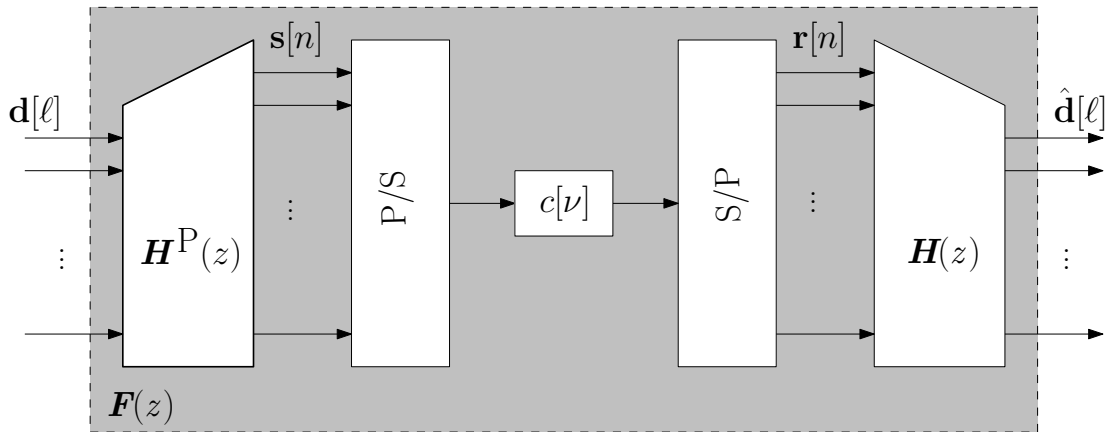


Figure 4.4: Polyphase components of the OS-FBMC system with synthesis and analysis filter banks and the channel impulse response $\mathbf{c}[\nu]$.

that the cross-talk between non-adjacent subchannels is kept sufficiently small. Aliasing between adjacent subchannels cannot be entirely suppressed by the DFT filter bank but is removed due to the OQAM arrangement. However, any delay or time-dispersion of the channel $c[\nu]$ will destroy orthogonality and result in inter-symbol (ISI) and inter-carrier interference (ICI) in the output $\hat{\mathbf{d}}[l]$. Therefore, I explore a synchronisation and equalisation approach next.

4.3 Equalisation of an FBMC/OQAM System

4.3.1 Equivalent Transmission System

First, the sub-channel transfer functions of the inner FBMC system are described in Figs. 4.2, 4.3, and 4.4 which can be represented as a polynomial matrix $\mathbf{F}(z) : \mathbb{C} \rightarrow \mathbb{C}^{M \times M} \bullet \circ \mathbf{F}[n]$. Considering the channel impulse response $c[\nu]$ together with the multiplexer and demultiplexer in Figs. 4.3 and 4.4, this subsystem can be characterised by a pseudo-circulant polyphase matrix $\mathbf{C}(z) : \mathbb{C} \rightarrow \mathbb{C}^{K \times K}$ [103],

$$\mathbf{C}(z) = \begin{bmatrix} C_0(z) & C_1(z) & \dots & C_{K-1}(z) \\ z^{-1}C_{K-1}(z) & C_0(z) & \dots & C_{K-2}(z) \\ \vdots & & \ddots & \vdots \\ z^{-1}C_1(z) & \dots & z^{-1}C_{K-1} & C_0(z) \end{bmatrix}, \quad (4.1)$$

which comprises the K polyphase components $C_\mu(z)$ of the channel transfer function $C(z) = \sum_{\nu=0}^{K-1} c[\nu] z^{-\nu}$. These are defined as

$$C_\mu(z) = \sum_{\nu=0}^{K-1} C_\mu(z^K) z^{-\nu}, \quad (4.2)$$

or alternatively can be obtained from the channel impulse $c[\nu]$ via

$$C_\mu(z) = \sum_{\nu} c[K\nu + \mu] z^{-\nu}. \quad (4.3)$$

Using the polyphase synthesis and analysis matrices for the FBMC systems shown in Figs. 4.3 and 4.4, the equivalent system $\mathbf{F}(z)$ can be obtained as

$$\mathbf{F}(z) = \mathbf{H}(z)\mathbf{C}(z)\mathbf{H}^p(z). \quad (4.4)$$

If $F_{ij}(z)$ is the element in the i th row and j th column of $\mathbf{F}(z)$ in (4.4), for the FBMC/OQAM system, it represents the transfer function between the j th signal in the input vector $\mathbf{u}[n]$ and the i th signal in the output vector $\mathbf{y}[n]$, while for the OS-FBMC system, it represents the transfer function between the signals in $\hat{d}_j[\ell]$ and $\hat{d}_i[\ell]$. Thus, the diagonal elements $F_{mm}(z)$, $m = 1 \dots M$, represent the per-subchannel transfer functions. There is no interference between the subbands in OS-FBMC thanks to utilising guard bands as shown in Fig. 4.7, while due to the frequency selectivity of a prototype filter such as PHYDYAS, cross-talk is

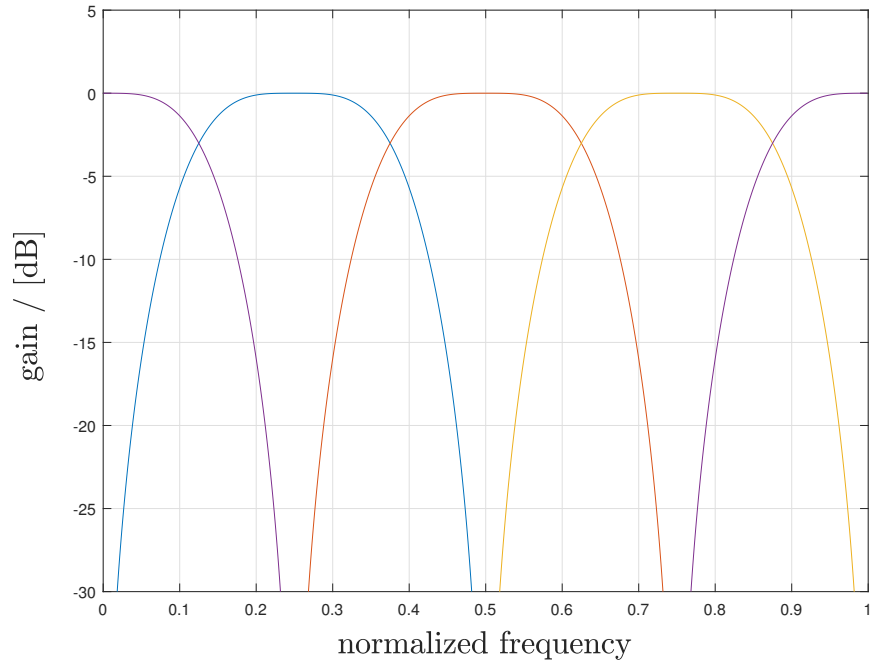


Figure 4.5: Magnitude response of subchannels in an FBMC/OQAM with $M = 4$ using PHYDYAS prototype filter.

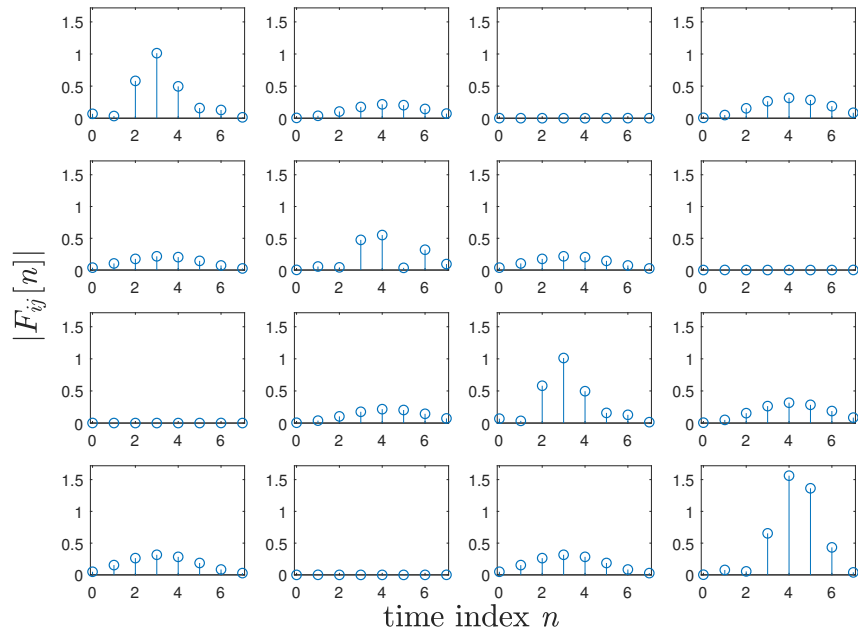


Figure 4.6: Example of a 4×4 polynomial channel matrix $\mathbf{F}(z)$ for an FBMC/OQAM system using PHYDYAS prototype filter.

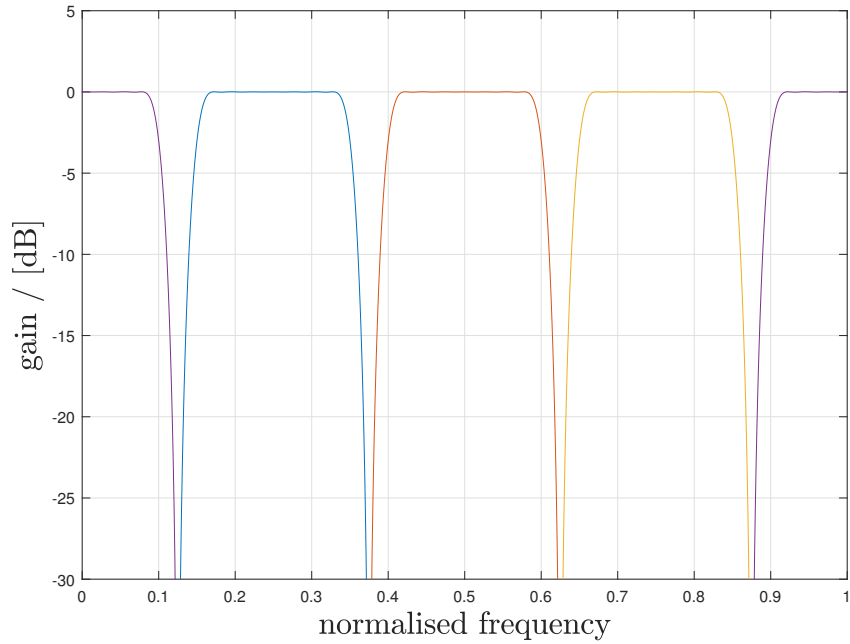


Figure 4.7: Magnitude response of subchannels in an OS-FBMC with $M = 4$.

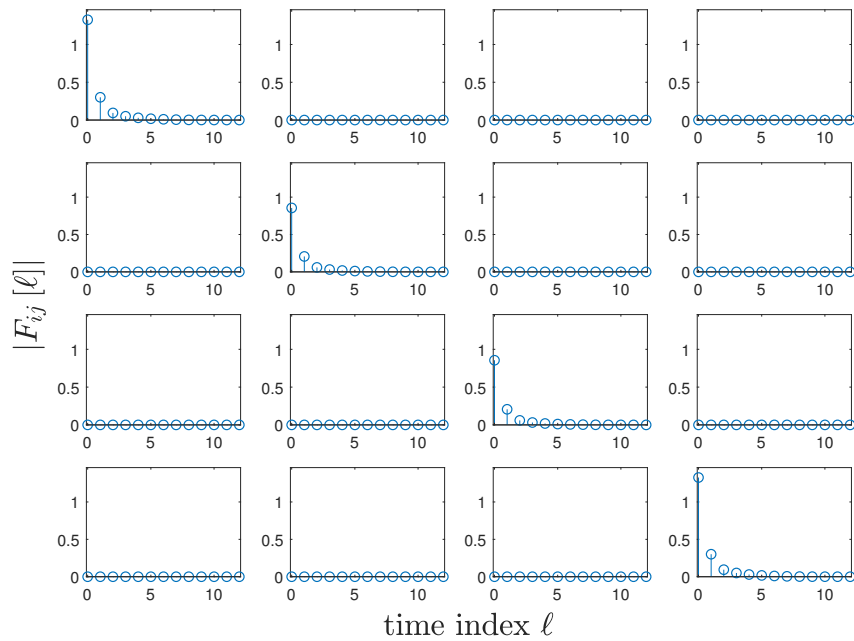


Figure 4.8: Example of a 4×4 polynomial channel matrix $\mathbf{F}(z)$ for an OS-FBMC system using upsampling factor $K = 5$.

introduced but restricted to adjacent bands only as depicted in Fig. 4.5 such that

$$F_{ij}(z) \approx 0, \quad \forall (M-1) > |\text{mod}_M i - \text{mod}_M j| > 1, \quad (4.5)$$

$$i, j = 1 \cdots M.$$

The structure of $\mathbf{F}(z)$ of the FBMC/OQAM system using the PHYDYAS prototype is therefore tri-diagonal, including non-zero corner elements irrespective of the channel polyphase matrix $\mathbf{C}(z)$ as depicted in Fig. 4.6. On the other hand, the OS-FBMC system is free of ICI due to exploiting guard bands therefore, $\mathbf{F}(z)$ in this case will be a diagonal matrix as shown in Fig. 4.8.

Example. An example of $\mathbf{F}(z)$ for an FBMC/OQAM and OS-FBMC systems with $M = 4$ sub-channels is obtained for a channel $c[\nu]$ of length 4 with random Gaussian channel coefficients. The components of $\mathbf{F}(z)$ are determined by channel sounding, and are depicted in Figs. 4.6 and 4.8. Moreover, $\mathbf{F}(z)$ can be obtained also using (4.1-4)

4.3.2 Equalisation of FBMC System

Because the first stage of the OQAM post-processing alternately discards the real and imaginary parts of $y_m[n]$, $m = 1 \dots M$, achieving a transparent system such that

$$\hat{\mathbf{d}}[\ell] \approx \mathbf{d}[\ell - \Delta\tau], \quad (4.6)$$

where $\Delta\tau \in \mathbb{N}$ represents some delay. The condition (4.6) exploits the alternate discarding of real and imaginary parts of $\mathbf{y}[n]$ in the OQAM post-processing, and reflects the overall synchronisation and equalisation of the FBMC/OQAM system and leads to a simple solution below.

Since an equaliser must cancel ICI, it requires cross-talk terms akin to $\mathbf{F}(z)$. Therefore, this chapter proposes a polynomial matrix equaliser $\mathbf{W}(z)$ inserted between the AFB and OQAM post-processing in the receiver, as shown in Fig. 4.2. This assumes that $\mathbf{F}(z)$ is available, i.e. that it can either be obtained via channel sounding directly, or synthesised according to (4.4) based on the measured channel impulse response $c[\nu]$ with $\mathbf{H}(z)$ known. This equaliser is obtained by calculating a polynomial singular value decomposition (PSVD, [52, 104, 105]),

$$\mathbf{F}(z) \approx \mathbf{U}(z)\mathbf{\Sigma}(z)\mathbf{V}^P(z), \quad (4.7)$$

where $\mathbf{U}(z)$ and $\mathbf{V}(z)$ are paraunitary or lossless matrices such that

$$\mathbf{U}(z)\mathbf{U}^P(z) = \mathbf{U}^P(z)\mathbf{U}(z) = \mathbf{I}, \quad (4.8)$$

$$\mathbf{V}(z)\mathbf{V}^P(z) = \mathbf{V}^P(z)\mathbf{V}(z) = \mathbf{I}. \quad (4.9)$$

The matrix $\mathbf{\Sigma}(z)$ is diagonal,

$$\mathbf{\Sigma}(z) = \text{diag}\{\sigma_1(z) \cdots \sigma_M(z)\}, \quad (4.10)$$

and contains the polynomial singular values $\sigma_m(z)$, $m = 1 \dots M$.

Based on the polynomial SVD in (4.7), the equaliser $\mathbf{W}(z)$ can be determined as

$$\mathbf{W}(z) = \mathbf{F}^\dagger(z) \approx \mathbf{V}(z)\mathbf{\Sigma}^\dagger(z)\mathbf{U}^P(z), \quad (4.11)$$

where $\{\cdot\}^\dagger$ denotes the pseudo-inverse process which will be discussed later in this chapter. Therefore, the inversion of $\mathbf{F}(z)$ reduces to the calculation of its PSVD, and the inversion of the singular values.

4.4 Polynomial Matrix Inversion via PSVD

To calculate $\mathbf{W}(z) = \mathbf{F}^\dagger(z)$ first requires determining the PSVD of $\mathbf{F}(z)$ via (4.7). Three general options have been discussed for the calculation of PSVD in the literature: there is a direct iterative calculation [104], an iterative calculation using a polynomial QR approach [105], and the route via two polynomial eigenvalue decompositions (PEVDs) [52]. The availability of enhanced PEVD algorithms such as the sequential matrix diagonalisation (SMD) approach [53] or multiple-shift SMD [106] have motivated the latter.

Like other PEVD algorithms, SMD is applicable to polynomial matrices $\mathbf{A}(z)$ that possess the parahermitian property, such that $\mathbf{A}(z) = \mathbf{A}^P(z)$. By forming two such parahermitian matrices, and two approximate PEVDs [52, 107] using e.g. the SMD algorithm [53] can be calculated:

$$\mathbf{R}_1(z) = \mathbf{F}(z)\mathbf{F}^P(z) \approx \mathbf{U}(z)\mathbf{S}_1(z)\mathbf{U}^P(z), \quad (4.12)$$

$$\mathbf{R}_2(z) = \mathbf{F}^P(z)\mathbf{F}(z) \approx \mathbf{V}(z)\mathbf{S}_2(z)\mathbf{V}^P(z). \quad (4.13)$$

This determines the two paraunitary matrices for (4.7). If $\mathbf{F}(z)$ is square, it is expected that

$$\mathbf{\Sigma}(z) = \mathbf{S}_1(z)\mathbf{S}_1^P(z) = \mathbf{S}_2(z)\mathbf{S}_2^P(z). \quad (4.14)$$

However, unless $\mathbf{\Sigma}(z)$ is constrained (e.g. to be minimum phase), it cannot be directly extracted from $\mathbf{S}_1(z)$ and $\mathbf{S}_2(z)$. Instead

$$\mathbf{\Sigma}(z) = \mathbf{V}(z)\mathbf{F}(z)\mathbf{U}^P(z) \quad (4.15)$$

can be evaluated in order to determine the polynomial singular values in $\mathbf{\Sigma}(z)$.

To determine $\Sigma^\dagger(z)$ requires the inversion of the polynomial singular values in (4.11), i.e.

$$\Sigma^\dagger(z) = \text{diag}\{\sigma_1^{-1}, \sigma_2^{-1}, \dots, \sigma_M^{-1}\}. \quad (4.16)$$

Since $\sigma_m(z)$, $m = 1 \dots M$ is generally non-minimum phase, zeros of $\sigma_m(z)$ inside the unit circle will lead to causal components of $\sigma_m^{-1}(z)$, while roots of $\sigma_m(z)$ outside the unit circle will result in anti-causal components of $\sigma_m^{-1}(z)$. The inversion can be performed by several approaches, akin to the inversion of polynomial eigenvalues in [108], such as by calculating the roots of $\sigma_m^{-1}(z)$, determining their residues for a partial fraction expansion, and then approximating the poles by appropriately truncating their causal or anti-causal geometric series representations. Here, for an inverse $w_m(z)$ of the m th eigenvalue,

$$\sigma_m(z) w_m(z) \approx z^{-\Delta} \quad (4.17)$$

is required, where Δ is a suitable delay. As a rule of thumb for inverse system identification, it is recommended that $\Delta = \frac{L}{2}$ where L is the length of the inverse, in order to account for the non-minimum phase nature of $\sigma_m(z)$ [73].

To use a least squares approximation, a vector $\boldsymbol{\sigma}_m \in \mathbb{C}^K$ holds the K coefficients of $\sigma_m(z)$, $m = 1 \dots M$. The aim is to find a vector $\mathbf{w}_m \in \mathbb{C}^L$ holding the L coefficients of $w_m(z)$ such that

$$\mathbf{w}_{m,\text{opt}} = \arg \min_{\mathbf{w}_m} \| [\mathbf{I}_{L-K+1} \otimes (\boldsymbol{\sigma}_m^T \mathbf{J}_K)] \mathbf{w}_m - \mathbf{p} \|_2, \quad (4.18)$$

with \mathbf{J}_K an $K \times K$ reverse identity matrix, \otimes denoting a Kronecker product, and $\mathbf{p} \in \mathbb{N}^{L-K+1}$ a pinning vector containing zeros except for a one in the Δ th position. A solution can be found by a pseudo-inversion of the convolutional

matrix

$$\mathbf{A}_m = \mathbf{I}_{L-K+1} \otimes (\boldsymbol{\sigma}_m^T \mathbf{J}_K), \quad (4.19)$$

such that $\mathbf{w}_{m,\text{opt}} = \mathbf{A}_m^\dagger \mathbf{p}$ [109]. Alternatively, an iterative method such as the recursive least squares (RLS) algorithm can be invoked [110].

Example. Applying a polynomial singular value decomposition as laid out above for the earlier example of an $M = 4$ FBMC/OQAM equivalent transmission matrix $\mathbf{F}(z)$ in Fig. 4.6 yields the matrix $\boldsymbol{\Sigma}(z)$ characterised in Fig. 4.9. The matrix is sufficiently diagonalised, but reveals a rank deficiency of $\mathbf{F}(z)$, as half of the singular values are zero. Inspecting the source model for $\mathbf{F}(z)$ in (4.4), since the inner factor $\mathbf{C}(z)$ is an $\frac{M}{2} \times \frac{M}{2}$ polynomial matrix, the overall rank cannot exceed $\frac{M}{2}$. To avoid the inversion of singular values that are either zero everywhere, or have zeros within a vicinity of the unit circle, the pseudo-inversion of a polynomial matrix has to be explored.

4.5 Polynomial Matrix Pseudo-Inverse

Within this chapter, the aim has been to invert a square polynomial $\mathbf{F}(z)$. To add both robustness to the inversion approach but also to include more general, rectangular matrices $\mathbf{F}(z) : \mathbb{C} \rightarrow \mathbb{C}^{N \times M}$, a polynomial matrix pseudo-inverse is discussed as an extension of the pseudo-inverse of a constant matrix [109]. For general $N \times M$ matrices, the PEVD steps (4.12) and (4.13) will yield paraunitary matrices $\mathbf{U}(z) : \mathbb{C} \rightarrow \mathbb{C}^{N \times N}$ and $\mathbf{V}(z) : \mathbb{C} \rightarrow \mathbb{C}^{M \times M}$. However, instead of directly inverting the diagonal components of $\boldsymbol{\Sigma}(z) : \mathbb{C} \rightarrow \mathbb{C}^{N \times M}$ as suggested earlier, I select

$$\boldsymbol{\Sigma}^{-1}(z) = \text{diag}\{w_1(z), \dots, w_{\min(M,N)}(z)\}, \quad (4.20)$$

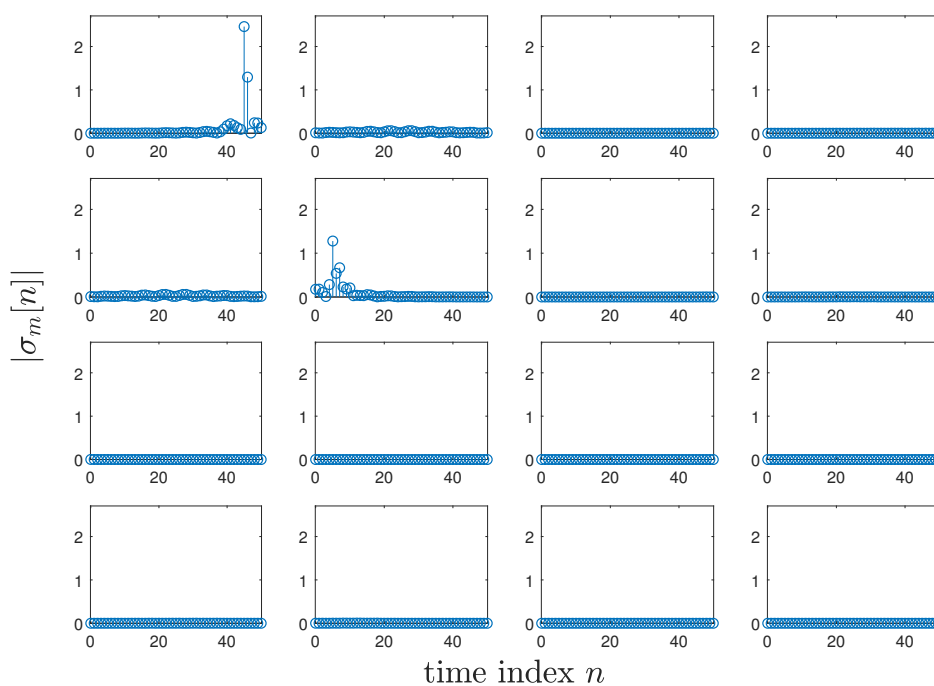


Figure 4.9: Example of 4×4 diagonal matrix $\Sigma(z)$, containing its diagonal terms $\sigma_m[n] \bullet - \circ \sigma_m(z)$, with all cross-terms zero or very nearly so.

where $w_m(z)$ now is the inverse of $\sigma_m(z)$ for finite $\sigma_m(z)$, and $w_m(z) = 0$ for $|\sigma_m(z)| < \epsilon_1 \forall z$, with ϵ_1 a small constant.

For a numerical evaluation, the L coefficients of $w_m(z)$ are collated in the vector \mathbf{w}_m , and with the earlier definitions of the singular value vectors $\boldsymbol{\sigma}_m$, the convolutional matrix \mathbf{A}_m , and the pinning vector \mathbf{p} , the inverse is determined as

$$\mathbf{w}_m = \begin{cases} 0 & \text{for } \|\boldsymbol{\sigma}_m\|_2 \leq \epsilon_1, \\ \mathbf{A}_m^H (\mathbf{A}_m \mathbf{A}_m^H + \epsilon_2 \mathbf{I}_{L-K+1})^{-1} \mathbf{p} & \text{for } \|\boldsymbol{\sigma}_m\|_2 > \epsilon_1. \end{cases} \quad (4.21)$$

The small constant $\epsilon_1 > 0$ determines a threshold below which a singular value is treated as numerically zero. A second constant, ϵ_2 , implements a regularisation to mitigate spectral zeros in $\sigma_m(z)$ or zeros close to the unit circle. A larger value for ϵ_2 may result in faster decaying responses in $w_m(z)$, but also introduces a bias into the original solution in ((4.18)).

Example. For an $M = 8$ channel FBMC/OQAM system using the PHYDYAS prototype filter over a dispersive channel $c[\nu]$ of length 4, the equivalent channel polynomial matrix $\mathbf{F}(z)$ is shown in Fig. 4.10. Because the spectral overlapping between the subbands is limited to the direct adjacent neighbours, the polynomial channel matrix $\mathbf{F}(z)$ has the form of a tri-diagonal matrix with the two corner elements being non-zero.

The polynomial matrix $\boldsymbol{\Sigma}(z)$ is obtained according to (4.15) as depicted in Fig. 4.11. $\boldsymbol{\Sigma}(z)$ appears to be a diagonal matrix with reduced rank ($\frac{M}{2} = 4$) as discussed earlier. According to (4.11), the resulting pseudo-inverse polynomial matrix $\mathbf{W}(z) = \mathbf{F}^\dagger(z)$ with a structure of a tri-diagonal plus the two non-zero corner elements is shown in Fig. 4.12. The multiplication output of $\mathbf{F}(z)$ with $\mathbf{W}(z)$ is not an identity matrix as shown in Fig. 4.13 due to the rank deficiency

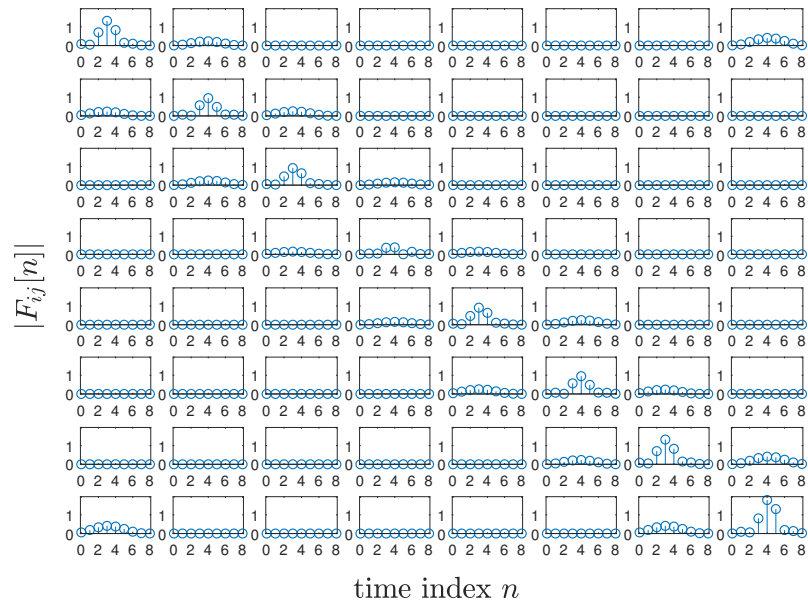


Figure 4.10: Example of a 8×8 polynomial channel matrix $\mathbf{F}(z)$ for a FBMC/OQAM system using PHYDYAS prototype filter over a dispersive channel $c[\nu]$ with length of 4.

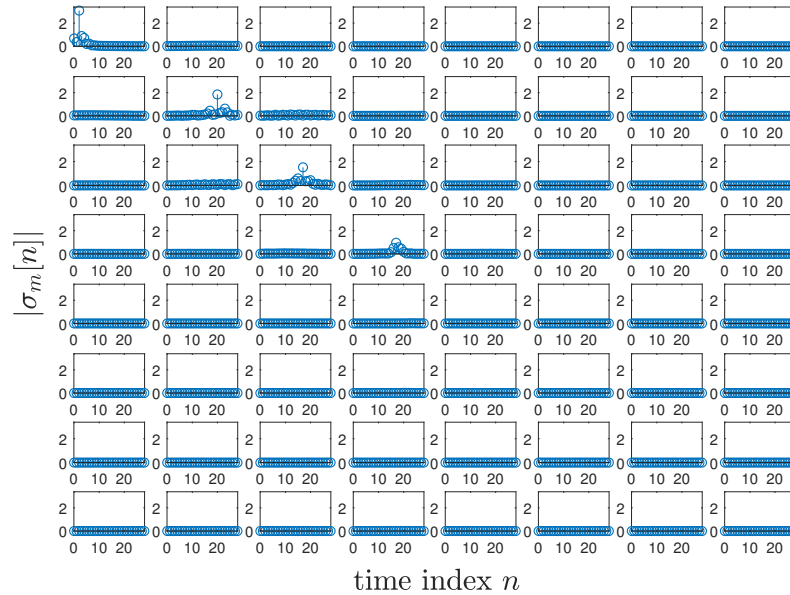


Figure 4.11: Example of 8×8 diagonal matrix $\Sigma(z)$, containing its diagonal terms $\sigma_m[n] \bullet \circ \sigma_m(z)$, with all cross-terms zero or very nearly so over a dispersive channel $c[\nu]$ with length of 4.

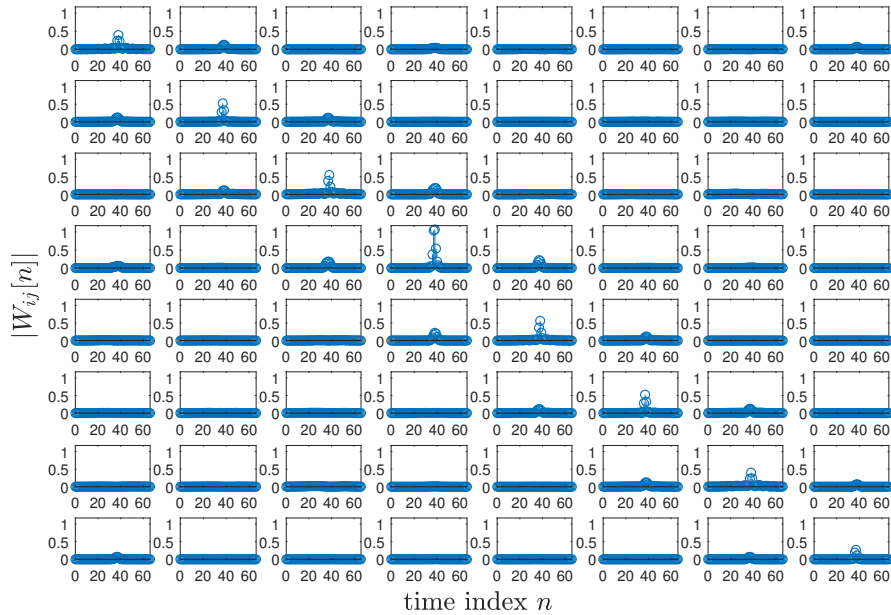


Figure 4.12: Example of a 8×8 polynomial equaliser matrix $\mathbf{W}(z)$ of an FBMC/OQAM using PHYDYAS prototype filter.

of $\mathbf{F}(z)$. However, when including the OQAM pre- and post-processing, and considering the MIMO channel matrix between the input $\mathbf{d}[\ell]$ and $\hat{\mathbf{d}}[\ell]$, such that

$$\hat{\mathbf{d}}[\ell] = \mathbf{G}[\ell] * \mathbf{d}[\ell], \quad (4.22)$$

the system in Fig. 4.14 emerges, which is now free of ISI and ICI.

For the resulting pseudo-inverse, the $\frac{M}{2}$ finite singular values possess zeros close to the unit circle are leading to amplification of the noise in the equaliser. Therefore, the usage of the constant ϵ_2 in the equalisation process aims to minimise that amplification. Based on the simulation of the proposed equalisation approach applied for an FBMC/OQAM system with $M = 4$ over 2000 realisations of Gaussian channel of order 10, the measured SER when using different values of the regularisation constant ϵ_2 at SNR of 15 dB is drawn in Fig. 4.15.

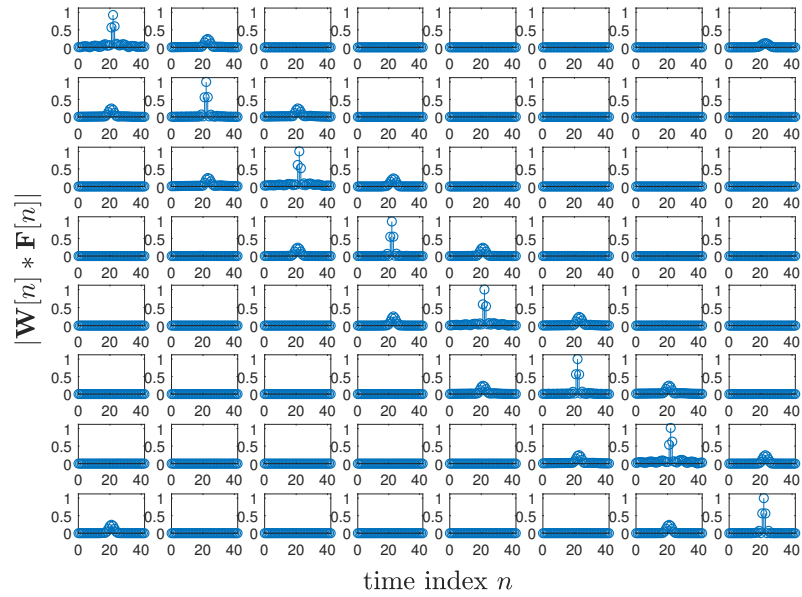


Figure 4.13: Example for the joint channel transmission matrix $\mathbf{F}(z)$ and its pseudo-inverse $\mathbf{F}^\dagger(z)$ for an $M = 8$ channel FMBC/OQAM system including a dispersive channel $c[\nu]$ of length 4 when using PHYDYAS prototype filter.

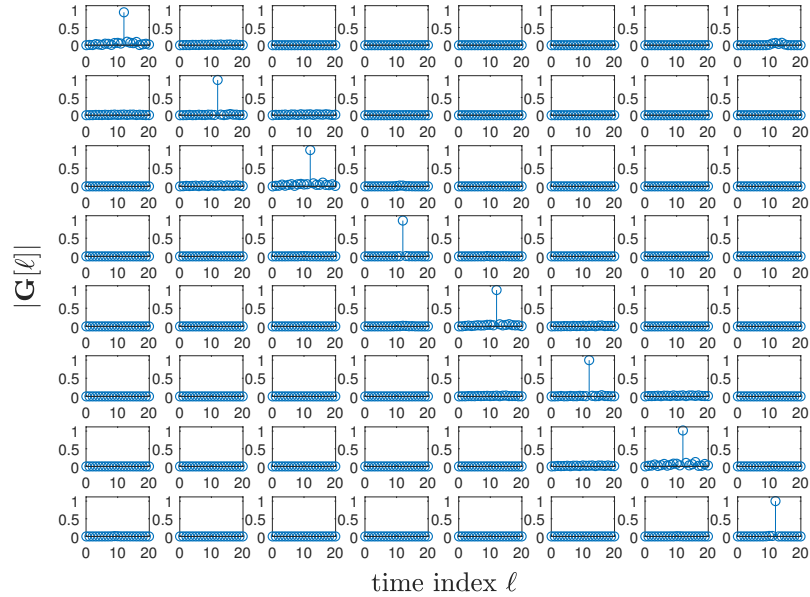


Figure 4.14: Example for the overall equalised polynomial matrix $\mathbf{G}[\ell]$, for an FMBC/OQAM system with $M = 8$ over a dispersive channel $c[\nu]$ of length 4 when using the PHYDYAS prototype filter.

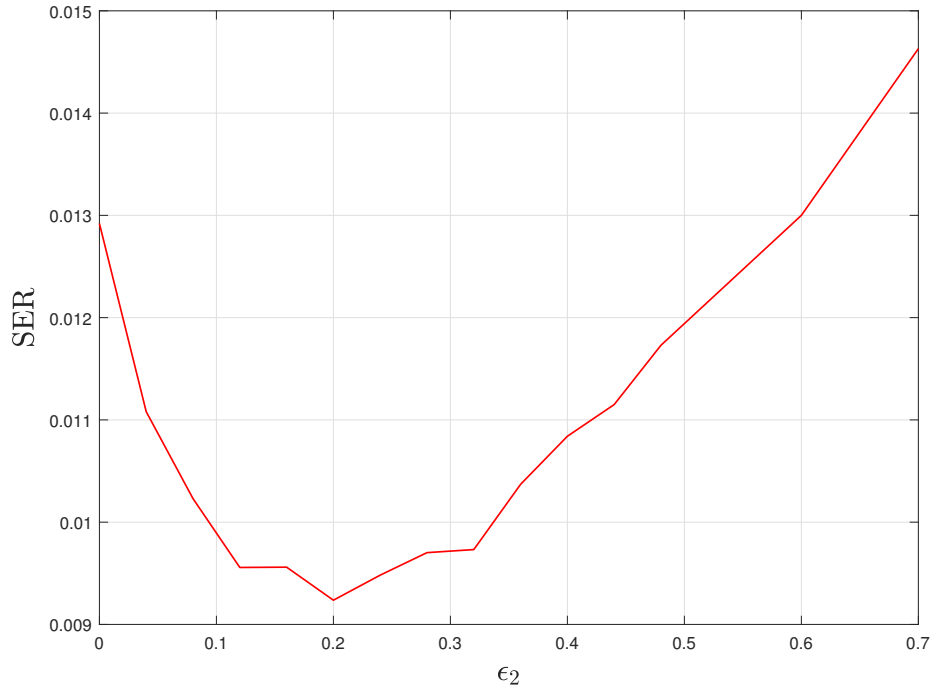


Figure 4.15: SER vs regularisation coefficient (ϵ_2) at SNR of 15 dB for the equalised FBMC/OQAM system with $M = 4$ over a dispersive channel of length of 10 coefficients

It can be noted that there is an optimum value of ($\epsilon_2 = 0.2$) which achieves the minimum SER. The impact of ϵ_2 has significant effects on the inversion process as shown in Fig. 4.16. In Fig. 4.16, ψ is a factor that reflects the level of the residual interference in the output polynomial matrix $\mathbf{G}[\ell]$ when compared to the identity matrix \mathbf{I} as

$$\psi = \left\| \sum_{\ell} \mathbf{G}[\ell] - \mathbf{I}\delta[\ell] \right\|_{\text{F}}. \quad (4.23)$$

Throughout the simulation, the probability density function (PDF) of the factor ψ was calculated when using $\epsilon_2 = \{0, 0.2\}$ as shown in Fig. 4.16. It can be noted the improvements of using $\epsilon_2 = 0.2$ on the PDF(ψ) compared to the case of not using ϵ_2 at all. Fig. 4.17 depicts a comparison in the symbol error ratio (SER) performances of a per-subband equaliser and the proposed equaliser when applied

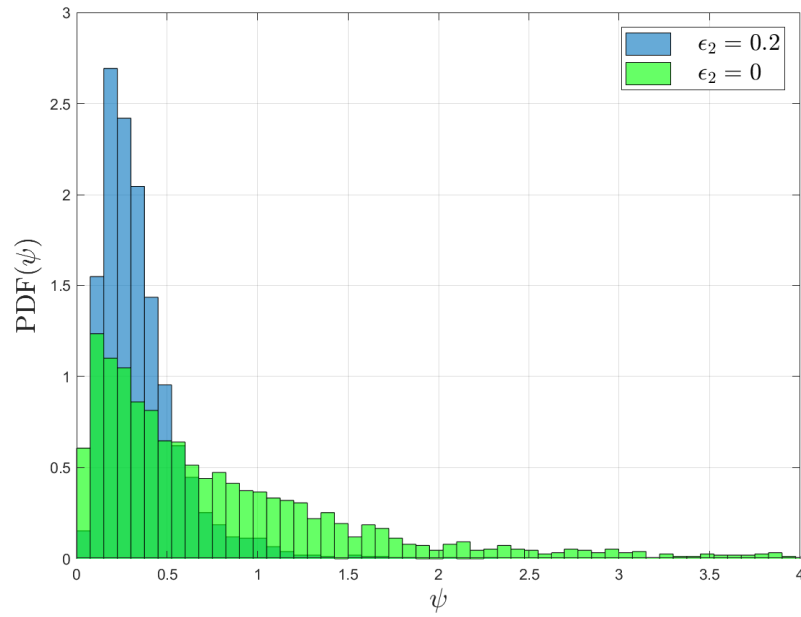


Figure 4.16: The PDF of ψ with and without using a regularisation coefficient ϵ_2 during the inversion process of $\mathbf{F}(z)$ for an FBMC/OQAM system with $M = 4$ using PHYDYAS prototype filter over a dispersive channel with length of 10.

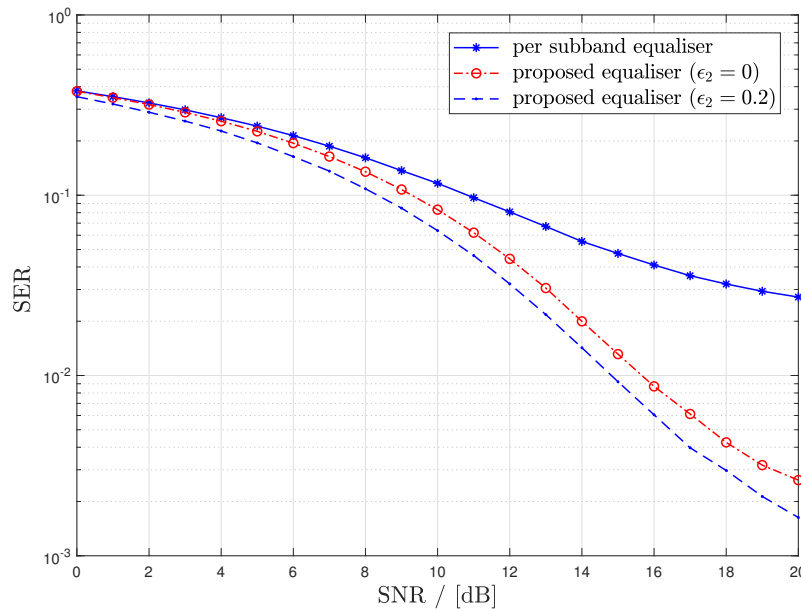


Figure 4.17: SER performances of a per-subband equaliser and the proposed multiband equaliser for FBMC/OQAM with $M = 4$ over a dispersive channel $c[\nu]$ of length 10.

to an FBMC/OQAM system using the PHYDYAS prototype filter with $M = 4$ subbands over a dispersive channel of length 10. It can be noted that the proposed equaliser achieves better SER performance than the per-subband equaliser due to considering the cross-talk terms in the proposed equalisation approach while the performance of the per-subband equaliser is negatively affected by the residual interference induced by the permitted spectral overlapping between subcarriers in FBMC/OQAM. Moreover, the SER performance was enhanced due to using the regularisation constant $\epsilon_2 = 0.2$.

4.6 Concluding Remarks

This chapter has analysed an FBMC/OQAM system, which is known to suffer from ISI and ICI between at least adjacent subchannels in presence of a dispersive channel impulse response. A polynomial matrix formulation has been proposed for an equivalent channel transfer function, which includes the filter bank components and channel. The equalisation of this system was attempted by means of polynomial matrix algebra. Since the matrix in the proposed approach is rank deficient by default, a polynomial pseudo-inverse was introduced to address this problem. The equalisation leads to a solution, that together with OQAM pre- and post-processing can eliminate ISI and ICI.

Chapter 5

Equalisation of Multi-Antenna FBMC/OQAM

As it has been pointed out in previous chapters, filter bank based multicarrier orthogonal quadrature amplitude modulation (FBMC/OQAM) as a transmultiplexing technique has attracted a lot of attention. This is due to its distinction from other multicarrier modulation techniques in terms of its attaining of maximum spectral efficiency, which is a critical demand in the development of modern communication systems. As the previous chapter has highlighted, intersymbol interference (ISI) and inter-carrier interference (ICI) result from the transmission over dispersive single-input-single-output (SISO) channels. When using FBMC/OQAM techniques in a multiple-input-multiple-output (MIMO) environment, the challenge of dealing with ISI and ICI is further exacerbated by the presence of spatial interference. This chapter therefore first describes the transfer functions (including all temporal and spatial interference terms) by polynomial matrices. The equalisation of this system can then be performed by a proposed

polynomial matrix pseudo-inverse. Two numerical examples for this approach are presented.

5.1 Introduction

Filter bank based multicarrier (FBMC) modulation methods are a strong candidate for 5th generation communications systems and beyond because of their robustness to synchronisation errors when compared to orthogonal frequency division multiplexing (OFDM) systems [24, 29]. Different from OFDM, in FBMC subcarriers retain a higher frequency-selectivity. Even though recent practical measurements indicate that for a well-synchronised FBMC system, single tap equalisers may be sufficient [111], generally significant dispersion has to be considered [70, 71], if not through long channel impulse response then through insufficient timing synchronisation of the receiver [35]. As a result, significant inter-symbol interference (ISI) arises.

Amongst the different FBMC choices, a critically sampled DFT filter bank combined with judicious interleaving of real and imaginary parts akin to offset-quadrature amplitude modulation (OQAM) has attracted attention as it reaches maximum spectrum efficient yet retains orthogonality at least for the real part of the transmitted symbols [7]. Due to critical sampling, at least adjacent subbands overlap spectrally, causing inter-carrier interference (ICI) in the receiver. Thus equalisers cannot operate per-band but need to incorporate cross-terms with at least adjacent bands akin to early subband filtering schemes such as [98]. Nevertheless, the high spectral efficiency of FBMC/OQAM has motivated numerous solutions that aim to solve this problem [2, 35, 111, 112].

When considering FBMC/OQAM for transmission over MIMO channels, the interference situation is worsened by additional inter-antenna interference (IAI) terms in addition to ISI and ICI. This is generally seen as a significant problem, and substantial efforts have been undertaken to combat these interference terms — see e.g. early works in [113], or more recently in [70, 71] or the review in [2]. The majority of these publications has targetted the joint design of precoders and equalisers, which can enable significant benefits if the channel is known to both receiver and transmitter.

In the absence of channel state information at the transmitter, often efforts have to be restricted to equalisation, and the aim of this chapter is to propose such an approach. The proposed design is based on the modelling of the inner part of the FBMC/OQAM system — including the filter banks and the MIMO channel, which are responsible for dispersion and synchronisation errors — by an equivalent polynomial channel matrix. The algebraic techniques are used for such matrices to find an equaliser. The polynomial notation and problem formulation of a broadband communication systems is not new — see e.g. [114] for a SISO and [71] for a MIMO precoder and equaliser — but solutions to such problems have not been straightforward: Mertins [114] only formulates the problem without solving it, while Mestre *et al.* [71] use a frequency domain approach — a so-called analytic singular value decomposition [115, 116]. I here rely on novel polynomial matrix formulations [50] and associated algorithms [52, 53, 103, 117] to calculate a polynomial matrix pseudo-inverse as equaliser as a MIMO extension of the work in [35]. The advantage of these polynomial matrix techniques lies in the coherent treatment of the problem, which avoids the challenge of association of bin-wise solutions from DFT bin to DFT bin such as encountered in [71].

This chapter is organised as follows: Sec. 5.2 reviews the MIMO FBMC/OQAM system model, which motivates the description of the MIMO channel combined with the synthesis and analysis filter banks of the FBMC/OQAM system by an equivalent channel matrix in Sec. 5.3. The equalisation of the MIMO-FBMC/OQAM system via the pseudo-inversion of this equivalent channel matrix is the topic of Sec. 5.4, followed by numerical examples in Secs. 5.5 and 5.6. Concluding remarks are presented in Sec. 5.7.

5.2 System Model

An FBMC/OQAM system for a MIMO channel with N_T transmitters and N_R receivers is outlined in Fig. 5.1. For a brief description of FBMC/OQAM, with reference to Fig. 5.1, for simplicity I first assume the single input single output case with $N_T = N_R = K = 1$, and $\mathbf{W}[n] \circ \bullet \mathbf{W}(z) = \mathbf{I}_M$.

In the inner, shaded part of the FBMC system in Fig. 5.1, a DFT-modulated filter bank with a synthesis filter bank (SFB) and an analysis filter bank (ASB) multiplexes a signal vector $\mathbf{u}[n] \in \mathbb{C}^M$ across the channel, employing an upsampling ratio of $M/2$. In the receiver, the signal is demultiplexed into $\mathbf{x}[n] \in \mathbb{C}^M$. For a DFT filter bank to permit maximum symbol density (and hence maximum spectral efficiency) while satisfying good localisation in both time and frequency domains, the orthogonality of the system has to be relaxed. In FBMC/OQAM the relaxation of conditions is achieved by restricting orthogonality to the real part only by judiciously assigning alternating real and imaginary values in $\mathbf{d}[\ell] \in \mathbb{C}^M$ to $\mathbf{u}[n] \in \mathbb{C}^M$ through a staggering and de-staggering process [7] akin to an OQAM modulation. As a result, the index n runs twice as fast as the time index ℓ . Through this, partial orthogonality is enforced, such that $\hat{\mathbf{d}}[\ell] = \mathbf{d}[\ell]$ if the

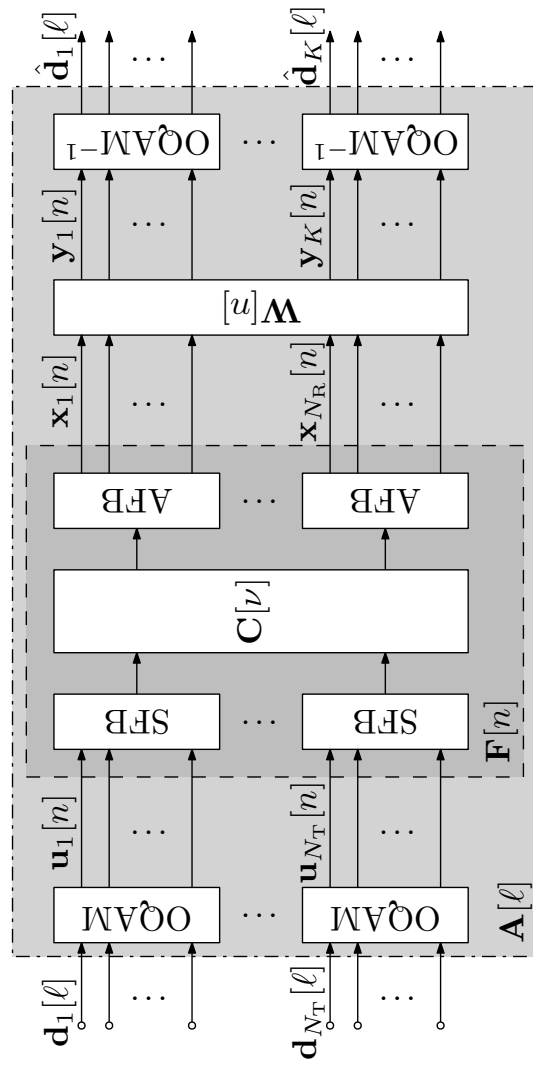


Figure 5.1: FBMC/OQAM system transmultiplexing signals over a MIMO channel $\mathbf{C}[\nu]$ with N_T transmitters and N_R receivers, and with an equaliser $\mathbf{W}[n]$.

channel is transparent.

The MIMO scenario assumes that K spatial transmit channels can be formed, where $K = \min\{N_T, N_R\}$. An FBMC/OQAM block is applied to each of the transmitters and receivers, as shown in Fig. 5.1. An equaliser $\mathbf{W}[n] \in \mathbb{C}^{MK \times MN_R}$, applied prior to the OQAM de-staggering in the receiver, has the aim of equalising and synchronising the overall system. This is similar to the equaliser and synchroniser in [35], but here also aims to mitigate spatial or inter-antenna-interference.

5.3 Equivalent Polynomial Channel Matrix

In order to later define the equaliser $\mathbf{W}(z) \bullet \text{---} \circ \mathbf{W}[n]$, first the inner FBMC component of Fig. 5.1 is described. For this, a polyphase notation of the analysis and synthesis filter banks is utilised. With M channels and an oversampling factor of 2, the polyphase analysis matrix $\mathbf{H}(z) : \mathbb{C} \rightarrow \mathbb{C}^{M \times M/2}$ is an $M \times \frac{M}{2}$ polynomial matrix. Similarly, a synthesis filter bank can be described by a polyphase synthesis matrix $\mathbf{G}(z) : \mathbb{C} \rightarrow \mathbb{C}^{M/2 \times M}$, where for a DFT filter bank, the polyphase synthesis matrix $\mathbf{G}(z)$ is the parahermitian of the polyphase analysis matrix, i.e.

$$\mathbf{G}(z) = \mathbf{H}^P(z) = \mathbf{H}^H(1/z^*). \quad (5.1)$$

To form filter banks, these polyphase realisations are combined with parallel-to-serial (p/s) and serial-to-parallel (s/p) converters, as depicted in Fig. 5.2.

If $C_{n_R, n_T}(z)$ is the channel transfer function between the n_T th transmitter, $n_T = 1 \dots N_T$, and the n_R th receiver, $n_R = 1 \dots N_R$, the MIMO system transfer function between the p/s input vector $\mathbf{s}_{n_T}[n]$ and the s/p output vector $\mathbf{r}_{n_R}[n]$ is

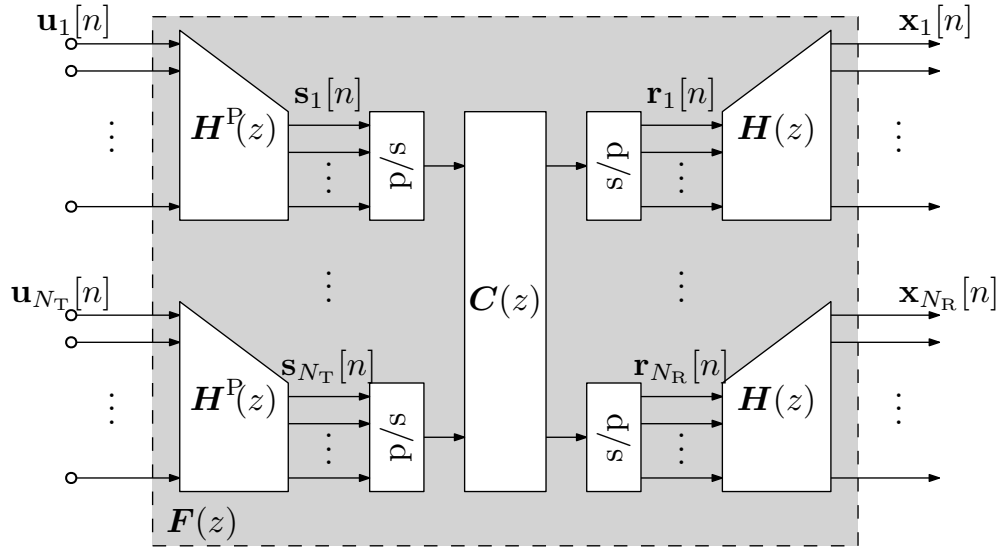


Figure 5.2: Inner component of the MIMO FBMC/OQAM system in polyphase notation.

the pseudo-circulant matrix $\mathbf{C}_{n_R, n_T}(z) : \mathbb{C} \rightarrow \mathbb{C}^{M/2 \times M/2}$ [35, 103],

$$\mathbf{C}_{n_R, n_T}(z) = \begin{bmatrix} C_0(z) & C_1(z) & \cdots & C_{\frac{M}{2}-1}(z) \\ z^{-1}C_{\frac{M}{2}-1}(z) & C_0(z) & \cdots & C_{\frac{M}{2}-2}(z) \\ \vdots & \vdots & \ddots & \vdots \\ z^{-1}C_1(z) & \cdots & z^{-1}C_{\frac{M}{2}-1}(z) & C_0(z) \end{bmatrix}. \quad (5.2)$$

For notational brevity, the subscripts $\{\cdot\}_{n_R, n_T}$ have been omitted from the r.h.s. of the above equation, which comprises of the $\frac{M}{2}$ type-I polyphase components $C_\mu(z)$, $\mu = 1 \dots \frac{M}{2}$ of $\mathbf{C}_{n_R, n_T}(z)$ [99] such that

$$C_{n_R, n_T}(z) = \sum_{\mu=0}^{\frac{M}{2}-1} C_\mu(z^{\frac{M}{2}}) z^{-\mu} \quad (5.3)$$

describes the channel between the n_T th transmitter and n_R th receiver.

The overall MIMO transfer function between the concatenated filter bank

inputs $[\mathbf{u}_1^H[n] \dots \mathbf{u}_{N_T}^H[n]]^H$ in the transmitter and the concatenated vector of filter bank outputs $[\mathbf{x}_1^H[n] \dots \mathbf{x}_{N_R}^H[n]]^H$ in the receiver is described by the matrix $\mathbf{F}[n] \circ \bullet \mathbf{F}(z)$, which forms the shaded system part in Figs. 5.1 and 5.2. With the demultiplexed MIMO channel matrix $\mathbf{C}(z) : \mathbb{C} \rightarrow \mathbb{C}^{(N_R M/2) \times (N_T M/2)}$,

$$\mathbf{C}(z) = \begin{bmatrix} \mathbf{C}_{1,1}(z) & \dots & \mathbf{C}_{1,N_T}(z) \\ \vdots & \ddots & \vdots \\ \mathbf{C}_{N_R,1}(z) & \dots & \mathbf{C}_{N_R,N_T}(z) \end{bmatrix} \quad (5.4)$$

which spans the system between $[\mathbf{s}_1^H[n] \dots \mathbf{s}_{N_T}^H[n]]^H$ and $[\mathbf{r}_1^H[n] \dots \mathbf{r}_{N_R}^H[n]]^H$ in Fig. 5.2, the channel matrix $\mathbf{F}(z)$ becomes

$$\mathbf{F}(z) = (\mathbf{I}_{N_R} \otimes \mathbf{H}(z)) \mathbf{C}(z) (\mathbf{I}_{N_T} \otimes \mathbf{H}^P(z)) , \quad (5.5)$$

where \otimes denotes the Kronecker product.

A few properties of $\mathbf{F}(z)$ can be inferred from its structure in (5.5). Firstly, even though $\mathbf{F}(z) : \mathbb{C} \rightarrow \mathbb{C}^{(N_R M) \times (N_T M)}$, the reduced dimension of $\mathbf{C}(z)$ forces the polynomial rank [118] of $\mathbf{F}(z)$ to

$$\text{rank}\{\mathbf{F}(z)\} \leq \frac{KM}{2} , \quad (5.6)$$

where $K = \min\{N_R, N_T\}$. Secondly, if the DFT filter bank described by $\mathbf{H}(z)$ is constructed for a standard FBMC/OQAM system via [102], then energy will only leak between adjacent bands at most. Therefore, $\mathbf{F}(z)$ will be sparse with a block structure, where each $M \times M$ sub-block only contain nonzero elements along its diagonal, its first off-diagonals, and in its upper right and lower left corner elements.

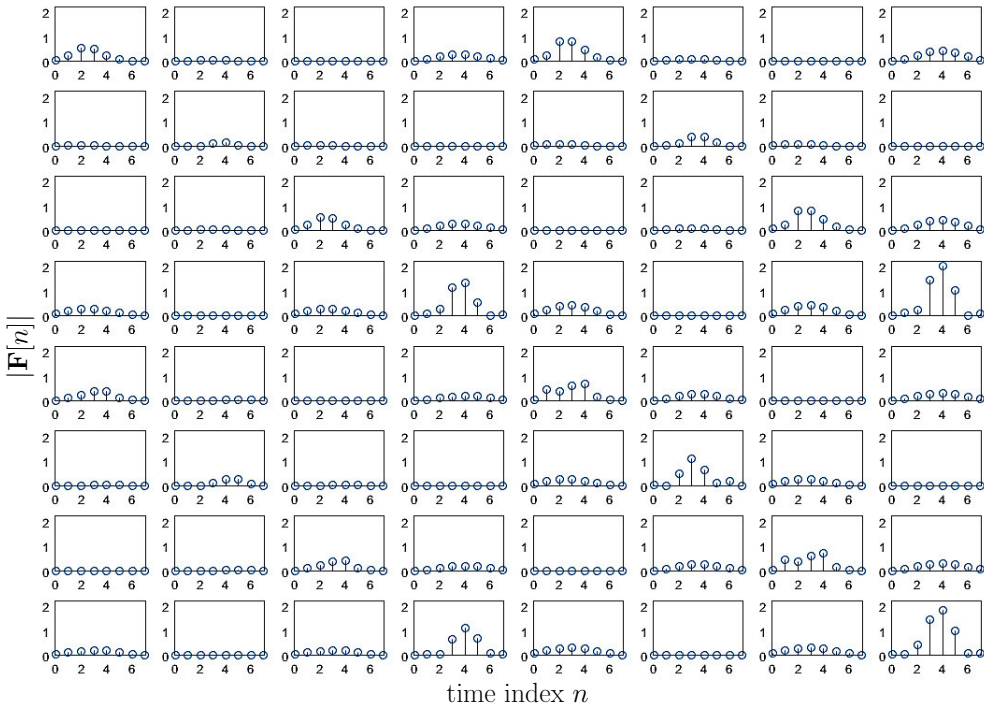


Figure 5.3: Example for the equivalent polynomial channel matrix $\mathbf{F}(z) \bullet\text{---}\circ \mathbf{F}[n]$ of a channel with $N_T = 2$ transmitters and $N_R = 2$ receivers, and $M = 4$ subchannels.

Example. The channel matrix $\mathbf{F}[n]$ for a MIMO-FBMC/OQAM system with a 2×2 random MIMO channel containing impulse responses of length 5, and $M = 4$ subbands is shown in Fig. 5.3. The transfer function $\mathbf{F}(z)$ is an 8×8 sparse polynomial matrix. The two lower left hand and upper right hand 4×4 blocks of $\mathbf{F}[n]$ represent the inter-antenna interference paths, thus creating a matrix structure that differs from the nearly tri-diagonal system of Chap. 4. The Channel polynomial matrix $\mathbf{F}[n]$ can be obtained either by sounding the channel or algebraically by calculating it according to (5.5).

5.4 MIMO FBMC/OQAM Equalisation

Based on the equivalent channel model derived in Sec. 5.2, the equalisation of this system will be explored. The overall setup in Fig. 5.1 contains a subblock $\mathbf{W}[n] \circ \bullet \mathbf{W}(z)$ which directly follows the equivalent channel $\mathbf{F}[n] \circ \bullet \mathbf{F}(z)$ prior to OQAM de-staggering of the retrieved K spatial channels of the system. The purpose of this equaliser block is to restore the orthogonality of the real part of the combined system $\mathbf{W}(z)\mathbf{F}(z)$. Due to the rank-deficiency of $\mathbf{F}(z)$, this equaliser relies on the pseudo-inverse, which is calculated via the singular value decomposition of a polynomial matrix [52, 104]. While the SVD of a polynomial matrix can also be calculated directly [104], the approach here — akin to Chap. 4 — evaluates the PEVD of two matrices $\mathbf{R}_1(z) : \mathbb{C} \rightarrow \mathbb{C}^{MN_R \times MN_R}$ and $\mathbf{R}_2(z) : \mathbb{C} \rightarrow \mathbb{C}^{MN_T \times MN_T}$ such that

$$\mathbf{R}_1(z) = \mathbf{F}(z)\mathbf{F}^P(z) \approx \mathbf{U}(z)\mathbf{\Lambda}_1(z)\mathbf{U}^P(z) \quad (5.7)$$

$$\mathbf{R}_2(z) = \mathbf{F}^P(z)\mathbf{F}(z) \approx \mathbf{V}(z)\mathbf{\Lambda}_2(z)\mathbf{V}^P(z) . \quad (5.8)$$

The factorisations on the r.h.s. of (5.7) and (5.8) are polynomial EVDs with paraunitary $\mathbf{U}(z) : \mathbb{C} \rightarrow \mathbb{C}^{MN_R \times MN_R}$ and $\mathbf{V}(z) : \mathbb{C} \rightarrow \mathbb{C}^{MN_T \times MN_T}$, such that

$$\mathbf{U}(z)\mathbf{U}^P(z) = \mathbf{U}^P(z)\mathbf{U}(z) = \mathbf{I}_{MN_R} \quad (5.9)$$

$$\mathbf{V}(z)\mathbf{V}^P(z) = \mathbf{V}^P(z)\mathbf{V}(z) = \mathbf{I}_{MN_T} . \quad (5.10)$$

The approximation signs in (5.7) and (5.8) account for the approximate nature of the decomposition achieved by iterative polynomial EVD algorithms in e.g. [52, 53, 103, 117] but also for the fact that the true EVD of the parahermitian matrices $\mathbf{R}_1(z)$ and \mathbf{R}_2 is almost always infinite in length [50], such that only approximations by polynomials are possible. The terms $\mathbf{\Lambda}_i(z)$, $i = 1, 2$ are diag-

onal parahermitian matrices that approximate the – again likely infinite [50] — eigenvalues of $\mathbf{R}_1(z)$ and \mathbf{R}_2 by Laurent polynomials.

With the help of (5.7) and (5.8) via the evaluation $\mathbf{S}(z) = \mathbf{U}^P(z)\mathbf{F}(z)\mathbf{V}(z)$, the approximate polynomial SVD is determined as

$$\mathbf{F}(z) \approx \mathbf{U}(z)\mathbf{\Sigma}(z)\mathbf{V}^P(z) . \quad (5.11)$$

The diagonal matrix $\mathbf{\Sigma}(z)$ is not necessarily square: $\mathbb{C} \rightarrow \mathbb{C}^{MN_R \times MN_T}$,

$$\mathbf{\Sigma}(z) = \text{diag}\{\sigma_1(z), \sigma_2(z), \dots, \sigma_{MK}(z)\} , \quad (5.12)$$

holds the approximate singular values of $\mathbf{F}(z)$ [52], extracted from the diagonal of $\mathbf{S}(z)$ by neglecting any of its remaining small off-diagonal elements.

The approximate pseudo-inverse of $\mathbf{F}(z)$ is now possible via its SVD in (5.11), such that

$$\mathbf{F}^\dagger(z) \approx \mathbf{V}(z)\mathbf{\Sigma}^\dagger(z)\mathbf{U}^P(z) . \quad (5.13)$$

Pseudo-inverting $\mathbf{\Sigma}(z)$ means inverting all singular values $\sigma_i(z)$, $i = 1 \dots MK$, as long as these are non-zero, and matrix transposition such that $\mathbf{\Sigma}^\dagger(z) : \mathbb{C} \rightarrow \mathbb{C}^{MN_T \times MN_R}$. Due to the rank deficiency of $\mathbf{F}(z)$, at least half of the singular values will be zero, i.e. $\sigma_i(z) = 0 \forall i = (M\frac{K}{2} + 1) \dots MK$. The inversion of polynomial terms can be accomplished by partial fraction expansion of $1/\sigma_i(z)$ and approximation of first order terms by geometric series [108], or adaptively using LMS or RLS algorithms [35].

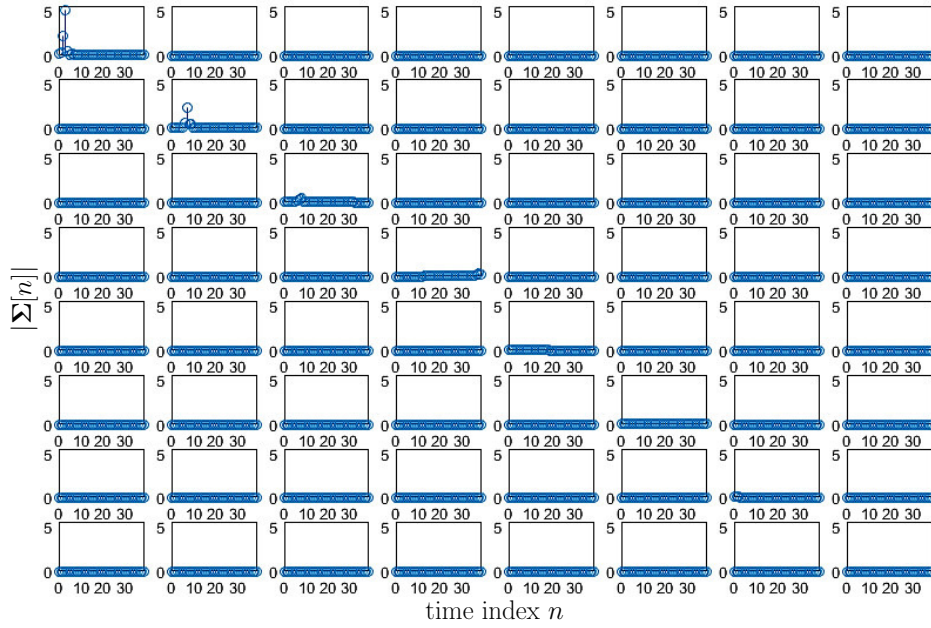


Figure 5.4: Matrix $\Sigma[n] \circ \bullet \Sigma(z)$ of approximate singular values of $\mathbf{F}[n]$ as characterised in Fig. 5.3.

5.5 Numerical Example I

A first example elaborates on the equivalent polynomial channel matrix $\mathbf{F}(z)$ as characterised in Fig. 5.3. The matrix $\Sigma[n] \circ \bullet \Sigma(z)$ of approximate singular values is calculated via the multiple-shift SMD algorithm [117], and yields the coefficients shown in Fig. 5.4. The singular values are arranged in descending order, noting that algorithms such as SMD encourage (or in the case of SBR2 can be proven to converge to [119]) spectral majorisation. With $K = 2$, the $MK/2 = 4$ non-zero singular values can be found in the top upper left-hand corner of $\Sigma(z)$.

The spectra of the non-zero singular values, i.e. the evaluation of $\sigma_i(z)$ on the unit circle for $z = e^{j\Omega}$, is shown in Fig. 5.5, which shows the approximate spectral

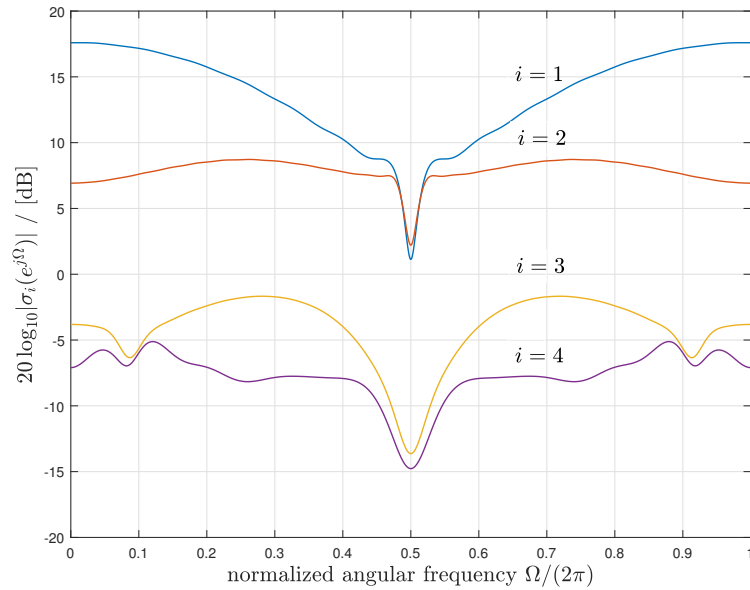


Figure 5.5: Evaluation of non-singular values of $\mathbf{F}(z)$ in Fig. 5.3 on the unit circle.

majorisation, such that

$$\sigma_i(e^{j\Omega}) \gtrsim \sigma_{i+1}(e^{j\Omega}), \quad i = 1 \dots 3, \forall \Omega. \quad (5.14)$$

If singular values exhibit strong attenuation or even spectral nulls, their inversion should include a regularisation term ϵ_2 as in (4.20), which is particularly aiming to avoid noise amplification by the equaliser in the presence of channel noise. Fig. 5.6 depicts the impact of ϵ_2 on the SER performance of the equalised system shown in Fig. 5.8 at SNR = 17dB, the optimum value of ϵ_2 in this example is 0.05. The optimum value of ϵ_2 can be obtained via simulating the equalisation process of an FBMC/OQAM system over many channel realisations e.g. 1000 realisations using different values of ϵ_2 and averaging the measured SER at a certain SNR e.g. 17 dB. It can be noted from Fig. 5.6 that for the of values of ϵ_2 in the range $[0, 0.05]$, the SER performance improved when ϵ_2 increases and obtaining the

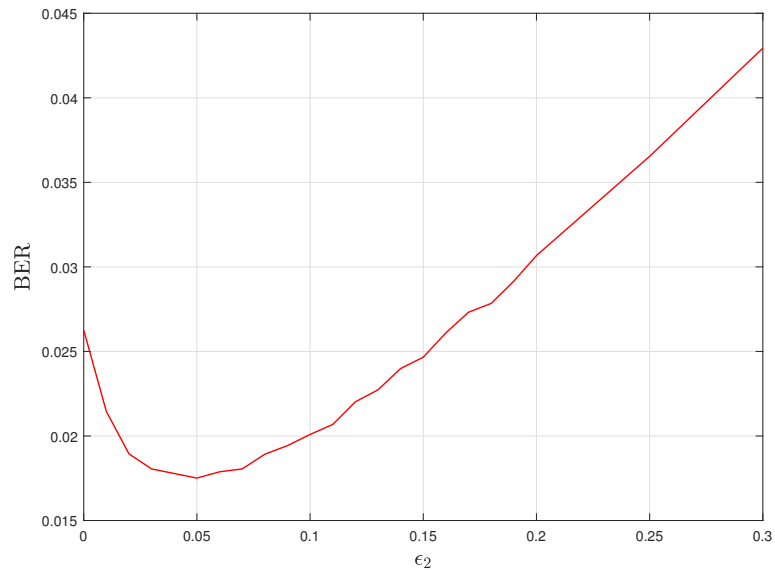


Figure 5.6: SER vs regularisation coefficient (ϵ_2) at SNR of 15 dB for the equalised MIMO-FBMC/OQAM system in Fig. 5.8.

optimum SER performance at the value of 0.05. However, when increasing the value of $\epsilon_2 > 0.05$, the SER performance decays. The impact of using $\epsilon_2 = 0.05$ on the inversion process of $\mathbf{F}(z)$ to obtain the equaliser polynomial matrix $\mathbf{W}(z)$ is depicted in Fig. 5.9 which can be obtained according to (4.23). Fig. 5.9 reflects the slight difference in the PDF(ψ) when using $\epsilon_2 = 0.05$ and the case when not using the regularisation term during the inversion process of $\mathbf{F}[n]$. The SER performance of the equalised MIMO-FBMC/OQAM system using $\epsilon_2 = \{0, 0.5\}$ is shown in Fig. 5.10.

The response of the concatenation of the equivalent polynomial channel matrix and the equaliser, $\mathbf{W}(z)\mathbf{F}(z) \bullet \circ \mathbf{W}[n] * \mathbf{F}[n]$, is shown in Fig. 5.7. Since $\mathbf{F}(z)$ is rank deficient, the system inversion cannot yield an identity matrix. As shown in Fig. 5.7, it can be noted that the up right and down left 4×4 elements in the polynomial matrix possess approximately zero elements i.e. the IAI is

suppressed due to equalisation process. Moreover, the top left and bottom right 4×4 elements are shown to be a tri-diagonal non-zeros elements in addition to the two corner elements similar to the case of SISO-FBMC/OQAM. However, sounding the overall MIMO-FBMC/OQAM system of Fig. 5.1 between the inputs $\mathbf{d}_i[\ell]$ and outputs $\hat{\mathbf{d}}_j[\ell]$, $i, j = 1, 2$, i.e. I measure the system $\mathbf{A}[\ell]$ such that $\hat{\mathbf{d}}[\ell] = \mathbf{A}[\ell] * \mathbf{d}[\ell]$ with $\mathbf{d}[\ell] = [\mathbf{d}_1^H[\ell], \mathbf{d}_2^H[\ell]]^H$ and $\hat{\mathbf{d}}[\ell] = [\hat{\mathbf{d}}_1^H[\ell], \hat{\mathbf{d}}_2^H[\ell]]^H$ as shown in Fig. 5.1, it yield the response depicted in Fig. 5.8. This response approximates an identity matrix, i.e. inter-symbol, inter-carrier, as well as inter-antenna interference terms have been suppressed by the proposed equaliser.

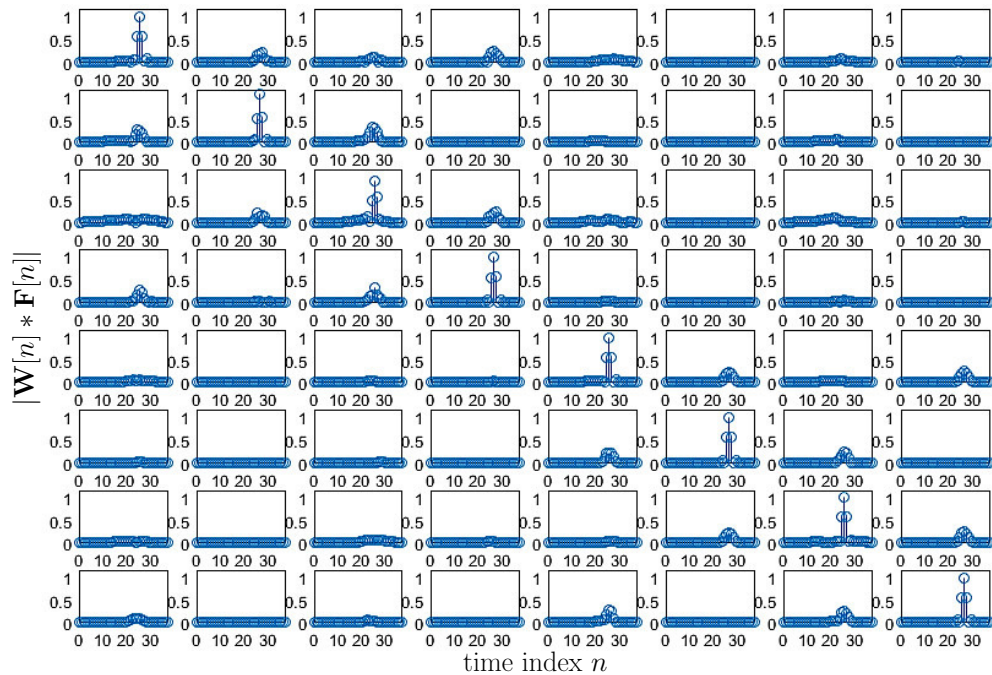


Figure 5.7: Overall response of the equivalent channel $\mathbf{F}(z)$ $\bullet\text{---}\circ \mathbf{F}[n]$, including inner FBMC system of Fig. 5.2, and the equaliser $\mathbf{W}(z)$ $\bullet\text{---}\circ \mathbf{W}[n]$.

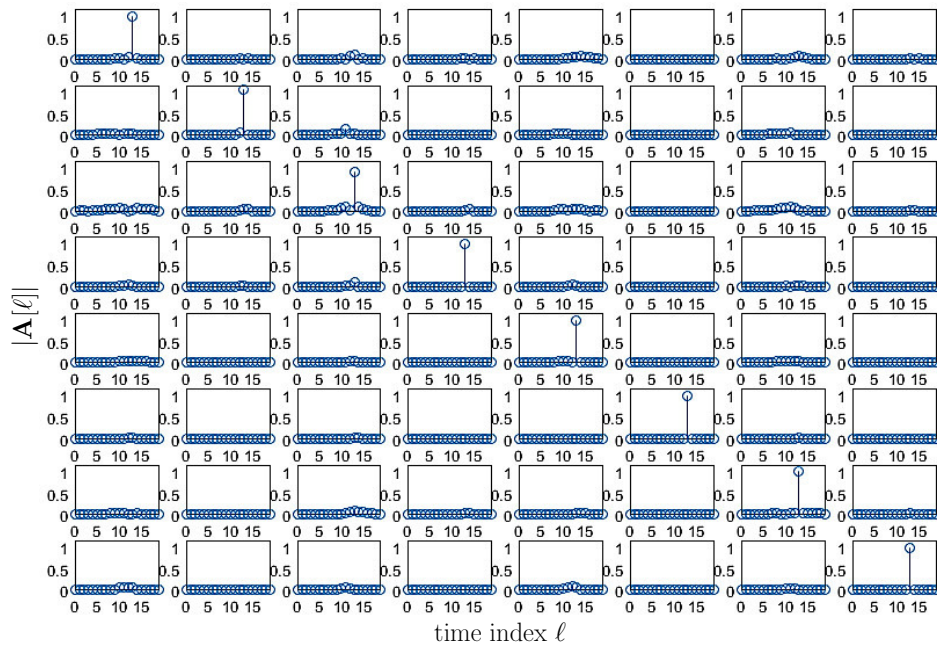


Figure 5.8: Response $\mathbf{A}[\ell]$ of the overall MIMO-FBMC/OQAM system as highlighted in Fig. 5.1.

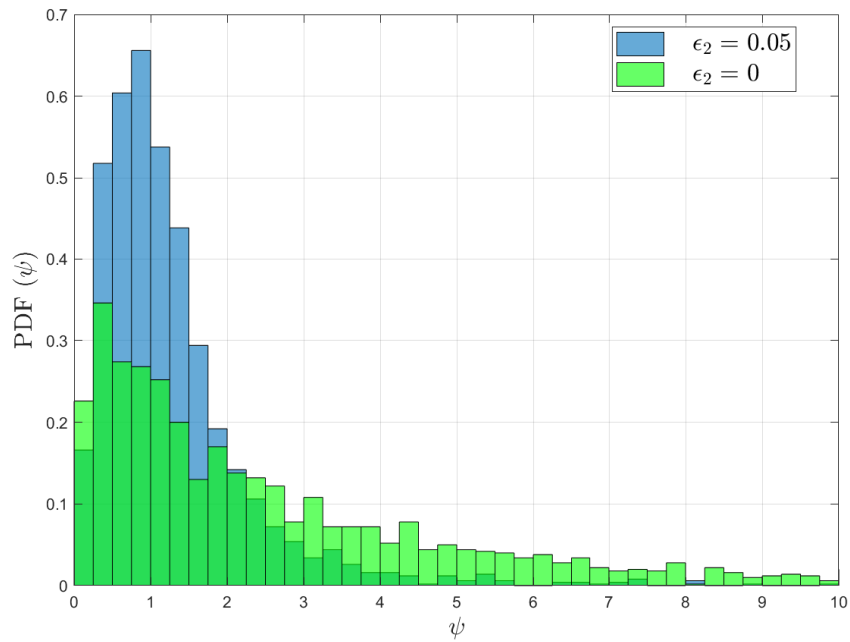


Figure 5.9: The PDF of ψ with and without using a regularisation constant ϵ_2 during the inversion process of $\Sigma(z)$.

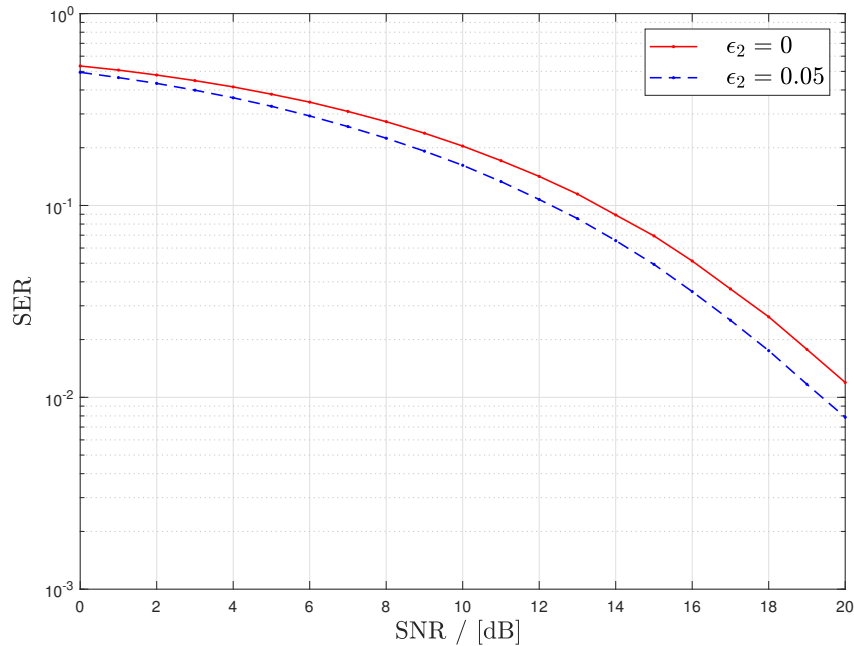


Figure 5.10: SER Vs SNR for an FBMC/OQAM system over 2×2 MIMO channel when using regularisation coefficient $\epsilon_2 = \{0, 0.05\}$ during the equalisation process.

5.6 Numerical Example II

In this section, a another example is presented for an FBMC/OQAM system using $M = 4$ over a dispersive MIMO channel $\mathbf{C}(z)$ utilising 2 antennas at the transmitter ($N_T = 2$) and 3 antennas at the receiver ($N_R = 3$). The MIMO channel polynomial matrix $\mathbf{C}(z)$ is of order 5 with a Gaussian distribution coefficients. Fig. 5.11 depicts the equivalent channel polynomial matrix $\mathbf{F}(z)$ with a size of $(N_R M \times N_T M)$ according to (5.5) which also can be obtained by channel sounding. As shown in Fig. 5.11, the channel polynomial matrix $\mathbf{F}[n]$ has a rectangular structure in this case different from that in the previous example shown in Fig. 5.3 due to using 3 antennas in the receiver. Accordingly, the poly-

nomial matrix $\mathbf{\Sigma}(z)$ has also rectangular form and contains the singular values of $\mathbf{F}(z)$ on its main diagonal as shown in Fig. 5.12. The polynomial matrix $\mathbf{\Sigma}(z)$ is approximate diagonal matrix and obtained via PSVD for the polynomial channel matrix $\mathbf{F}(z)$ based on (5.7-11). Due to the rank deficiency of $\mathbf{F}(z)$, the polynomial matrix $\mathbf{\Sigma}(z)$ possess only 4 non zero elements on its main diagonal representing the polynomial singular elements which are spectrally majorised as depicted in Fig. 5.13.

The equaliser for that system is based on the proposed approach which explained in Section 5.4 by inverting the non-zero singular values $\sigma_i(z), i = 1 \dots \frac{KM}{2}$, to obtain the polynomial equaliser matrix $\mathbf{F}^\dagger(z)$ according to (5.13). The output of the inner system equalisation $\mathbf{W}(z)\mathbf{F}(z)$ is shown in Fig. 5.14 which indicates the suppressing of ICI. The overall equalised system after applying the OQAM algorithm $\mathbf{A}(z)$ is shown in Fig. 5.15 which appear to be an approximate identity matrix -i.e all types of interferences (ISI,ICI, and IAI) are suppressed.

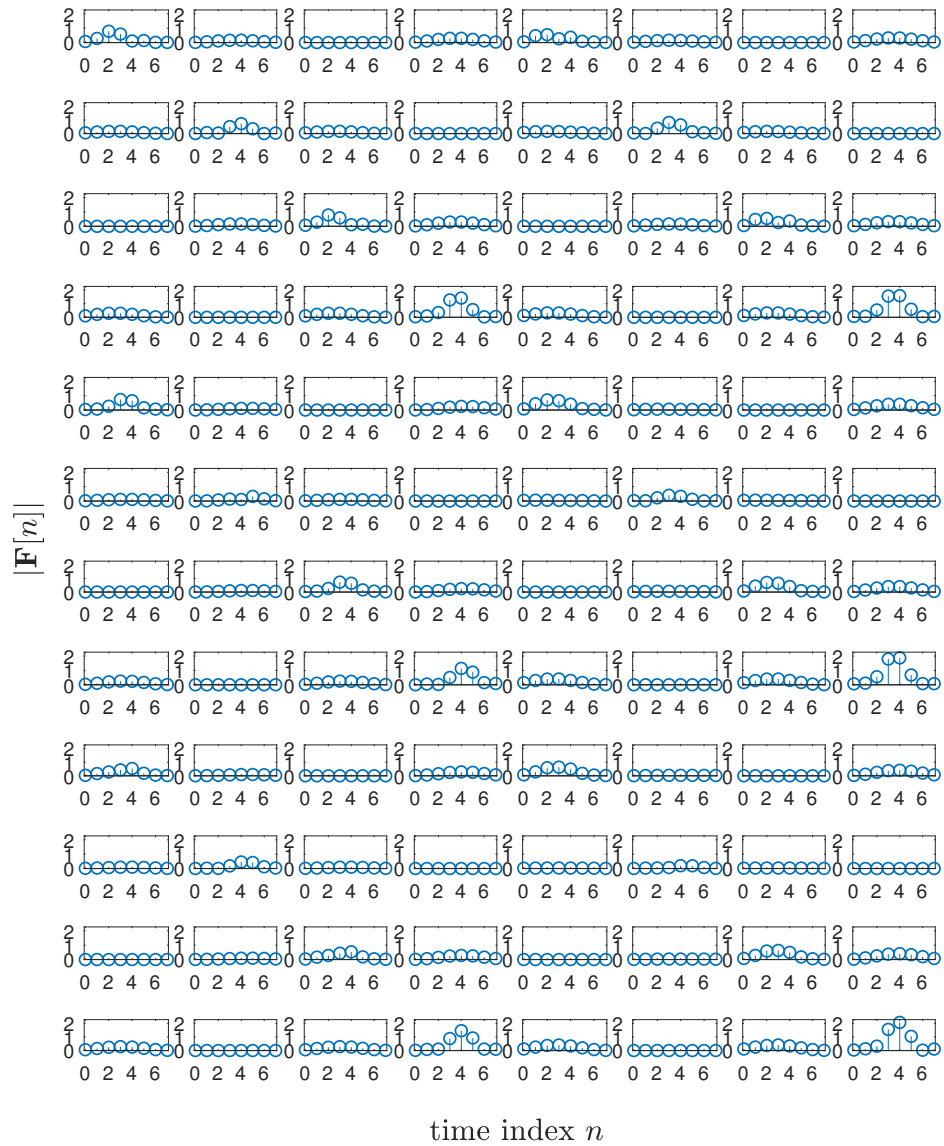


Figure 5.11: The equivalent polynomial channel matrix $\mathbf{F}[n]$ of an 2×3 MIMO FBMC/OQAM system with $M = 4$ over a dispersive MIMO channel of length 5.

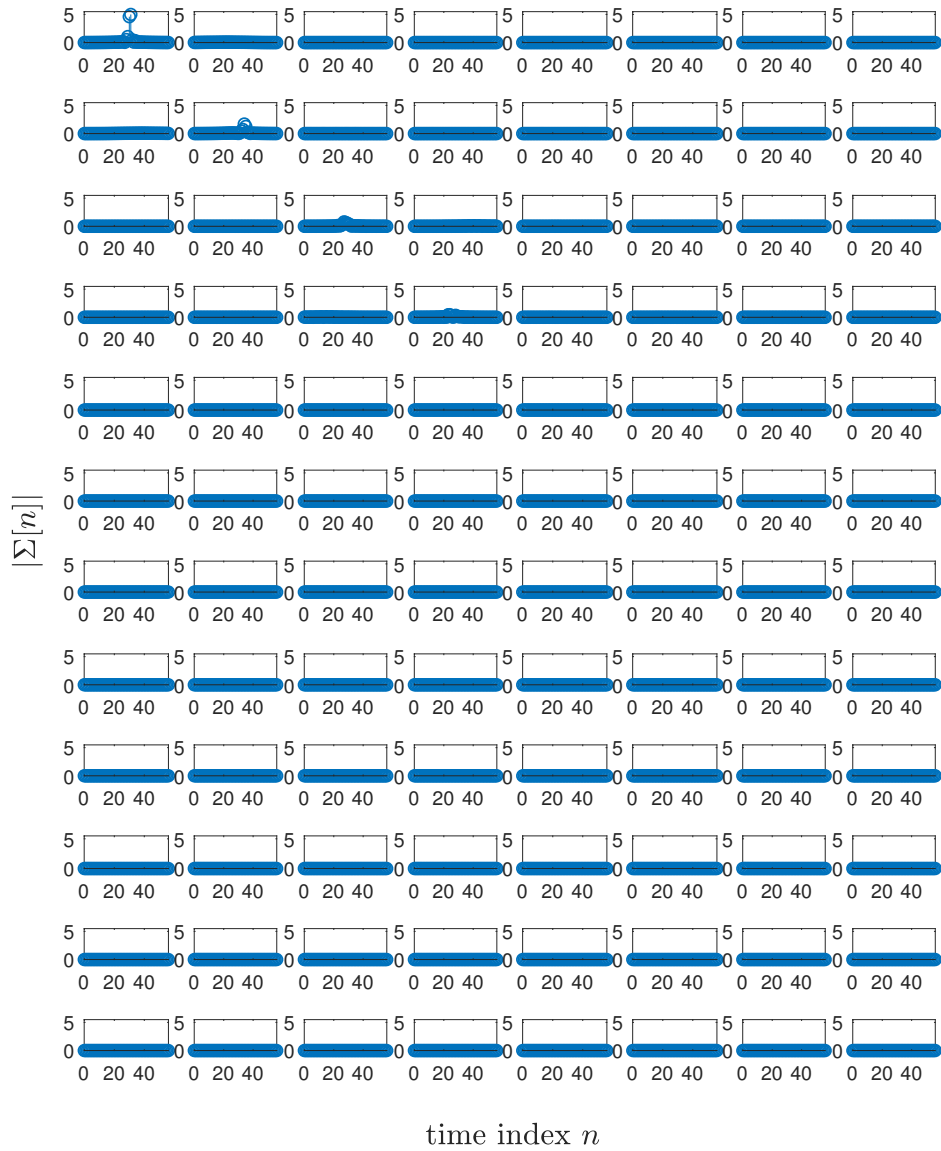


Figure 5.12: The diagonal matrix $\Sigma(z) \bullet \circ \Sigma[n]$ which contains the singular values of $F(z)$ as depicted in Fig. 5.11 .

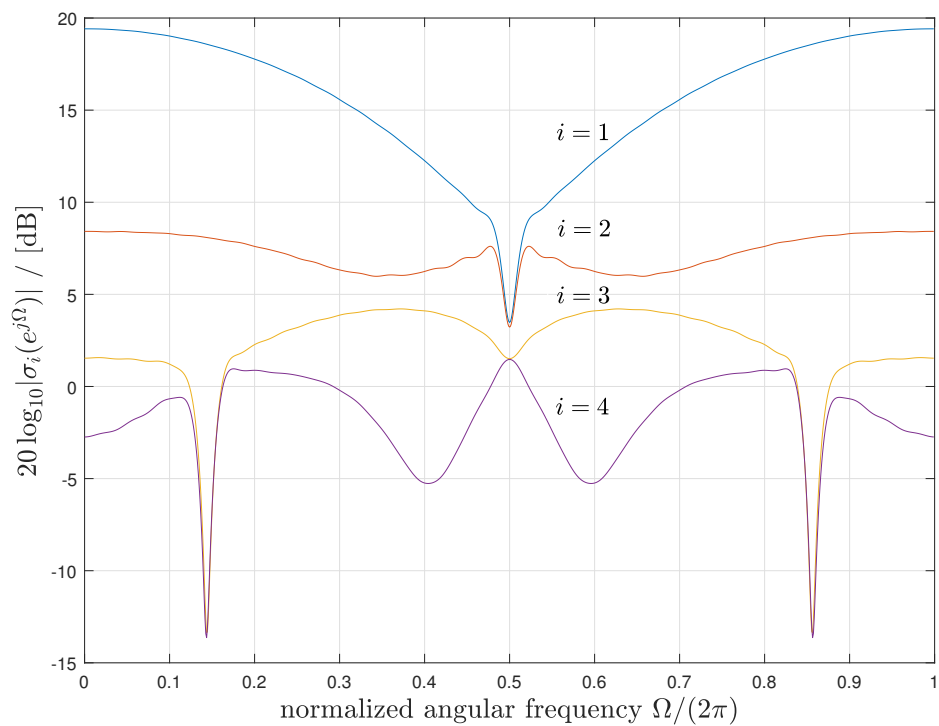


Figure 5.13: Magnitude response of the non-zero singular values of $\mathbf{F}(z)$ in Fig. 5.11.

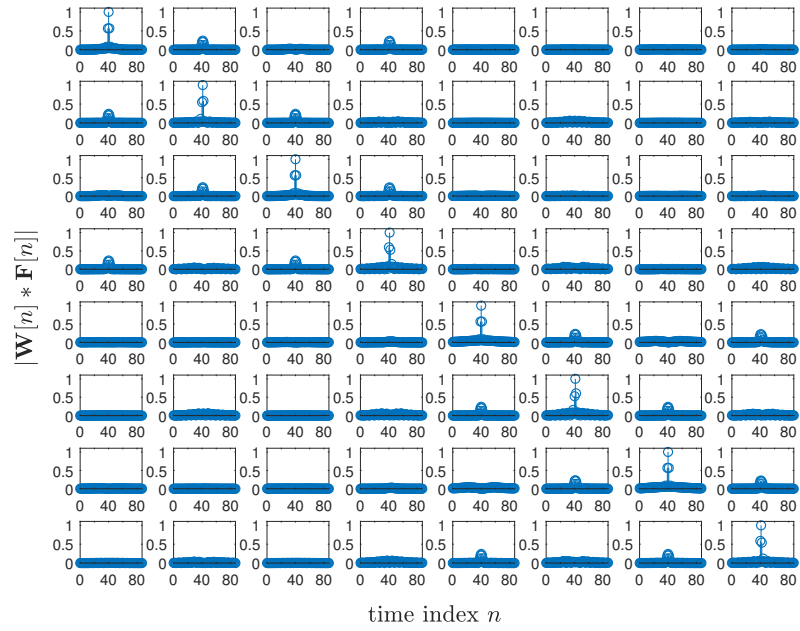


Figure 5.14: The joint channel polynomial matrix $\mathbf{F}(z)$ and its pseudo inverse $\mathbf{F}^\dagger(z)$.

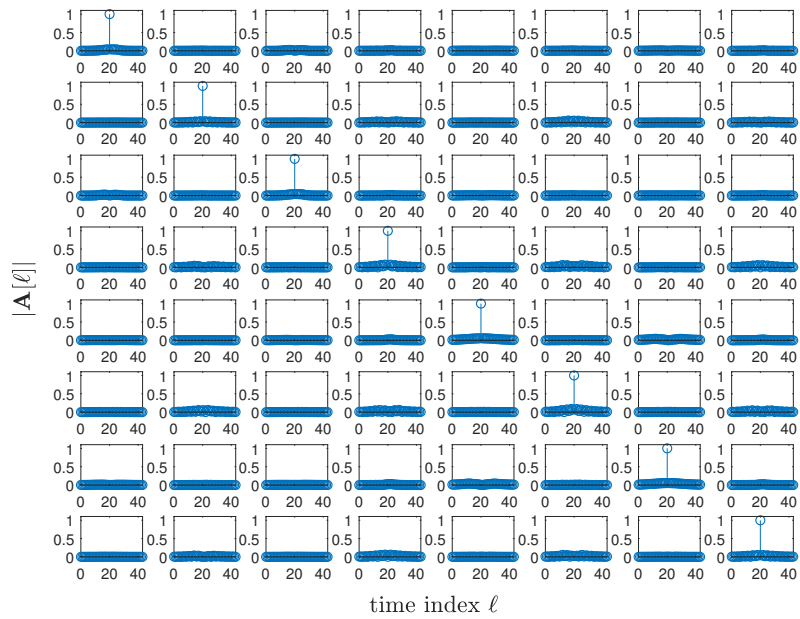


Figure 5.15: Response $\mathbf{A}[\ell]$ of the overall 2×3 MIMO-FBMC/OQAM system as highlighted in Fig. 5.11.

5.7 Conclusions

This chapter has investigated the equalisation of an FBMC/OQAM system when extended to a multiple-input multiple-output channel. The equivalent response of the inner MIMO-FBMC/OQAM system comprising the filter banks for transmultiplexing as well as the MIMO channel itself, was presented in the form of a polynomial matrix which reflects the different types of distortion (inter-symbol, inter-carrier, and inter-antenna interferences) affecting the system performance. Our proposed equaliser is based on this equivalent channel model characterised by a polynomial matrix. Its structurally imposed rank-deficiency has motivated pseudo-inverse. The presented numerical examples have shown that this system is capable of equalising the overall MIMO-FBMC/OQAM system.

Chapter 6

Conclusions and Future Work

6.1 Conclusions

This thesis has investigated filter bank based multicarrier (FBMC) modulation, which in the evolving 5th generation wireless communications systems is a competitor to conventional OFDM. FBMC systems generally offer higher frequency selectivity and better robustness towards synchronisation errors compared to OFDM. However, unlike OFDM, in dispersive channel conditions, FBMC approaches still retain some frequency selectivity, thus necessitating equalisation. Amongst these FBMC approaches, FBMC orthogonal quadrature amplitude modulation (FBMC/OQAM) is a particular, critically sampled FBMC system, which exhibits maximum spectral efficiency. This thesis therefore has focussed on the equalisation of FBMC/OQAM systems.

Chapter 3 has compared FBMC/OQAM with an oversampled FBMC system over a dispersive SISO channel, with a per-subband equaliser. This equaliser

was chosen to have fractional spacing in order to permit better equalisation/synchronisation in case the channel imposed a non-integer symbol period delay. Updated by the CMA and the concurrent CMA-DD algorithms, the equalisers were able to suppress the ISI. The simulation results showed the equalisation robustness of the OS-FBMC system, which due to its guard bands is ICI free, compared to FBMC/OQAM which suffers from ICI between next-adjacent bands. Although the OQAM system is capable of suppressing the interference between adjacent subchannels when transmitting over an ideal channel, the orthogonality of the system is lost when transmitting over dispersive channels.

Chapters 4 and 5 have derived the equivalent channel transfer function for FBMC/OQAM modulation over SISO and MIMO channels, respectively, which includes the filter bank components and channel, and is modelled in the form of a polynomial matrix. Hence, an equaliser for such FBMC/OQAM systems is proposed which inverts the channel polynomial matrix. The rank deficiency of the channel polynomial matrix requires the use of a polynomial pseudo-inverse instead, which is derived in this thesis. The proposed equaliser in addition to the OQAM system is shown to approximately suppress ISI and ICI in case of SISO transmission.

When transmitting with FBMC/OQAM over a MIMO channel, the received signal will not only be distorted by ISI and ICI, as in SISO, but will also suffer from inter-antenna interference which degrades the system performance significantly. The different types of MIMO-FBMC/OQAM interference (ISI, ICI, and IAI) are reflected in the equivalent channel polynomial matrix, which has been derived in Chapter 5. In order to mitigate all interference terms in the MIMO-FBMC/OQAM system, the pseudo inverse of the channel polynomial matrix is extended to the MIMO case. Numerical examples elaborate that all interference

types affecting MIMO-FBMC/OQAM system can be effectively mitigated.

With the FBMC/OQAM equalisation solutions proposed in this thesis, it is possible to utilise this spectrally efficient transmultiplexing scheme over dispersive channels. These schemes are particularly attractive if channel state information can only be relied upon in the receiver.

6.2 Future Work

Based on the topics presented in this thesis, further investigations of the FBMC/OQAM issues in the SISO and MIMO environments can be studied. Some ideas to the future work are presented below.

Power allocation and bit loading. When transmitting over a dispersive channel, the FBMC/OQAM subcarriers will be affected by different fading levels. If, as in the SER simulations of Chapters 3 and 4, the system transmit power is equally allocated among the subchannels which are loaded with the same symbol constellation, the average performance of the overall system will be dominated by the worst subchannel performance [120, 121]. In order to improve the performance and/or maximise the capacity of the FBMC/OQAM system, the resources (power, bits) can be reallocated among the subchannels according to their SNR. As a starting point, several algorithms presented in e.g. [95, 120, 122, 123] can be investigated to be adapted to the FBMC/OQAM system in conjunction with the proposed equaliser approach in this thesis to improve the system performance and/or increase the capacity.

Forward error correction coded FBMC/OQAM. Throughout the thesis, the investigated FBMC/OQAM system was using uncoded symbols. Forward error correction codes would play an important role in enhancing the system performance. Some work has been done in the context of FBMC in [124–126], therefore applying coded symbol streams to the equalised FBMC/OQAM system can be expected to lead to enhancements in the overall system reliability, and therefore help to assess the proposed equalisation and synchronisation solutions as part of an overall communication systems.

Computational complexity evaluation of the proposed equalisation schemes. Computational complexity is an important aspect if the proposed scheme was to be adopted for a practical application. Therefore, the first step would be the measurements of the computational complexity of the proposed equalisation schemes in terms of multiply-accumulates (MACs), or, since this is difficult for iterative polynomial matrix factorisation algorithms such as SBR2 or SMD, the CPU time. In a second step, the system complexity would be improved by investigating less complex and efficient PSVD algorithms based on recent efforts in [127–130], or the reduction of the polynomial order based on e.g. [131–133].

Performance comparison of the proposed equalisation approaches with realistic benchmarks. It would be very interesting to compare the performance of the proposed equalisation scheme with the approaches investigated in [2, 39, 70, 112], even though some of these schemes perform both equalisation and precoding, and as such also require channel state information in the transmitter.

Abbreviations

3G	3rd generation wireless communications
4G	4th generation wireless communications
5G	5th generation wireless communications
AFB	analysis filter bank
AWGN	additive white Gaussian noise
SER	symbol error rate
CMA	constant modulus algorithm
CMT	cosine modulated multitone
CP	cyclic prefix
DAB	digital audio broadcasting
DD	decision-direct
DFT	Discrete Fourier transform
DVB	digital video broadcasting
FBMC	filter bank multicarrier
FCE	fractionally spaced equaliser
FMT	filtered multitone
FIR	finite impulse response
FSE	fractionally spaced equalisers
IAI	interantenna interference
ICI	intercarrier interference
ISI	intersymbol interference
LTE	long term evolution

Abbreviations

MCM	multicarrier modulation
MIMO	multiple input multiple output
OFDM	orthogonal frequency division multiplexing
OS-FBMC	oversampled filter-bank based multicarrier
OQAM	offset quadrature amplitude modulation
PHYDYAS	physical layer for dynamic access and cognitive radio
PEVD	polynomial eigenvalue decomposition
PSVD	polynomial singular value decomposition
RLS	recursive least squares
SMD	sequential matrix diagonalisation
SNR	signal to noise ratio
SISO	single-input single-output
SMT	staggered multitoned
SFB	synthesis filter bank
WLAN	wireless local area networks
WiMAX	worldwide interoperability for microwave access

Mathematical Notation

General Notations

a	scalar quantity
\mathbf{a}	vector quantity
\mathbf{A}	matrix quantity
$a[n]$	a function of the discrete variable n
$\mathbf{A}(z)$	z-transform of a discrete function $A[n]$
$\mathbf{A}(e^{j\omega})$	descrete Fourier transform of $A[n]$

Relations and Operators

$\bullet - \circ$	transform pair, e.g. $F[n] \bullet - \circ F(z)$
$(\cdot)^*$	complex conjugate
$(\cdot)^T$	transpose operation,
$(\cdot)^P$	ParaHermitian operation, e.g. $(\mathbf{F}^P(z) = \mathbf{F}^H(1/z^*))$
$(\cdot)^{-1}$	inverse
$(\cdot)^\dagger$	pseudo-inverse
$ \cdot $	magnitude operator
$\ \cdot\ _F$	Frobenius norm of (\cdot)
$\ \cdot\ _2$	Euclidean norm of (\cdot)

Mathematical Notation

$\uparrow K$	upsampling by a K factor
$\downarrow K$	downsampling by a K factor
\otimes	Kronecker product
$\Re(\cdot)$	the real part of the complex quantity (\cdot)
$\Im(\cdot)$	the imaginary part of the complex quantity (\cdot)
$*$	convolution operation
$\text{diag}(\cdot)$	diagonal matrix with elements (\cdot)
$\min(\cdot)$	select the minimum value in (\cdot)
$\text{rank}\{\mathbf{F}\}$	rank of \mathbf{F} (number of linearly independent rows in \mathbf{F})

Sets and Spaces

\mathbb{C}	set of complex numbers
$\mathbb{C}^{M \times N}$	set of $M \times N$ matrices with complex entries
\mathbb{R}	set of real numbers
$\mathbb{R}^{M \times N}$	set of $M \times N$ matrices with real entries

Symbols and Variables

μ_{CM}	CM step size
μ_{DD}	DD step size
ψ_{CM}	CM step size
ψ_{DD}	DD step size
$\Sigma(z)$	diagonal matrix contains the polynomial singular values $\sigma_m(z)$
ϵ_1	threshold constant
ϵ_2	regularisation constant
γ	constant modules
$\sigma_m(z)$	transfer function of the m th polynomial singular values of $\mathbf{F}(z)$

$F_i(z)$	transfer function of the i th filter in the SFB
$\mathbf{F}(z)$	FBMC/OQAM channel polynomial matrix
$H_i(z)$	transfer function of the i th filter in the AFB
\mathbf{I}	identity matrix
L_c	channel length
L_f	filter length
L_P	length of the prototype filter $P[m]$
M	number of subchannels of the FBMC system
N_T	number of transmit antennas in a MIMO system
N_R	number of receive antennas in a MIMO system
V	overlapping factor
$P[m]$	prototype filter impulse response
$W_{i(CM)}$	i th polyphase component of the FS-CMA equaliser, $i = 0, 1$
$\mathbf{W}[n]$	FBMC/OQAM equaliser polynomial matrix

References

- [1] S. Chen and J. Zhao. “The requirements, challenges, and technologies for 5G of terrestrial mobile telecommunication,” *IEEE Communications Magazine*, vol. 52, no. 5, pp. 36–43, 2014.
- [2] A. I. Perez-Neira, M. Caus, R. Zakaria, D. L. Ruyet, E. Kofidis, M. Haardt, X. Mestre, and Y. Cheng. “MIMO signal processing in offset-QAM based filter bank multicarrier systems,” *IEEE Transactions on Signal Processing*, vol. 64, no. 21, pp. 5733–5762, Nov. 2016.
- [3] Q. Li, X. E. Lin, J. Zhang, and W. Roh. “Advancement of MIMO technology in WiMAX: From IEEE 802.16 d/e/j to 802.16 m,” *IEEE Communications Magazine*, vol. 47, no. 6, pp. 100–107, June 2009.
- [4] B. A. Bjerke. “LTE-advanced and the evolution of LTE deployments,” *IEEE Wireless Communications*, vol. 18, no. 5, pp. 4–5, Oct. 2011.
- [5] J. A. Bingham. “Multicarrier modulation for data transmission: An idea whose time has come,” *IEEE Communications magazine*, vol. 28, no. 5, pp. 5–14, 1990.
- [6] J. Fang, Z. You, I. T. Lu, J. Li, and R. Yang. “Comparisons of filter bank multicarrier systems,” in *IEEE Long Island Systems, Applications and Technology Conference - LISAT*, Farmingdale, NY, USA, May 2013.
- [7] P. Siohan, C. Siclet, and N. Lacaille. “Analysis and design of OFDM/OQAM systems based on filterbank theory,” *IEEE Transactions on Signal Processing*, vol. 50, no. 5, pp. 1170–1183, May 2002.

- [8] M. Caus and A. I. Perez-Neira. “Transmitter-receiver designs for highly frequency selective channels in MIMO FBMC systems,” *IEEE Transactions on Signal Processing*, vol. 60, no. 12, pp. 6519–6532, 2012.
- [9] K. Fazel and S. Kaiser. *Multi-Carrier and Spread Spectrum Systems*. John Wiley & Sons, 2003.
- [10] H. Schulze and C. Luders. *Theory and applications of OFDM and CDMA: Wideband wireless communications*. John Wiley & Sons, 2005.
- [11] Y. Zhao and S.-G. Haggman. “Sensitivity to doppler shift and carrier frequency errors in OFDM systems-the consequences and solutions,” *Proceedings of Vehicular Technology Conference - VTC*, vol. 3, pp. 1564–1568, Atlanta, GA, USA, Apr. 1996.
- [12] J. Lee, H.-L. Lou, D. Toumpakaris, and J. M. Cioff. “Effect of carrier frequency offset on OFDM systems for multipath fading channels,” *IEEE Global Telecommunications Conference - GLOBECOM*, vol. 6, pp. 3721–3725, Dallas, TX, USA, Nov. 2004.
- [13] I. Barhumi, G. Leus, and M. Moonen. Time-varying FIR equalization for doubly selective channels. *IEEE Transactions on Wireless Communications*, 4(1):202–214, January 2005.
- [14] L. Rugini, P. Banelli, and G. Leus. Simple equalization of time-varying channels for OFDM. *IEEE Communications Letters*, 9(7):619–621, July 2005.
- [15] I. Barhumi, G. Leus, and M. Moonen. Equalization for OFDM over doubly selective channels. *IEEE Transactions on Signal Processing*, 54(4):1445 – 1458, April 2006.
- [16] R. N. Mitra and D. P. Agrawal. “5G mobile technology: A survey,” *ICT Express*, vol. 1, no. 3, pp. 132–137, 2015.
- [17] F. Schaich and T. Wild. “Waveform contenders for 5G-OFDM vs. FBMC vs. UPMC,” *IEEE 6th International Symposium on Communications, Control and Signal Processing -ISCCSP*, pp. 457–460, Athens, Greece, May 2014.

- [18] F. Schaich, T. Wild, and Y. Chen. “Waveform contenders for 5G-suitability for short packet and low latency transmissions,” *IEEE 79th Vehicular Technology Conference -VTC Spring*, pp. 1–5, Seoul, South Korea, May 2014.
- [19] H. Lin. “Filter bank OFDM: A new way of looking at FBMC,” *IEEE International Conference on Communication Workshop (ICCW)*, pp. 1077–1082, London, UK, Jun. 2015.
- [20] P. Chevalier, D. Le Ruyet, and R. Chauvat. “Maximum likelihood Alamouti receiver for filter bank based multicarrier transmissions,” *Proceedings of the 20th International ITG Workshop on Smart Antennas (WSA)*, pp. 1–7, Munich, Germany, Mar. 2016.
- [21] S. A. Cheema, K. Naskovska, M. Attar, B. Zafar, and M. Haardt. “Performance comparison of space time block codes for different 5G air interface proposals,” *Proceedings of the 20th International ITG Workshop on Smart Antennas (WSA)*, pp. 1–7, Munich, Germany, Mar. 2016.
- [22] G. Wunder, et al. “5GNOW: Intermediate frame structure and transceiver concepts,” *Globecom Workshops (GC Wkshps)*, pp. 565–570, Austin, TX, USA, Dec. 2014.
- [23] P. Banelli, S. Buzzi, G. Colavolpe, A. Modenini, F. Rusek, and A. Ugolini. “Modulation formats and waveforms for 5G networks: Who will be the heir of OFDM?: An overview of alternative modulation schemes for improved spectral efficiency,” *IEEE Signal Processing Magazine*, vol. 31, no. 6, pp. 80–93, Oct. 2014.
- [24] R. Gerzaguet, et al. “The 5G candidate waveform race: A comparison of complexity and performance,” *EURASIP Journal on Wireless Communications and Networking*, vol. 2017, no. 1, p. 13, Oct. 2017.
- [25] C. Kim, Y. H. Yun, K. Kim, and J. Y. Seol. “Introduction to QAM-FBMC: From waveform optimization to system design,” *IEEE Communications Magazine*, vol. 54, no. 11, pp. 66–73, Nov. 2016.

- [26] M. Schellmann, Z. Zhao, H. Lin, P. Siohan, N. Rajatheva, V. Luecken, and A. Ishaque. “FBMC-based air interface for 5G mobile: Challenges and proposed solutions,” *9th International Conference on Cognitive Radio Oriented Wireless Networks and Communications (CROWNCOM)*, pp. 102–107, Oulu, Finland, Jun. 2014.
- [27] B. Farhang-Boroujeny. “Filter bank multicarrier modulation: A waveform candidate for 5G and beyond,” *Advances in Electrical Engineering*, vol. 2014, Oct. 2014.
- [28] S. Mirabbasi and K. Martin. “Overlapped complex-modulated transmultiplexer filters with simplified design and superior stopbands,” *IEEE Transactions on Circuits and Systems II: Analog and Digital Signal Processing*, vol. 50, no. 8, pp. 456–469, Aug. 2003.
- [29] B. Farhang-Boroujeny. “OFDM versus filter bank multicarrier,” *IEEE signal processing magazine*, vol. 28, no. 3, pp. 92–112, Apr. 2011.
- [30] G. Cherubini, E. Eleftheriou, and S. Olcer. “Filtered multitone modulation for very high-speed digital subscriber lines,” *IEEE Journal on Selected Areas in Communications*, vol. 20, no. 5, pp. 1016–1028, 2002.
- [31] A. Viholainen, T. Saramaki, and M. Renfors. “Nearly perfect-reconstruction cosine-modulated filter bank design for vdsl modems,” *The 6th IEEE International Conference on Electronics, Circuits and Systems (ICECS)*, vol. 1, pp. 373–376, Pafos, Cyprus, Sep. 1999.
- [32] R. W. Chang. “Synthesis of band-limited orthogonal signals for multichannel data transmission,” *Bell Labs Technical Journal*, vol. 45, no. 10, pp. 1775–1796, 1966.
- [33] B. Saltzberg. “Performance of an efficient parallel data transmission system,” *IEEE Transactions on Communication Technology*, vol. 15, no. 6, pp. 805–811, 1967.
- [34] B. Hirosaki. “An orthogonally multiplexed qam system using the discrete fourier transform,” *IEEE Transactions on Communications*, vol. 29, no. 7, pp. 982–989, 1981.

- [35] A. Nagy and S. Weiss. “Synchronisation and equalisation of an FBMC/OQAM system by a polynomial matrix pseudo-inverse,” *IEEE International Symposium on Signal Processing and Information Technology*, Bilbao, Spain, Dec. 2017.
- [36] N. Holte. “MMSE equalization of OFDM/OQAM systems for channels with time and frequency dispersion,” *International Conference on Wireless Communications & Signal Processing*, pp. 1–5, Nanjing, China, Nov. 2009.
- [37] R. Nissel and M. Rupp. “OFDM and FBMC/OQAM in doubly-selective channels: Calculating the bit error probability,” *IEEE Communications Letters*, vol. 21, no. 6, pp. 1297–1300, 2017.
- [38] S. M. J. A. Tabatabaee and H. Zamiri-Jafarian. “Per-subchannel joint equalizer and receiver filter design in OFDM/OQAM systems,” *IEEE Transactions on Signal Processing*, vol. 64, no. 19, pp. 5094–5105, 2016.
- [39] L. Marijanovic, S. Schwarz, and M. Rupp. “MMSE equalization for FBMC transmission over doubly-selective channels,” *International Symposium on Wireless Communication Systems (ISWCS)*, pp. 170–174, Poznan, Poland, Sep. 2016.
- [40] B. S. Chang, C. Da Rocha, D. Le Ruyet, and D. Roviras. “On the use of precoding in FBMC/OQAM systems,” *ITS*, Manaus, Brazil, Sep, 2010.
- [41] O. De Candido, S. A. Cheema, L. G. Baltar, M. Haardt, and J. A. Nossek. “Downlink precoder and equalizer designs for multi-user MIMO FBMC/OQAM,” *Proceedings of the 20th International ITG Workshop on Smart Antennas*, pp. 1–8, Munich, Germany, Mar. 2016.
- [42] F. Rottenberg, X. Mestre, D. Petrov, F. Horlin, and J. Louveaux. “Parallel equalization structure for MIMO FBMC-OQAM systems under strong time and frequency selectivity,” *IEEE Transactions on Signal Processing*, vol. 65, no. 17, pp. 4454–4467, 2017.
- [43] C. Mavrokefalidis, A. Rontogiannis, E. Kofidis, A. Beikos, and S. Theodoridis. “Efficient adaptive equalization of doubly dispersive channels in MIMO-

- FBMC/ OQAM systems,” *11th International Symposium on Wireless Communications Systems (ISWCS)*, pp. 308–312, Barcelona, Spain, Aug. 2014.
- [44] A. Scaglione, G. B. Giannakis, and S. Barbarossa. Redundant Filterbank Precoders and Equalizers. I. Unification and Optimal Designs. *IEEE Transactions on Signal Processing*, 47(7):1988–2006, July 1999.
- [45] A. Scaglione, G. B. Giannakis, and S. Barbarossa. Redundant Filterbank Precoders and Equalizers. II. Blind Channel Estimation, Synchronization, and Direct Equalization. *IEEE Transactions on Signal Processing*, 47(7):2007–2022, July 1999.
- [46] A. Scaglione, G. B. Giannakis, and S. Barbarossa. Filterbank Transceivers Optimizing Information Rate in Block Transmission over Dispersive Channels. *IEEE Transactions on Information Theory*, 45(4):1019–1032, April 1999.
- [47] A. Mertins. MMSE Design of Redundant FIR Precoders for Arbitrary Channel Lengths. *IEEE Transactions on Signal Processing*, 51(9):2402–2409, September 2003.
- [48] X. Mestre and D. Gregoratti. A parallel processing approach to filterbank multicarrier MIMO transmission under strong frequency selectivity. In *IEEE International Conference on Acoustics, Speech and Signal Processing*, pages 8078–8082, May 2014.
- [49] M. Caus and A.I. Perez-Neira. Multi-stream transmission for highly frequency selective channels in MIMO-FBMC/OQAM systems. *IEEE Transactions on Signal Processing*, 62(4):786–796, February 2014.
- [50] S. Weiss, J. Pestana, and I. K. Proudler. “On the existence and uniqueness of the eigenvalue decomposition of a parahermitian matrix,” *IEEE Transactions on Signal Processing*, vol. 66, no. 10, pp. 2659–2672, May 2018.
- [51] M. Bellanger, *et al.* “FBMC physical layer: a primer,” *PHYDYAS*, vol. 25, no. 4, Jan. 2010.

- [52] J. G. McWhirter, P. D. Baxter, T. Cooper, S. Redif, and J. Foster. “An EVD algorithm for para-hermitian polynomial matrices,” *IEEE Transactions on Signal Processing*, vol. 55, no. 5, pp. 2158–2169, May 2007.
- [53] S. Redif, S. Weiss, and J. G. McWhirter. “Sequential matrix diagonalization algorithms for polynomial EVD of parahermitian matrices,” *IEEE Transactions on Signal Processing*, vol. 63, no. 1, pp. 81–89, Jan. 2015.
- [54] A. Nagy and S. Weiss. “Channel equalisation of a MIMO FBMC/OQAM system using a polynomial matrix pseudo-inverse,” *10th IEEE sensor array and multichannel signal processing workshop*, Sheffield, UK, July 2018.
- [55] A. A. Nagy and S. Weiss. “Comparison of filter-bank based multicarrier systems with fractionally spaced equalisation,” *11th IMA International Conference on Mathematics in Signal Processing*, Birmingham, UK, Dec. 2016.
- [56] X. Mestre *et al.* “EMPhAtiC enhanced multicarrier techniques for professional ad-hoc and cell-based communications,” Apr. 2015.
- [57] P. Popovski *et al.* “METIS mobile and wireless communications enablers for the twenty-twenty information society,” Apr. 2014.
- [58] A. Viholainen, T. Ihalainen, T. H. Stitz, M. Renfors, and M. Bellanger. “Prototype filter design for filter bank based multicarrier transmission,” *17th European Signal Processing Conference*, pp. 1359–1363, Glasgow, UK, Aug. 2009.
- [59] H. G. Feichtinger and T. Strohmer, editors. *Gabor Analysis and Algorithms — Theory and Applications*. Birkhäuser, Boston, MA, October 1997.
- [60] A. Viholainen, M. Bellanger, and M. Huchard. “PHYDYAS physical layer for dynamic access and cognitive radio, prototype filter and structure optimization,” *IEEE Wireless Communications*, Jan. 2009.
- [61] G. J. Foschini and M. J. Gans. “On limits of wireless communications in a fading environment when using multiple antennas,” *Wireless personal communications*, vol. 6, no. 3, pp. 311–335, 1998.

- [62] G. J. Foschini. “Layered space-time architecture for wireless communication in a fading environment when using multi-element antennas,” *Bell labs technical journal*, vol. 1, no. 2, pp. 41–59, 1996.
- [63] E. Telatar. “Capacity of multi-antenna gaussian channels,” *European Transactions on Emerging Telecommunications Technologies*, vol. 10, no. 6, pp. 585–595, 1999.
- [64] S. M. Alamouti. “simple transmit diversity technique for wireless communications,” *IEEE Journal on selected areas in communications*, vol. 16, no. 8, pp. 1451–1458, 1998.
- [65] V. Tarokh and H. Jafarkhani. “A differential detection scheme for transmit diversity,” *IEEE journal on selected areas in communications*, vol. 18, no. 7, pp. 1169–1174, 2000.
- [66] J. Mietzner, R. Schober, L. Lampe, W. H. Gerstacker, and P. A. Hoeher. “Multiple-antenna techniques for wireless communications—a comprehensive literature survey,” *IEEE communications surveys & tutorials*, vol. 11, no. 2, 2009.
- [67] M. J. Bocus, A. Doufexi, and D. Agrafiotis. “Performance evaluation of MIMO-OFDM/OQAM in time-varying underwater acoustic channels,” *IEEE OCEANS-Anchorage*, pp. 1–6, 2017.
- [68] C. Li and Q. Yang. “Optical OFDM/OQAM for the future fiber-optics communications,” *Procedia engineering*, vol. 140, pp. 99–106, 2016.
- [69] A. M. Tonello and F. Pecile. “Analytical results about the robustness of FMT modulation with several prototype pulses in time-frequency selective fading channels,” *IEEE Transactions on Wireless Communications*, vol. 7, no. 5, pp. 1634–1645, May. 2008.
- [70] M. Caus and A. Perez-Neira. “Multi-stream transmission for highly frequency selective channels in MIMO-FBMC/OQAM systems,” *IEEE transactions on signal processing*, vol. 62, no. 4, pp. 786–796, Dec. 2014.

- [71] X. Mestre and D. Gregoratti. “A parallel processing approach to filter-bank multicarrier MIMO transmission under strong frequency selectivity,” *IEEE International Conference on Acoustics, Speech and Signal Processing (ICASSP)*, pp. 8078–8082, Florence, Italy, May 2014.
- [72] S. Weiss, A. P. Millar, R. W. Stewart, and M. D. Macleod. “Performance of transmultiplexers based on oversampled filter banks under variable oversampling ratios,” *18th European Signal Processing Conference*, pp. 2181–2185, Aalborg, Denmark, Aug. 2010.
- [73] B. Widrow and E. Walach. “*Adaptive inverse control*,” Prentice Hall, 1995.
- [74] T. I. Laakso, V. Valimaki, M. Karjalainen, and U. K. Laine. “Splitting the unit delay [FIR/all pass filters design],” *IEEE Signal Processing Magazine*, vol. 13, no. 1, pp. 30–60, Jan. 1996.
- [75] J. R. Treichler, I. Fijalkow, and C. R. Johnson. “Fractionally Spaced Equalizers: How Long Should They Really Be?,” *IEEE Signal Processing Magazine*, vol. 13, no. 3, pp. 65–81, May. 1996.
- [76] F. C. C. D. Castro, M. D. Castro, and D. Arantes. “Concurrent blind deconvolution for channel equalization,” *IEEE International Conference on Communications*, pp. 366–371, Helsinki, Finland, Aug. 2001.
- [77] M. Hedef and S. Weiss. “Concurrent constant modulus algorithm and decision directed scheme for synchronous DS/CDMA equalisation,” *IEEE 13th Workshop on Statistical Signal Processing*, pp. 203–208, Bordeaux, France, Jul. 2005.
- [78] S. Chen and E. Chng. “Concurrent constant modulus algorithm and soft decision directed scheme for fractionally-spaced blind equalization,” *IEEE International Conference on Communications*, pp. 2342–2346, Paris, France, Jun. 2004.
- [79] S. Chen and E. Chng. “Fractionally spaced blind equalization with low complexity concurrent constant modulus algorithm and soft decision-directed scheme,” *International Journal of Adaptive Control and Signal Processing*, vol. 19, no. 6, pp. 471–484, 2005.

- [80] S. Weiss and R. W. Stewart. “Fast implementation of oversampled modulated filter banks,” *Electronics Letters*, vol. 36, no. 17, pp. 1502–1503, Aug. 2000.
- [81] H. Mohamad, S. Weiss, M. Rupp, and L. Hanzo. “Fast adaptation of fractionally spaced equalisers,” *Electronics Letters*, vol. 38, no. 2, pp. 96–98, Jan. 2002.
- [82] R. Johnson, P. Schniter, T. J. Endres, J. D. Behm, D. R. Brown, and R. A. Casas. “Blind equalization using the constant modulus criterion: A review,” *Proceedings of the IEEE*, vol. 86, no. 10, pp. 1927–1950, Oct. 1998.
- [83] V. Zarzoso and P. Comon. “Optimal step-size constant modulus algorithm,” *IEEE Transactions on communications*, vol. 56, no. 1, 2008.
- [84] M. Failli. “Digital land mobile radio communications. COST 207,” Luxembourg, Mar. 1989.
- [85] T. Ihalainen, T. H. Stitz, M. Rinne, and M. Renfors. “Channel equalization in filter bank based multicarrier modulation for wireless communications,” *EURASIP Journal on Advances in Signal Processing*, vol. 2007, no. 1, p. 049389, Nov. 2006.
- [86] D. S. Waldhauser and J. A. Nossek. “MMSE equalization for bandwidth efficient multicarrier systems,” *IEEE International Symposium on Circuits and Systems*, 4 pp.-5394, Island of Kos, Greece, May 2006.
- [87] D. S. Waldhauser, L. G. Baltar, and J. A. Nossek. “MMSE subcarrier equalization for filter bank based multicarrier systems,” *IEEE 9th Workshop on Signal Processing Advances in Wireless Communications*, pp. 525–529, Recife, Brazil, Jul. 2008.
- [88] D. S. Waldhauser, L. G. Baltar, and J. Nossek. “Adaptive equalization for filter bank based multicarrier systems,” *IEEE International Symposium on Circuits and Systems*, pp. 3098–3101, Seattle, WA, USA, May 2008.
- [89] A. Ikhlef and J. Louveaux. “Per subchannel equalization for MIMO FBMC/OQAM systems,” *IEEE Pacific Rim Conference on Communications*,

- Computers and Signal Processing*, pp. 559–564, Victoria, BC, Canada, Aug. 2009.
- [90] L. G. Baltar, D. S. Waldhauser, and J. A. Nossek. “MMSE subchannel decision feedback equalization for filter bank based multicarrier systems,” *IEEE International Symposium on Circuits and Systems*, pp. 2802–2805, Taipei, Taiwan, May 2009.
- [91] D. S. Waldhauser, L. G. Baltar, and J. A. Nossek. “Adaptive decision feedback equalization for filter bank based multicarrier systems,” *IEEE International Symposium on Circuits and Systems*, pp. 2794–2797, Taipei, Taiwan, May 2009.
- [92] X. Mestre, M. Majoral, and S. Petschinger. “An asymptotic approach to parallel equalization of filter bank based multicarrier signals,” *IEEE Transactions on Signal Processing*, vol. 61, no. 14, pp. 3592–3606, Jul. 2013.
- [93] T. Ihalainen, T. H. Stitz, and M. Renfors. “Efficient per-carrier channel equalizer for filter bank based multicarrier systems,” *IEEE International Symposium on Circuits and Systems*, vol. 4, pp. 3175–3178, Kobe, Japan, May 2005.
- [94] G. Ndo, H. Lin, and P. Siohan, and W. Roh. “FBMC/OQAM equalization: Exploiting the imaginary interference,” *IEEE 23rd International Symposium on Personal, Indoor and Mobile Radio Communications - (PIMRC)*, pp. 2359–2364, Sydney, NSW, Australia, Sep. 2012.
- [95] J. Zhang, A. Nimr, and M. Haardt. “Joint design of multi-tap filters and power control for FBMC/OQAM based two-way decode-and-forward relaying systems in highly frequency selective channels,” *IEEE International Conference on Acoustics, Speech and Signal Processing (ICASSP)*, pp. 2439–2443, Brisbane, QLD, Australia, Apr. 2015.
- [96] B. S. Chang, C. A. F. da Rocha, D. L. Ruyet, and D. Roviras. “On the effect of ISI in the error performance of precoded FBMC/OQAM systems,” *18th Asia-Pacific Conference on Communications (APCC)*, pp. 987–991, Jeju Island, South Korea, Oct. 2012.

- [97] W. Chung, C. Kim, S. Choi, and D. Hong. “Synchronization sequence design for FBMC/OQAM systems,” *IEEE Transactions on Wireless Communications*, vol. 15, no. 10, pp. 7199–7211, Oct. 2016.
- [98] A. Gilloire and M. Vetterli. “Adaptive filtering in subbands with critical sampling: Analysis, experiments, and application to acoustic echo cancellation,” *IEEE Transactions on Signal Processing*, vol. 40, no. 8, pp. 1862–1875, Aug. 1992.
- [99] P. P. Vaidyanathan. *Multirate systems and filter banks*, Prentice Hall, Englewood Cliffs, 1993.
- [100] Z. Cvetkovic and M. Vetterli. “Oversampled filter banks,” *IEEE Transactions on Signal Processing*, vol. 46, no. 5, pp. 1245–1255, May 1998.
- [101] S. Weiss and R.W. Stewart. Fast Implementation of Oversampled Modulated Filter Banks. *Electronics Letters*, 36(17):1502–1503, August 2000.
- [102] M. G. Bellanger. “Specification and design of a prototype filter for filter bank based multicarrier transmission,” *IEEE International Conference on Acoustics, Speech, and Signal Processing*, vol. 4, pp. 2417–2420, Salt Lake City, UT, USA, May 2001
- [103] S. Redif, J. G. McWhirter, and S. Weiss. “Design of FIR paraunitary filter banks for subband coding using a polynomial eigenvalue decomposition,” *IEEE Transactions on Signal Processing*, vol. 59, no. 11, pp. 5253–5264, Nov. 2011.
- [104] J. G. McWhirter. “An algorithm for polynomial matrix SVD based on generalised Kogbetliantz transformations,” *18th European Signal Processing Conference*, pp. 457–461, Aalborg, Denmark, Aug. 2010.
- [105] J. A. Foster, J. G. McWhirter, M. R. Davies, and J. A. Chambers. “An algorithm for calculating the QR and singular value decompositions of polynomial matrices,” *IEEE Transactions on Signal Processing*, vol. 58, no. 3, pp. 1263–1274, Mar. 2010.

- [106] J. Corr, K. Thompson, S. Weiss, J. McWhirter, S. Redif, and I. Proudler. “Multiple shift maximum element sequential matrix diagonalisation for parahermitian matrices,” *IEEE Workshop on Statistical Signal Processing*, pp. 312–315, Gold Coast, Australia, Jun. 2014.
- [107] S. Weiss, J. Pestana, and I. K. Proudler. On the existence and uniqueness of the eigenvalue decomposition of a parahermitian matrix. *IEEE Transactions on Signal Processing*, 66(10):2659–2672, May 2018.
- [108] S. Weiss, A. P. Millar, and R. W. Stewart. “Inversion of parahermitian matrices,” in 18th European Signal Processing Conference,” *18th European Signal Processing Conference*, pp. 447–451, Aalborg, Denmark, Aug. 2010.
- [109] G. H. Golub and C. F. V. Loan. *Matrix computations*, The Johns Hopkins University Press, Baltimore, Maryland, 3rd edition, 1996.
- [110] S. Haykin. *Adaptive Filter Theory*, Prentice Hall, Englewood Cliffs, 2nd edition, 1991.
- [111] R. Nissel, S. Schwarz, and M. Rupp. “Filter bank multicarrier modulation schemes for future mobile communications,” *IEEE Journal on Selected Areas in Communications*, vol. 35, no. 8, pp. 1768–1782, Aug. 2017.
- [112] X. Mestre and D. Gregoratti. “Parallelized structures for MIMO FBMC under strong channel frequency selectivity,” *IEEE Transactions on Signal Processing*, vol. 64, no. 5, pp. 1200–1215, Mar. 2016.
- [113] T. Ihalainen, A. Ikhlef, J. Louveaux, and M. Renfors. “Channel equalization for multi-antenna FBMC/OQAM receivers,” *IEEE Transactions on Vehicular Technology*, vol. 60, no. 5, pp. 2070–2085, Jun. 2011.
- [114] A. Mertins. “MMSE design of redundant FIR precoders for arbitrary channel lengths,” *IEEE Transactions on Signal Processing*, vol. 51, no. 9, pp. 2402–2409, Sep. 2003.
- [115] B. De Moor and S. Boyd. “Analytic properties of singular values and vectors,” *Katholic Univ. Leuven, Belgium Tech. Rep.*, vol. 28, 1989.

- [116] A. Bunse-Gerstner, R. Byers, V. Mehrmann, and N. K. Nicols. “Numerical computation of an analytic singular value decomposition of a matrix valued function,” *Numer. Math.*, vol. 60, no. 6, pp. 1–40, 1991.
- [117] J. Corr, K. Thompson, S. Weiss, I. K. Proudler, and J. G. McWhirter. “Row-shift corrected truncation of paraunitary matrices for PEVD algorithms,” *23rd European Signal Processing Conference (EUSIPCO)*, pp. 849–853, Nice, France, Aug. 2015.
- [118] V. Belevitch. *Classical Network Theory*, Holden-Day, 1968.
- [119] J. McWhirter and Z. Wang. “A novel insight to the SBR2 algorithm for diagonalising para-hermitian matrices,” *11th IMA International Conference on Mathematics in Signal Processing*, Birmingham, UK, Dec. 2016.
- [120] W. Al-Hanafy and S. Weiss. “Suboptimal greedy power allocation schemes for discrete bit loading,” *The Scientific World Journal*, vol. 2013, June 2013.
- [121] S. Nader-Esfahani and M. Afrasiabi. “Simple bit loading algorithm for OFDM-based systems,” *IET communications*, vol. 1, no. 3, pp. 312–316, 2007.
- [122] D. P. Palomar and J. R. Fonollosa. “Practical algorithms for a family of waterfilling solutions,” *IEEE transactions on Signal Processing*, vol. 53, no. 2, pp. 686–695, 2005.
- [123] M. Caus and A. I. Perez-Neira. “A suboptimal power allocation algorithm for FBMC/OQAM,” *IEEE 13th International Workshop on Signal Processing Advances in Wireless Communications (SPAWC)*, pp. 189–193, Cesme, Turkey, Jun. 2012.
- [124] M. Caus, M. Navarro, X. Mestre, and A. Perez-Neira. “Link adaptation in FBMC/OQAM systems using NB-LDPC codes,” *European Conference on Networks and Communications (EuCNC)*, pp. 11–15, Athens, Greece, Jun. 2016.

- [125] L. Mathews and S. S. Pillai. “Performance of turbo coded FBMC based MIMO systems,” *IEEE International Conference on Computational Intelligence and Computing Research (ICIC)*, pp. 1–5, Chennai, India, Dec. 2016
- [126] S. Jo and J.-S. Seo. “Tx scenario analysis of FBMC based LDM system,” *ICT Express*, vol. 1, no. 3, pp. 138–142, 2015.
- [127] J. Corr, K. Thompson, S. Weiss, J.G. McWhirter, and I.K. Proudler. Cyclic-by-row approximation of iterative polynomial EVD algorithms. In *Sensor Signal Processing for Defence*, pages 1–5, Edinburgh, Scotland, Sept 2014.
- [128] J. Corr, K. Thompson, S. Weiss, I.K. Proudler, and J.G. McWhirter. Reduced search space multiple shift maximum element sequential matrix diagonalisation algorithm. In *IET/EURASIP Intelligent Signal Processing*, London, UK, December 2015.
- [129] Fraser K. Coutts, Jamie Corr, Keith Thompson, Stephan Weiss, Ian Proudler, and John G. McWhirter. Memory and complexity reduction in parahermitian matrix manipulations of PEVD algorithms. In *24th European Signal Processing Conference*, Budapest, Hungary, August 2016.
- [130] F.K. Coutts, J. Corr, K. Thompson, S. Weiss, I.K. Proudler, and J.G. McWhirter. Complexity and search space reduction in cyclic-by-row PEVD algorithms. In *50th Asilomar Conference on Signals, Systems and Computers*, Pacific Grove, CA, November 2016.
- [131] Chi Hieu Ta and S. Weiss. Shortening the order of paraunitary matrices in SBR2 algorithm. In *6th International Conference on Information, Communications & Signal Processing*, pages 1–5, Singapore, December 2007.
- [132] J. Corr, K. Thompson, S. Weiss, I.K. Proudler, and J.G. McWhirter. Row-shift corrected truncation of paraunitary matrices for PEVD algorithms. In *23rd European Signal Processing Conference*, pages 849–853, Nice, France, August/September 2015.
- [133] J. Corr, K. Thompson, S. Weiss, I.K. Proudler, and J.G. McWhirter. Shortening of paraunitary matrices obtained by polynomial eigenvalue decomposi-

tion algorithms. In *Sensor Signal Processing for Defence*, Edinburgh, Scotland, September 2015.